BIOACTIVE SCAFFOLDS FOR BONE REGENERATION

M.T. Poldervaart, MD, MSc

Bioactive scaffolds for bone regeneration. Mischa Tamara Poldervaart PhD thesis, Utrecht University, University Medical Center Utrecht, Utrecht, The Netherlands.

This research forms part of the Project P2.04 BONE-IP of the research program of the BioMedical Materials Institute, co-founded by the Dutch Ministry of Economic Affairs. The research in this thesis was financially supported by: Anna Fonds | NOREF.

ISBN: 9789462338142

Layout and printing: Gildeprint, Enschede, The Netherlands.

Cover art: Lona Aalders.

Bioactive scaffolds for bone regeneration

Bioactieve constructen voor botregeneratie
(met een samenvatting in het Nederlands)

Proefschrift

ter verkrijging van de graad van doctor aan de Universiteit Utrecht op gezag van de rector magnificus, prof.dr. G.J. van der Zwaan, ingevolge het besluit van het college voor promoties in het openbaar te verdedigen op dinsdag 28 november 2017 des avonds te 6.00 uur

door

Mischa Tamara Poldervaart
geboren op 1 december 1982
te Dordrecht

Promotoren: Prof. dr. W.J.A. Dhert
Prof. dr. F.C. Öner

Copromotor: Dr. J. Alblas

Dit proefschrift werd (mede) mogelijk gemaakt met financiële steun van:
Nederlandse Orthopaedische Vereniging
Dutch Spine Society
Nederlandse Vereniging voor Biomaterialen en Tissue Engineering
OLVG Amsterdam
Anna Fonds | NOREF
Smith & Nephew
Push Braces
Bauerfeind
Tromp Medical BV
BISLIFE Foundation
Chipsoft

Voor MJ

TABLE OF CONTENTS

CHAPTER 1

General introduction

CLINICAL PROBLEM

Bone healing

Bone has the ability to regenerate itself during the process of repair. After injury, external or internal immobilization can facilitate this physiological process of bone regeneration. When this healing process fails, for example due to pathological processes, excessive motion, infection or sequestration by avascular necrosis, this can lead to nonunion of fractures. Nonunions are defined as fractures that lack potential to heal without an intervention, such as application of a bone graft or bone graft substitute material. Bone grafting procedures to prevent or treat nonunions are performed in about half of the 3 million musculoskeletal procedures per year in the United States [1]. Worldwide bone grafting procedures are performed in 2.2 million orthopedic procedures annually [2].

First documented applications of the bone graft

Interestingly, the first documented bone grafting procedure was already described in 1668 in a book by Dutch surgeon Job van Meek'ren [3]. It mentioned a report from a Russian missionary about the use of a piece of dog skull to fill a soldiers' cranial defect. The transplant was removed 2 years later to regain access to the church, from which the soldier was excommunicated because of the xenograft, even though healing was reported to be 'perfect'.

In 1820 German surgeon Philips von Walter was the first to describe autologous bone grafting, successfully filling of a cranial defect after trepanation [4,5]. The procedure was first described as bone grafting in 1861 *'greffe osseuse'* by Leopold Ollier from Lyon in '*Traité expérimental et clinique de la régénération des os et de la production artificielle du tissu osseux'*, a document that also stated that *"implanted bone fragments are viable if they include the periosteum, which is the most important viability factor of the graft"*.

Autologous bone grafts

In present time, autografting is considered the gold standard in bone grafting procedures. The calcified extracellular matrix of an autograft provides stability, osteoconductivity, growth factors to induce vasculogenesis and osteogenesis and contains cells that play a crucial part in the regenerative process. Unfortunately there are also disadvantages in the use of autograft bone, such as limited availability, the need for an extra surgery, and side effects and complications associated with the harvesting procedure. Even substantial complications, such as pelvic fractures, nerve damage, vascular damage and (wound) infection have been reported [6]. The most commonly reported complication, occurring in approximately 20% of patients, is persistent pain at the harvest site [7], although this donor site morbidity may be overestimated due to inability to differentiate this pain from residual lower back pain [8].

Allogeneic bone grafts

Allogeneic bone grafts, and associated products such as demineralized bone matrix (DMB) are the second most applied bone grafts (1/3 of the procedures in North America). Processing of the donor bone tissue (such as freeze drying, irradiation and multiple washing steps) is costly and impairs its performance compared to unprocessed bone, damaging the osteoconductive and osteoinductive properties. Secondly, the use of allograft introduces the risk of infectious disease transfer. Donor bone is also limited in availability.

Alternatives to bone grafting

Calcium sulfate (Plaster of Paris) was the first reported artificial bone graft in 1894 [9]. Since then, many different biomaterials have been used as bone replacement materials. New products are continuously developed and tested and bone graft substitutes have grown out to a 2.5 billion dollar per year industry [1]. Scaffold materials vary from titanium[10] to bioactive glass[11] to polymers[12], but by far the mostly used bone substitutes are ceramics. Ceramics are often produced from hydroxyapatite (HA, a main component of bone and teeth), tri-calcium phosphate (TCP) and mixtures of these two, known as biphasic calcium phosphate (BCP) [13]. Current bone substitute materials usually do not perform as well as bone grafts. Ideally bone graft substitutes need to be biocompatible and osteoconductive, and are preferably osteoinductive, easy to handle, off-the-shelf available and biodegradable [14].

Problem definition

The disadvantages of autologous bone grafts and the inferiority of graft substitutes point to a great need for alternative methods to reconstruct bone defects. Tissue engineered bone constructs are considered a promising approach to a new generation of bioactive bone substitutes [15].

THE CLASSICAL TRIAS OF TISSUE ENGINEERING

Tissue engineering is an emerging multidisciplinary field that converges knowledge and techniques from biology, medicine and engineering; it aims to progress towards the development of compounds, tissues or organs that can replace defective or lost tissues or organs [16,17]. Classically, three important components can be involved in the bone tissue engineering approach. Application of a scaffold (carrier) material, which can be seeded with cells, and potentially combined with bioactive factors that can attract endogenous cells, induce vascularization or stimulate cell differentiation in seeded as well as host cells. These three components are discussed in depth in the following paragraphs.

Requirements for successful tissue engineered bone grafts

The aimed location for application of tissue engineered bone grafts largely dictates the requirements of the use of each component. At orthotopic locations, conditions for forming and maintaining bone are principally already present. The need for cell-based approaches is limited, as many stem cells are present in and around the periosteum. Due to mechanical loading, scaffold materials with mechanical properties that closely resemble that of the bone are desirable. At ectopic locations, there is no mechanical loading, nor a preexisting bone environment, which makes application of bone forming cells, bioactive factors and/or an osteoinductive scaffold material a prerequisite for bone formation [18].

When suitable tissue engineered bone grafts are upscaled to clinically relevant sizes, they exceed the acceptable distance (100µm - 1mm) for diffusion of oxygen and nutrients, causing central necrosis of the grafts. To overcome this problem, pre-vascularisation strategies, using cells or bioactive factors can be utilized [19,20].

I. Important cells in bone tissue engineering

The mesenchymal stromal cell (MSC)

In 1966 Friedenstein *et al*. identified a population of fibroblast-like cells retrieved from murine bone marrow biopsies, that demonstrated colony forming ability and osteogenic capacity [21]. These cells have since then been extensively studied and were named mesenchymal stem cells (MSCs) [22]. Isolation of these cells is mainly dependent on their potency to adhere to tissue culture plastic combined with a high expansion potential. The presence of cell markers CD105, CD73, CD90 and absence of cell markers CD45, CD34, CD14 or CD11b, and CD79α or CD19 and HLA-DR surface molecules, as well as their ability to differentiate into osteogenic, adipogenic and chondrogenic pathways *in vitro* confirm that these cells are MSCs [23]. Isolation of MSCs is no longer exclusively from bone marrow aspirates (although this is still the most commonly used cell source), but they can be isolated from adipose tissue [24], skin [25], umbilical cord [26], placenta [27], cord blood [28], dental pulp [29] and even breast milk [30]. The progress in characterization of the cells revealed that they are a rather heterogeneous population of which only a small fraction demonstrates real stem cell characteristics such as unlimited and asymmetric cell division, multi-lineage potential and repopulating capacity. These findings led to renaming of the cells to multipotent stromal cells (MSCs) [31,32]. It may be necessary for differentiation purposes to mature MSCs before implantation, which can be achieved by *in vitro* pre-culturing [33].

MSCs are an appealing base for cell-based therapies because they can be easily harvested, rapidly expanded *ex vivo*, are immuno-privileged, so they will not be rejected by

host cells in an allogeneic setting [34], are multipotent and have the capacity to home to injured tissue [35].

The endothelial progenitor cell (EPCs)

Bone is a highly vascularised tissue, therefore vascularization is a prerequisite to allow bone formation in tissue engineered constructs of clinically relevant dimensions [36]. Since tissue engineered bone constructs are devoid of vessel supply, a promising approach seems to be the addition of endothelial colony forming cells (ECFCs), that can be isolated from the circulation and can differentiate into endothelial cells that line blood vessels. ECFCs have a high capacity for proliferation and vessel formation *in vitro* and *in vivo* [37,38].

In 1997 Asahara *et al*. isolated, characterized and assessed *in vivo* function of human endothelial progenitor cells (EPCs) from peripheral blood [39]. This article presented a novel paradigm for neovascularisation by means of postnatal vasculogenesis and inspired a great interest in EPCs. The *in vitro* adherent EPCs expressed endothelial markers KDR, CD34, vWF, eNOS and VE-cadherin. As research on EPCs progressed it became apparent that most of the antigens that were selected as EPC markers can't discriminate EPCs from hematopoietic cells [40]. Cells that co-express the EPC markers with CD45, CD14 or CD115 are from the hematopoietic lineage, have limited proliferation capacity, do not form stable vessels *in vivo*, and are often denoted as early outgrowth or early EPCs. On the other hand, cells that show expression of CD34, CD133 and KDR and that are collectively named late EPCs or ECFCs, have a high proliferative potential, and form long lasting *de novo* vessels *in vivo* [37]. Different methods for harvesting and culturing EPCs are used, leading to appearance of different subtypes of EPCs (Figure 1). Culturing colony forming-Hill cells (CFU-Hill) is a process where non-adherent peripheral blood mononuclear cells (PB-MNCs) give rise to the colony. When the adherent PB-MNCs are cultured, colony circulating angiogenic cells (CAC, monocytes) and endothelial colony forming cells (ECFCs) arise. ECFCs, also termed blood outgrowth endothelial cells (BOECs), can be isolated from umbilical cord blood and peripheral blood, appear between day 7 and 14, with a cobblestone morphology. ECFCs are a well-described cell population that expresses CD31, CD105, CD144, CD146, cWF, KDR and AcLDL, and do not express CD14, CD45 or CD 115. ECFCs display high levels of telomerase [41]. Of all cells described in this paragraph, only ECFCs are able to give rise to endothelial progeny in a clonal fashion, form endothelial tubes with lumens *in vitro*, and form *de novo* vessels *in vivo*, thereby measuring up to the definition of true endothelial progenitor cells [38,40,42,43].

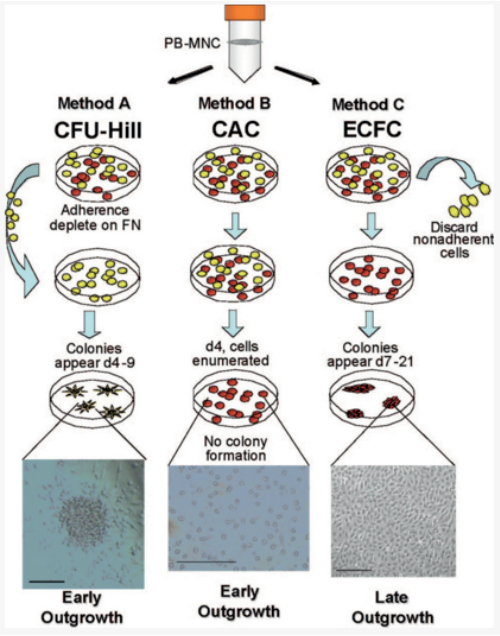

Figure 1. Common methods of EPC culture (from [40]).

II. Scaffold materials for bone tissue engineering

A scaffold is a structure that acts as the mechanical support and/or delivery system of the tissue-engineered construct. Scaffolds can be made from many materials, for example from naturally occurring polymers, synthetic materials or ceramics. Scaffolds may contain cells and/or bioactive factors that can signal cells, stimulating them to proliferate of differentiate. Ideally scaffold materials are biodegradable, and degrade at a rate that allows ingrowth of newly formed tissue, to maintain balance in mechanical stability [44].

The demands on the scaffold properties, such as biocompatibility, biodegradability, mechanical stability, and biological behavior of the construct determine the choice of the material. Scaffold properties can be further tailored by introduction of porosity and addition of functional groups. Porosity was conventionally introduced by molding, salt leaching, gas bubbling or freeze-drying applications, but recently 3D printing technology has enabled precise, predefined scaffold production with specific architecture [45]. 3D printing for production of bone substitute scaffolds will be introduced further in the section 'enabling technologies'.

Hydrogel scaffolds

Hydrogels are increasingly applied in regenerative medicine, as they can provide cells an aqueous environment leading to their unique biocompatibility and biodegradability [46]. They can be tailored into various shapes and sizes and functional groups can be incor-

porated to introduce desirable physical characteristics [47,48]. Hydrogels can be employed as scaffold materials that present signals to guide cellular processes and release proteins or drugs in a sustained fashion [49].

The performance of hydrogels as scaffold materials can be improved by introducing porosity, which lowers the diffusion distance of oxygen and other nutrients to the center of the construct [50]. By applying the 3D printing technology, desired porosity of hydrogel-based constructs is easily achieved [51].

Printable hydrogels need to allow the translation of computer designs to scaffold constructs, which requires a high degree of control over the gel deposition process. This degree of control remains a challenge, since stiffer gels are usually less suitable for cell culturing purposes [52]. The hydrogels that were applied for the experiments described throughout this thesis, were chosen based on cytocompatibility and suitable viscoelastic properties for 3D printing. These include the natural hydrogels alginate, Matrigel, hyaluronic acid and gelatin and their modified photosensitive counterparts and will be further introduced.

Alginate

Alginate is an non-toxic, biocompatible, FDA-approved anionic polysaccharide polymer, which gelates by addition of divalent cations such as Ca^{2+}, forming reversible ionic bridges between the polymer chains [53]. Alginate is very suitable as a material for 3D printing because it is a viscous, cell-friendly and rapidly crosslinkable hydrogel in which bone formation has been previously reported [54-56].

Matrigel

Matrigel is a gelatinous protein mixture secreted by Engelbreth-Holm-Swarm (EHS) mouse sarcoma cells. The main components of Matrigel are laminin, entactin, and collagen, which closely resemble the cultured cells' natural environment or niche [57]. It also contains growth factors that promote differentiation and proliferation of various cell types. The exact composition of Matrigel is subject to batch differences, and in order to use this hydrogel in 3D printing, mixing it with other hydrogels that have more rapid crosslinking capacities is advantageous.

Hyaluronic acid

Hyaluronic acid is an anionic, nonsulfated glycosaminoglycan that is present in connective, epithelial, and neural tissues. As one of the main components of the extracellular matrix, it is highly biocompatible and contributes significantly to cell proliferation and migration [58]. To enable 3D printing and hydrogel crosslinking, the viscosity of hyaluronic acid based hydrogels can be increased by addition of methacrylate groups that are UV-crosslinkable [59].

Ceramic scaffolds

The hydrogels in this thesis were in some studies supplemented with ceramics, in order to better mimic a bone environment for the cells. Naturally occurring as well as synthetically made calcium phosphate based biomaterials have been commonly applied as bone substitutes in orthopedic surgery, in the form of ceramics, powders or cements [60]. Calcium phosphate ceramics are acquired by heating non-metallic mineral salts at temperatures higher than 700°C, resulting in highly crystalline structures, a process known as sintering [61,62]. Ceramics very closely resemble the inorganic components of bone, and therefore their biocompatibility is high. Biphasic calcium phosphate (BCP) gives scaffolds mechanical support, it provides an osteoconductive environment for osteoblasts and the material can be resorbed and remodeled by osteoclasts. In our experiments a specific BCP that was sintered at 1150°C has been applied in granules, as this particular BCP even showed osteoinductivity *in vivo* [63,64]. The BCP granules were small enough to fit through the hydrogel deposition needle and were incorporated into 3D printed hydrogel scaffolds [65], or applied in the form of porous cylinders. The porous cylinders could be filled with growth factor containing hydrogels, by casting them into the BCP pores.

III. Bioactive Factors for bone tissue engineering

Growth factors are naturally occurring substances, usually proteins or steroid hormones that can stimulate cell proliferation and differentiation [66]. They regulate cellular functions by acting as signaling molecules, binding on transmembrane receptors, between cells [67]. In development they regulate tissue morphogenesis, angiogenesis and neurite outgrowth; in adults they play an important role in tissue homeostasis and tissue healing [68]. In the following paragraphs, the growth factors that are most promising for bone tissue engineering applications and that have been used for the work described in the current thesis are introduced, namely bone morphogenetic protein 2 (BMP-2) a strong osteoinductive stimulant, vascular endothelial growth factor (VEGF), which is an important factor for angiogenesis and vasculogenesis, and stromal cell derived factor 1α (SDF1α), a chemokine that is known to attract endogenous cells.

Bone morphogenetic protein (BMP-2)

In 1965 Marshall Urist, MD, identified a compound embedded in bone matrix with high osteoinductive capacity (both *in vitro* and *in vivo*), later named bone morphogenetic protein. It took several decades before growth factors could be manufactured in sufficient quantities. BMP-2 is one of the commercially available products. It stimulates MSCs towards osteogenic differentiation[69] and has been approved in the clinic for spinal fusion surgery and tibial nonunion [70]. Studies have shown that clinically applied BMP-2 products release the protein with a large initial burst [71]. The dosage that is used is much higher than the effective dose in order to compensate for the short half life time and

rapid degradation of the protein [72]. The use of BMP-2 in spinal fusion is associated with an increased risk of adverse events, such as ectopic bone formation, tissue swelling, infection and osteolysis. An increased risk of malignancies is also suspected for products applying the highest concentration [70,73].

In uncomplicated fracture healing, the BMP-2 gene is upregulated during the first four weeks after fracture [74]. This supports application of a more sustained release of the BMP-2 protein at physiological dosage or application of plasmid DNA encoding BMP-2 [75-77], as alternative and effective strategies in enhancing osteogenic differentiation and bone formation while reducing the risk of side effects and complications [78,79]. In this thesis BMP-2 in either form was applied as a stimulus for osteogenic differentiation and bone formation*, in vitro* and *in vivo*.

Vascular endothelial growth factor (VEGF)

A potent growth factor that can induce angiogenesis and vasculogenesis is VEGF [80]. VEGF is a heparin-binding, homodimeric glycoprotein, that prevents apoptosis of endothelial cells during embryogenesis [81]. The close relationship between osteogenesis and angiogenesis is underlined by the necessity of VEGF for early bone development [82], the upregulation of BMP-2 in endothelial cells when VEGF is supplemented, or hypoxia is induced [83], and by the finding that osteoblasts are able to produce VEGF under hypoxic circumstances [84,85]. Several publications reported on a synergistic effect of the combined application of BMP-2 and VEGF, leading to increased bone formation [86,87]. These promising reports led to the application of VEGF in our scaffolds, *in vitro* and *in vivo*.

Stromal cell-derived factor 1α (SDF-1α)

SDF-1α is a chemokine, that is strongly chemotactic for MSCs, lymphocytes and dendritic cells, acting via the CXCR4 receptor pathway [88-90]. During embryogenesis, the presence of SDF-1α results in migration of hematopoietic cells from the fetal liver to the bone marrow [91]. In adulthood, the chemokine can recruit EPCs, that are important for vascularization [88,92]. This finding implicates that addition of SDF-1α to tissue engineered constructs could result in recruitment of endogenous cells [93], hereby possibly eliminating the need for cell seeding in these scaffolds. When SDF-1α is applied in combination with BMP-2, a positive (possibly synergistic) effect on bone formation has been reported in literature, by recruiting more MSCs towards the osteogenic stimulus, hereby increasing its effect [94-96]. These promising observations were investigated in this thesis.

ENABLING TECHNOLOGIES

The vast progress that was made in the field of regenerative medicine in the past decades was partially provided by and development of novel enabling technologies such as controlled growth factor release and 3D bioprinting. Since these two techniques have been applied throughout this thesis, they will be introduced further in the following paragraphs.

Prolonged growth factor release via gelatin microparticles (GMPs)

The growth factors described here have in common that they are all quickly degraded in the bloodstream. BMP-2 [74], VEGF [97] and SDF-1α [98] have half life times of less than an hour. In order to accomplish prolonged presence of these factors at a desired location, controlled release vehicles can be applied. Gelatin microparticles (GMPs) are particularly suitable to deliver growth factors since growth factor is loaded onto them by simple diffusion. No potentially damaging chemical reactions are necessary to incorporate these fragile proteins, which are an issue in many other controlled release vehicles that are described in literature [99]. Gelatin is a natural product that is biocompatible and biodegradable. GMPs have been used dispersed in hydrogels, and as isolated particles to deliver a variety of growth factors [100,101]. GMPs were incorporated into 3D printed constructs in this thesis in order to establish a controlled release profile at a certain location, at a certain time, which control over scaffold properties in a more precise manner.

3D printing

Until recently, tissue-engineered construct mainly consisted of randomly distributed cells and growth factors within scaffolds. 3D bioprinting allows smart scaffold design, and mimicking native tissue complexity. This biomimicry is regarded as the next big step in tissue engineering, led by the hypothesis that increased resemblance of the native extracellular matrix will lead to improved cell and scaffold function [102-105].

3D bioprinting can contribute to this approach as computer made designs can be translated into scaffolds with a controlled spatial distribution of material, cells and growth factors [106]. Construct properties can be easily and reproducibly tuned in terms of porosity, size and shape.

Each scaffold material comes with its own possibility and limitations for 3D printing. For example, thermoplastic polymers are very suitable to 3D print complex architectures with, but they cannot contain any viable cells at the moment of deposition because of too high temperatures during the printing process. Cells can only be added to these scaffolds by post-seeding, a method far less accurate and controllable. Hydrogel scaffolds can contain cells and bioactive factors at the moment of deposition, so strands with specific contents that can be incorporated at specific scaffold sites, but scaffold

architecture can not be accomplished at the same spatial resolution as is possible with thermoplasts.

Although the 3D bioprinting technique is very promising, and encouraging results have been seen so far [103], challenges remain in the search for an optimal scaffold material [104]. Many requirements must be met in order to create a successful 3D printed scaffold material. The material must be of a fitting viscosity, and must be rapidly polymerizable in order to succeed in layer-by-layer deposition. Furthermore, cytocompatibility is essential to allow cell proliferation, differentiation and ingrowth [107]. The main reason for focusing on hydrogels as scaffold materials in this thesis is their excellent biocompatibility that allows cell inclusion prior to material deposition with the 3D printer.

RESEARCH AIMS AND QUESTIONS TO BE ADRESSED IN THIS

The overall aim of this thesis was to improve scaffold architecture and functionality for tissue engineering of bone compared to existing alternatives. First the beneficial effect of prolonged growth factor availability was investigated. Second, the influence of growth factor locations within the scaffolds was subject of investigation. Third the effects of combined application of growth factors were investigated.

Aim 1: To investigate the effect of prolonged growth factor availability in tissue engineered constructs. Specific questions are:

A. Does prolonged release of BMP-2 using GMPs lead to more osteogenic differentiation *in vitro* and bone formation *in vivo* compared to rapid growth factor release?

B. Does prolonged release of VEGF using GMPs lead to more vessel formation *in vivo* compared to rapid growth factor release?

Aim 2: To investigate the effect of growth factor location within tissue engineered constructs. Specific questions are:

A. Does regional application of BMP-2 lead to regional osteogenic differentiation *in vitro* and bone formation *in vivo*?

B. Does regional application of VEGF lead to regional vessel formation *in vivo*?

Aim 3: To investigate the (synergistic) effects of combined growth factors application within tissue engineered constructs. Specific questions are:

A. Does the combined addition of VEGF and/or SDF1 to BMP-2 laden constructs lead to enhanced bone formation *in vivo* compared to single addition of BMP-2?

B. Can synergistic effects of combined growth factor application be investigated in a novel, radiolucent bone chamber animal model?

OUTLINE OF THIS THESIS

In **chapter 2** sustained release of BMP-2 from GMPs was applied and tested in two animal models, in order to investigate specific questions 1A and 2A. MSC-laden, alginate scaffolds that contained BCP particles were first implanted subcutaneously in mice and analyzed for osteogenic differentiation *in vivo*. Secondly, BMP-2 from GMPs was applied in cell-free porous ceramic cylinders that were implanted subcutaneously in rats. Additionally, local application of BMP-2 laden GMPs was tested in regions of 3D printed constructs.

In **chapter 3** research aims 1 and 2 were further addressed by application of sustained release of a second growth factor, VEGF, from GMPs. This was tested in Matrigel plugs that contained hEPCs in an ectopic immuno-deficient mouse model. Then alginate was added to Matrigel to allow 3D printing, and regional application of VEGF was investigated.

In **chapter 4** research aims 1 and 3 were addressed in order to investigate endogenous MSC attraction by SDF1α and subsequent transfection with BMP-2, attempting to amplify the effect of the BMP-2 plasmid DNA. Synergy of the two growth factors was investigated by application of the sustained release of SDF1α from GMPs (aim 1) combined with application of BMP-2-encoding plasmid DNA (aim 3) in cell-seeded (gMSC) as well as cell-free constructs.

In **Chapter 5** research aim 3 was addressed, describing the design, application and efficacy of a novel, radiolucent bone chamber. This is an adapted tool for preclinical studies, in which biomaterials and growth factors can be tested at an orthotopic location. The possible synergy of the different growth factors that were used separately in the previous chapters was investigated in orthotopic and ectopic locations.

Chapters 6 focuses on addition of methacrylate groups to hydrogels in order to improve 3D printability. Better printing properties allow more in depth investigation of regional application of growth factors, as is described in our second aim. The methacrylated hydrogels were tested to investigate gel characteristics, biocompatibility and biodegradability. Also, the possibility of cell differentiation within these gels was subject of investigation.

The possible synergy of the different growth factors that were used separately in the previous chapters was investigated in orthotopic and ectopic locations in **Chapter 7**. Analysis of bone formation was performed classically using histomorphometry, the results were compared to μCT acquired data.

REFERENCE LIST

1. Desai BM. Osteobiologics. *Am J Orthop (Belle Mead NJ) 2007;36-4 Suppl:8-11*.
2. Giannoudis PV, Dinopoulos H, Tsiridis E. Bone substitutes: an update. *Injury 2005;36 Suppl 3:S20-7*.
3. Meek'ren jv. *Heel en geneeskonstige aanmerkingen*. Vol. Amsterdam, 1668.
4. de Boer HH. The history of bone grafts. *Clin Orthop Relat Res 1988-226:292-8*.
5. Donati D, Zolezzi C, Tomba P, Vigano A. Bone grafting: historical and conceptual review, starting with an old manuscript by Vittorio Putti. *Acta Orthop 2007;78-1:19-25*.
6. Seiler JG, 3rd, Johnson J. Iliac crest autogenous bone grafting: donor site complications. *J South Orthop Assoc 2000;9-2:91-7*.
7. Silber JS, Anderson DG, Daffner SD, Brislin BT, Leland JM, Hilibrand AS, Vaccaro AR, Albert TJ. Donor site morbidity after anterior iliac crest bone harvest for single-level anterior cervical discectomy and fusion. *Spine (Phila Pa 1976) 2003;28-2:134-9*.
8. Delawi D, Dhert WJ, Castelein RM, Verbout AJ, Oner FC. The incidence of donor site pain after bone graft harvesting from the posterior iliac crest may be overestimated: a study on spine fracture patients. *Spine (Phila Pa 1976) 2007;32-17:1865-8*.
9. Dreesman H. Uber Knochenplombierung. *Beitr Klin Chir 1894;9-804:804-10*.
10. Fujibayashi S, Neo M, Kim HM, Kokubo T, Nakamura T. Osteoinduction of porous bioactive titanium metal. *Biomaterials 2004;25-3:443-50*.
11. Rahaman MN, Day DE, Bal BS, Fu Q, Jung SB, Bonewald LF, Tomsia AP. Bioactive glass in tissue engineering. *Acta Biomater 2011;7-6:2355-73*.
12. Tuzlakoglu K, Reis RL. Biodegradable polymeric fiber structures in tissue engineering. *Tissue Eng Part B Rev 2009;15-1:17-27*.
13. Van der Stok J, Van Lieshout EM, El-Massoudi Y, Van Kralingen GH, Patka P. Bone substitutes in the Netherlands - a systematic literature review. *Acta Biomater 2011;7-2:739-50*.
14. Burg KJ, Porter S, Kellam JF. Biomaterial developments for bone tissue engineering. *Biomaterials 2000;21-23:2347-59*.
15. Habibovic P, de Groot K. Osteoinductive biomaterials--properties and relevance in bone repair. *J Tissue Eng Regen Med 2007;1-1:25-32*.
16. Langer R, Vacanti JP. Tissue engineering. *Science 1993;260-5110:920-6*.
17. Williams DF. On the nature of biomaterials. *Biomaterials 2009;30-30:5897-909*.
18. Geuze RE, Everts PA, Kruyt MC, Verbout AJ, Alblas J, Dhert WJ. Orthotopic location has limited benefit from allogeneic or autologous multipotent stromal cells seeded on ceramic scaffolds. *Tissue Eng Part A 2009;15-11:3231-9*.
19. Levenberg S, Rouwkema J, Macdonald M, Garfein ES, Kohane DS, Darland DC, Marini R, van Blitterswijk CA, Mulligan RC, D'Amore PA, Langer R. Engineering vascularized skeletal muscle tissue. *Nat Biotechnol 2005;23-7:879-84*.
20. Novosel EC, Kleinhans C, Kluger PJ. Vascularization is the key challenge in tissue engineering. *Adv Drug Deliv Rev 2011;63-4-5:300-11*.
21. Friedenstein AJ, Piatetzky S, II, Petrakova KV. Osteogenesis in transplants of bone marrow cells. *J Embryol Exp Morphol 1966;16-3:381-90*.
22. Caplan AI. Mesenchymal stem cells. *J Orthop Res 1991;9-5:641-50*.
23. Dominici M, Le Blanc K, Mueller I, Slaper-Cortenbach I, Marini F, Krause D, Deans R, Keating A, Prockop D, Horwitz E. Minimal criteria for defining multipotent mesenchymal stromal cells. The International Society for Cellular Therapy position statement. *Cytotherapy 2006;8-4:315-7*.

24. Zuk PA, Zhu M, Ashjian P, De Ugarte DA, Huang JI, Mizuno H, Alfonso ZC, Fraser JK, Benhaim P, Hedrick MH. Human adipose tissue is a source of multipotent stem cells. *Mol Biol Cell 2002;13-12: 4279-95*.
25. Shih DT, Lee DC, Chen SC, Tsai RY, Huang CT, Tsai CC, Shen EY, Chiu WT. Isolation and characterization of neurogenic mesenchymal stem cells in human scalp tissue. *Stem Cells 2005;23-7:1012-20*.
26. Sarugaser R, Lickorish D, Baksh D, Hosseini MM, Davies JE. Human umbilical cord perivascular (HUCPV) cells: a source of mesenchymal progenitors. *Stem Cells 2005;23-2:220-9*.
27. In 't Anker PS, Scherjon SA, Kleijburg-van der Keur C, de Groot-Swings GM, Claas FH, Fibbe WE, Kanhai HH. Isolation of mesenchymal stem cells of fetal or maternal origin from human placenta. *Stem Cells 2004;22-7:1338-45*.
28. Erices A, Conget P, Minguell JJ. Mesenchymal progenitor cells in human umbilical cord blood. *Br J Haematol 2000;109-1:235-42*.
29. Gronthos S, Brahim J, Li W, Fisher LW, Cherman N, Boyde A, DenBesten P, Robey PG, Shi S. Stem cell properties of human dental pulp stem cells. *J Dent Res 2002;81-8:531-5*.
30. Patki S, Kadam S, Chandra V, Bhonde R. Human breast milk is a rich source of multipotent mesenchymal stem cells. *Hum Cell 2010;23-2:35-40*.
31. Keating A. Mesenchymal stromal cells: new directions. *Cell Stem Cell 2012;10-6:709-16*.
32. Horwitz EM, Le Blanc K, Dominici M, Mueller I, Slaper-Cortenbach I, Marini FC, Deans RJ, Krause DS, Keating A. Clarification of the nomenclature for MSC: The International Society for Cellular Therapy position statement. *Cytotherapy 2005;7-5:393-5*.
33. Yoon E, Dhar S, Chun DE, Gharibjanian NA, Evans GR. In vivo osteogenic potential of human adipose-derived stem cells/poly lactide-co-glycolic acid constructs for bone regeneration in a rat critical-sized calvarial defect model. *Tissue Eng 2007;13-3:619-27*.
34. Klyushnenkova E, Mosca JD, Zernetkina V, Majumdar MK, Beggs KJ, Simonetti DW, Deans RJ, McIntosh KR. T cell responses to allogeneic human mesenchymal stem cells: immunogenicity, tolerance, and suppression. *J Biomed Sci 2005;12-1:47-57*.
35. Fong EL, Chan CK, Goodman SB. Stem cell homing in musculoskeletal injury. *Biomaterials 2011; 32-2:395-409*.
36. Gerber HP, Vu TH, Ryan AM, Kowalski J, Werb Z, Ferrara N. VEGF couples hypertrophic cartilage remodeling, ossification and angiogenesis during endochondral bone formation. *Nat Med 1999; 5-6:623-8*.
37. Yoder MC, Mead LE, Prater D, Krier TR, Mroueh KN, Li F, Krasich R, Temm CJ, Prchal JT, Ingram DA. Redefining endothelial progenitor cells via clonal analysis and hematopoietic stem/progenitor cell principals. *Blood 2007;109-5:1801-9*.
38. Critser PJ, Yoder MC. Endothelial Colony Forming Cell role in neoangiogenesis and tissue repair. *Curr Opin Organ Transplant 2010;15-1:68-72*.
39. Asahara T, Murohara T, Sullivan A, Silver M, van der Zee R, Li T, Witzenbichler B, Schatteman G, Isner JM. Isolation of putative progenitor endothelial cells for angiogenesis. *Science 1997;275-5302:964-7*.
40. Hirschi KK, Ingram DA, Yoder MC. Assessing identity, phenotype, and fate of endothelial progenitor cells. *Arterioscler Thromb Vasc Biol 2008;28-9:1584-95*.
41. Ingram DA, Mead LE, Tanaka H, Meade V, Fenoglio A, Mortell K, Pollok K, Ferkowicz MJ, Gilley D, Yoder MC. Identification of a novel hierarchy of endothelial progenitor cells using human peripheral and umbilical cord blood. *Blood 2004;104-9:2752-60*.
42. Ingram DA, Caplice NM, Yoder MC. Unresolved questions, changing definitions, and novel paradigms for defining endothelial progenitor cells. *Blood 2005;106-5:1525-31*.

43. Gremmels H, Fledderus JO, van Balkom BW, Verhaar MC. Transcriptome analysis in endothelial progenitor cell biology. *Antioxid Redox Signal 2011;15-4:1029-42.*
44. Hutmacher DW. Scaffolds in tissue engineering bone and cartilage. *Biomaterials 2000;21-24: 2529-43.*
45. Hollister SJ. Porous scaffold design for tissue engineering. *Nat Mater 2005;4-7:518-24.*
46. Slaughter BV, Khurshid SS, Fisher OZ, Khademhosseini A, Peppas NA. Hydrogels in regenerative medicine. *Adv Mater 2009;21-32-33:3307-29.*
47. Vermonden T, Fedorovich NE, van Geemen D, Alblas J, van Nostrum CF, Dhert WJ, Hennink WE. Photopolymerized thermosensitive hydrogels: synthesis, degradation, and cytocompatibility. *Biomacromolecules 2008;9-3:919-26.*
48. Bulpitt P, Aeschlimann D. New strategy for chemical modification of hyaluronic acid: preparation of functionalized derivatives and their use in the formation of novel biocompatible hydrogels. *J Biomed Mater Res 1999;47-2:152-69.*
49. Benoit DS, Schwartz MP, Durney AR, Anseth KS. Small functional groups for controlled differentiation of hydrogel-encapsulated human mesenchymal stem cells. *Nat Mater 2008;7-10:816-23.*
50. Karageorgiou V, Kaplan D. Porosity of 3D biomaterial scaffolds and osteogenesis. *Biomaterials 2005;26-27:5474-91.*
51. Fedorovich NE, Kuipers E, Gawlitta D, Dhert WJ, Alblas J. Scaffold Porosity and Oxygenation of Printed Hydrogel Constructs Affect Functionality of Embedded Osteogenic Progenitors. *Tissue Eng Part A 2011.*
52. Nicodemus GD, Bryant SJ. Cell encapsulation in biodegradable hydrogels for tissue engineering applications. *Tissue Eng Part B Rev 2008;14-2:149-65.*
53. Drury JL, Mooney DJ. Hydrogels for tissue engineering: scaffold design variables and applications. *Biomaterials 2003;24-24:4337-51.*
54. Stevens MM, Marini RP, Schaefer D, Aronson J, Langer R, Shastri VP. In vivo engineering of organs: the bone bioreactor. *Proc Natl Acad Sci U S A 2005;102-32:11450-5.*
55. Augst AD, Kong HJ, Mooney DJ. Alginate hydrogels as biomaterials. *Macromol Biosci 2006;6-8: 623-33.*
56. Wang L, Shelton RM, Cooper PR, Lawson M, Triffitt JT, Barralet JE. Evaluation of sodium alginate for bone marrow cell tissue engineering. *Biomaterials 2003;24-20:3475-81.*
57. Kleinman HK, Martin GR. Matrigel: basement membrane matrix with biological activity. *Semin Cancer Biol 2005;15-5:378-86.*
58. Noble PW. Hyaluronan and its catabolic products in tissue injury and repair. *Matrix Biol 2002;21-1: 25-9.*
59. Baier Leach J, Bivens KA, Patrick CW, Jr., Schmidt CE. Photocrosslinked hyaluronic acid hydrogels: natural, biodegradable tissue engineering scaffolds. *Biotechnol Bioeng 2003;82-5:578-89.*
60. De Long WG, Jr., Einhorn TA, Koval K, McKee M, Smith W, Sanders R, Watson T. Bone grafts and bone graft substitutes in orthopaedic trauma surgery. A critical analysis. *J Bone Joint Surg Am 2007;89-3:649-58.*
61. LeGeros RZ, Lin S, Rohanizadeh R, Mijares D, LeGeros JP. Biphasic calcium phosphate bioceramics: preparation, properties and applications. *J Mater Sci Mater Med 2003;14-3:201-9.*
62. Habibovic P, Yuan H, van der Valk CM, Meijer G, van Blitterswijk CA, de Groot K. 3D microenvironment as essential element for osteoinduction by biomaterials. *Biomaterials 2005;26-17:3565-75.*
63. Poldervaart MT, Wang H, van der Stok J, Weinans H, Leeuwenburgh SC, Oner FC, Dhert WJ, Alblas J. Sustained Release of BMP-2 in Bioprinted Alginate for Osteogenicity in Mice and Rats. *PLoS ONE 2013;8-8:e72610.*

64. Yuan H, Fernandes H, Habibovic P, de Boer J, Barradas AM, de Ruiter A, Walsh WR, van Blitterswijk CA, de Bruijn JD. Osteoinductive ceramics as a synthetic alternative to autologous bone grafting. *Proc Natl Acad Sci U S A 2010;107-31:13614-9.*
65. Loozen LW, F; Oner, FC; Dhert, WJA; Alblas, J Porous bioprinted constructs in BMP-2 non-viral gene therapy for bone tissue engineering. *JOURNAL OF MATERIALS CHEMISTRY B 2013;1-48:6619-26.*
66. Kempen DH, Creemers LB, Alblas J, Lu L, Verbout AJ, Yaszemski MJ, Dhert WJ. Growth factor interactions in bone regeneration. *Tissue Eng Part B Rev 2010;16-6:551-66.*
67. Talapatra S, Thompson CB. Growth factor signaling in cell survival: implications for cancer treatment. *J Pharmacol Exp Ther 2001;298-3:873-8.*
68. Fortier LA, Barker JU, Strauss EJ, McCarrel TM, Cole BJ. The role of growth factors in cartilage repair. *Clin Orthop Relat Res 2011;469-10:2706-15.*
69. Rickard DJ, Sullivan TA, Shenker BJ, Leboy PS, Kazhdan I. Induction of rapid osteoblast differentiation in rat bone marrow stromal cell cultures by dexamethasone and BMP-2. *Dev Biol 1994;161-1:218-28.*
70. Garrison KR, Shemilt I, Donell S, Ryder JJ, Mugford M, Harvey I, Song F, Alt V. Bone morphogenetic protein (BMP) for fracture healing in adults. *Cochrane Database Syst Rev 2010-6:CD006950.*
71. Jansen JA, Vehof JW, Ruhe PQ, Kroeze-Deutman H, Kuboki Y, Takita H, Hedberg EL, Mikos AG. Growth factor-loaded scaffolds for bone engineering. *J Control Release 2005;101-1-3:127-36.*
72. Poynton AR, Lane JM. Safety profile for the clinical use of bone morphogenetic proteins in the spine. *Spine (Phila Pa 1976) 2002;27-16 Suppl 1:S40-8.*
73. Simmonds MC, Brown JV, Heirs MK, Higgins JP, Mannion RJ, Rodgers MA, Stewart LA. Safety and effectiveness of recombinant human bone morphogenetic protein-2 for spinal fusion: a meta-analysis of individual-participant data. *Ann Intern Med 2013;158-12:877-89.*
74. Groeneveld EH, Burger EH. Bone morphogenetic proteins in human bone regeneration. *Eur J Endocrinol 2000;142-1:9-21.*
75. Wegman F, Bijenhof A, Schuijff L, Oner FC, Dhert WJ, Alblas J. Osteogenic differentiation as a result of BMP-2 plasmid DNA based gene therapy in vitro and in vivo. *Eur Cell Mater 2011;21:230-42; discussion 42.*
76. Wegman F, Geuze RE, van der Helm YJ, Cumhur Oner F, Dhert WJ, Alblas J. Gene delivery of bone morphogenetic protein-2 plasmid DNA promotes bone formation in a large animal model. *J Tissue Eng Regen Med 2012.*
77. Wegman F, van der Helm Y, Oner FC, Dhert W, Alblas J. BMP-2 plasmid DNA as a substitute for BMP-2 protein in bone tissue engineering. *Tissue Eng Part A 2013.*
78. Yamamoto M, Takahashi Y, Tabata Y. Controlled release by biodegradable hydrogels enhances the ectopic bone formation of bone morphogenetic protein. *Biomaterials 2003;24-24:4375-83.*
79. Cho TJ, Gerstenfeld LC, Einhorn TA. Differential temporal expression of members of the transforming growth factor beta superfamily during murine fracture healing. *J Bone Miner Res 2002;17-3:513-20.*
80. Santos MI, Reis RL. Vascularization in bone tissue engineering: physiology, current strategies, major hurdles and future challenges. *Macromol Biosci 2010;10-1:12-27.*
81. Ferrara N, Gerber HP, LeCouter J. The biology of VEGF and its receptors. *Nat Med 2003;9-6:669-76.*
82. Engsig MT, Chen QJ, Vu TH, Pedersen AC, Therkidsen B, Lund LR, Henriksen K, Lenhard T, Foged NT, Werb Z, Delaisse JM. Matrix metalloproteinase 9 and vascular endothelial growth factor are essential for osteoclast recruitment into developing long bones. *J Cell Biol 2000;151-4:879-89.*

83. Raida M, Heymann AC, Gunther C, Niederwieser D. Role of bone morphogenetic protein 2 in the crosstalk between endothelial progenitor cells and mesenchymal stem cells. *Int J Mol Med 2006; 18-4:735-9*.
84. Akeno N, Czyzyk-Krzeska MF, Gross TS, Clemens TL. Hypoxia induces vascular endothelial growth factor gene transcription in human osteoblast-like cells through the hypoxia-inducible factor-2alpha. *Endocrinology 2001;142-2:959-62*.
85. Deckers MM, van Bezooijen RL, van der Horst G, Hoogendam J, van Der Bent C, Papapoulos SE, Lowik CW. Bone morphogenetic proteins stimulate angiogenesis through osteoblast-derived vascular endothelial growth factor A. *Endocrinology 2002;143-4:1545-53*.
86. Kempen DH, Lu L, Heijink A, Hefferan TE, Creemers LB, Maran A, Yaszemski MJ, Dhert WJ. Effect of local sequential VEGF and BMP-2 delivery on ectopic and orthotopic bone regeneration. *Biomaterials 2009;30-14:2816-25*.
87. Patel ZS, Young S, Tabata Y, Jansen JA, Wong ME, Mikos AG. Dual delivery of an angiogenic and an osteogenic growth factor for bone regeneration in a critical size defect model. *Bone 2008;43-5: 931-40*.
88. Broxmeyer HE. Chemokines in hematopoiesis. *Curr Opin Hematol 2008;15-1:49-58*.
89. Otsuru S, Tamai K, Yamazaki T, Yoshikawa H, Kaneda Y. Circulating bone marrow-derived osteoblast progenitor cells are recruited to the bone-forming site by the CXCR4/stromal cell-derived factor-1 pathway. *Stem Cells 2008;26-1:223-34*.
90. Bleul CC, Fuhlbrigge RC, Casasnovas JM, Aiuti A, Springer TA. A highly efficacious lymphocyte chemoattractant, stromal cell-derived factor 1 (SDF-1). *J Exp Med 1996;184-3:1101-9*.
91. Askari AT, Unzek S, Popovic ZB, Goldman CK, Forudi F, Kiedrowski M, Rovner A, Ellis SG, Thomas JD, DiCorleto PE, Topol EJ, Penn MS. Effect of stromal-cell-derived factor 1 on stem-cell homing and tissue regeneration in ischaemic cardiomyopathy. *Lancet 2003;362-9385:697-703*.
92. Zheng H, Fu G, Dai T, Huang H. Migration of endothelial progenitor cells mediated by stromal cell-derived factor-1alpha/CXCR4 via PI3K/Akt/eNOS signal transduction pathway. *J Cardiovasc Pharmacol 2007;50-3:274-80*.
93. Eman RM, Oner FC, Kruyt MMP, Dhert W, Alblas J. Stromal cell-derived factor-1 stimulates cell recruitment, vascularization and osteogenic differentiation. *Tissue Eng Part A 2013*.
94. Ratanavaraporn J, Furuya H, Kohara H, Tabata Y. Synergistic effects of the dual release of stromal cell-derived factor-1 and bone morphogenetic protein-2 from hydrogels on bone regeneration. *Biomaterials 2011;32-11:2797-811*.
95. Higashino K, Viggeswarapu M, Bargouti M, Liu H, Titus L, Boden SD. Stromal cell-derived factor-1 potentiates bone morphogenetic protein-2 induced bone formation. *Tissue Eng Part A 2011;17-3-4:523-30*.
96. Chim H, Miller E, Gliniak C, Alsberg E. Stromal-cell-derived factor (SDF) 1-alpha in combination with BMP-2 and TGF-beta1 induces site-directed cell homing and osteogenic and chondrogenic differentiation for tissue engineering without the requirement for cell seeding. *Cell Tissue Res 2012;350-1:89-94*.
97. Eppler SM, Combs DL, Henry TD, Lopez JJ, Ellis SG, Yi JH, Annex BH, McCluskey ER, Zioncheck TF. A target-mediated model to describe the pharmacokinetics and hemodynamic effects of recombinant human vascular endothelial growth factor in humans. *Clin Pharmacol Ther 2002;72-1:20-32*.
98. Misra P, Lebeche D, Ly H, Schwarzkopf M, Diaz G, Hajjar RJ, Schecter AD, Frangioni JV. Quantitation of CXCR4 expression in myocardial infarction using 99mTc-labeled SDF-1alpha. *J Nucl Med 2008; 49-6:963-9*.

99. Danhier F, Ansorena E, Silva JM, Coco R, Le Breton A, Preat V. PLGA-based nanoparticles: an overview of biomedical applications. *J Control Release 2012;161-2:505-22.*
100. Ogawa T, Akazawa T, Tabata Y. In vitro proliferation and chondrogenic differentiation of rat bone marrow stem cells cultured with gelatin hydrogel microspheres for TGF-beta1 release. *J Biomater Sci Polym Ed 2010;21-5:609-21.*
101. Habraken WJ, Boerman OC, Wolke JG, Mikos AG, Jansen JA. In vitro growth factor release from injectable calcium phosphate cements containing gelatin microspheres. *J Biomed Mater Res A 2009;91-2:614-22.*
102. Shin H, Jo S, Mikos AG. Biomimetic materials for tissue engineering. *Biomaterials 2003;24-24: 4353-64.*
103. Fedorovich NE, Alblas J, Hennink WE, Oner FC, Dhert WJ. Organ printing: the future of bone regeneration? *Trends Biotechnol 2011.*
104. Malda J, Visser J, Melchels FP, Jungst T, Hennink WE, Dhert WJ, Groll J, Hutmacher DW. 25th anniversary article: Engineering hydrogels for biofabrication. *Adv Mater 2013;25-36:5011-28.*
105. Schuurman W, Khristov V, Pot MW, van Weeren PR, Dhert WJ, Malda J. Bioprinting of hybrid tissue constructs with tailorable mechanical properties. *Biofabrication 2011;3-2:021001.*
106. Fedorovich NE, Wijnberg HM, Dhert WJ, Alblas J. Distinct tissue formation by heterogeneous printing of osteo- and endothelial progenitor cells. *Tissue Eng Part A 2011;17-15-16:2113-21.*
107. Williams DF. On the mechanisms of biocompatibility. *Biomaterials 2008;29-20:2941-53.*

CHAPTER 2

Sustained release of BMP-2 in bioprinted alginate for osteogenicity in mice and rats

Michelle Poldervaart
Huanan Wang
Johan van der Stok
Harrie Weinans
Sander Leeuwenburgh
Cumhur Öner
Wouter Dhert
Jacqueline Alblas

PLoS One
2013 Aug 19;8(8):e72610

ABSTRACT

The design of bioactive three-dimensional (3D) scaffolds is a major focus in bone tissue engineering. Incorporation of growth factors into bioprinted scaffolds offers many new possibilities regarding both biological and architectural properties of the scaffolds. This study investigates whether the sustained release of bone morphogenetic protein 2 (BMP-2) influences osteogenicity of tissue engineered bioprinted constructs. BMP-2 loaded on gelatin microparticles (GMPs) was used as a sustained release system, which was dispersed in hydrogel-based constructs and compared to direct inclusion of BMP-2 in alginate or control GMPs. The constructs were supplemented with goat multipotent stromal cells (gMSCs) and biphasic calcium phosphate to study osteogenic differentiation and bone formation respectively. BMP-2 release kinetics and bioactivity showed continuous release for three weeks coinciding with osteogenicity. Osteogenic differentiation and bone formation of bioprinted GMP containing constructs were investigated after subcutaneous implantation in mice or rats. BMP-2 significantly increased bone formation, which was not influenced by the release timing. We showed that 3D printing of controlled release particles is feasible and that the released BMP-2 directs osteogenic differentiation *in vitro* and *in vivo*.

INTRODUCTION

For the treatment of large bone defects currently auto- or allograft bone grafts are being used. Both graft types have drawbacks such as limited availability of donor tissue, donor site morbidity (autograft) or inferior performance (allograft) [1,2]. Tissue engineered bone constructs could ideally reduce the need for donor bone; this is an important pillar in the field of regenerative medicine. Within these constructs signaling molecules such as growth factors are used to induce cellular growth, proliferation and differentiation [3,4].

BMP-2 is a potent osteoinductive growth factor (both *in vitro* and *in vivo*) that belongs to the transforming growth factor-β (TGF-β) protein superfamily. BMP-2 stimulates MSCs towards osteogenic differentiation [5] and has been used in the clinic for spinal fusion surgery and tibial fracture healing [6]. Protein delivery via a collagen sponge results in a BMP-2 presence of up to 8 days locally [7], resulting from a half-life of only 7-16 minutes systemically, due to fast degradation by proteinases [8]. Studies have shown that BMP-2 containing products that are used in the clinic release the protein with a large initial burst [9]. The dosage used in these clinical applications is much higher than the effective dose in order to compensate for the fast wash-out of the protein. The use of BMP-2 in spinal fusion is associated with an increased risk of bone overgrowth, problems due to exposed dura/nerves and osteolysis. An increased risk of malignancies is suspected for products applying the highest concentration [6,10]. In uncomplicated fracture healing, the gene coding for BMP-2 is upregulated for about four weeks after fracture, which supports the approach to strive for a more sustained release of the BMP-2 protein at lower dosage, as an alternative and effective strategy in enhancing osteogenic differentiation and bone formation while reducing the risk of side effects and complications [11-13]. To accomplish such a gradual and sustained release many controlled release vehicles have been described in literature; gelatin microparticles (GMPs) are particularly promising because growth factors can be incorporated into these microspheres by simple post-loading, thereby avoiding chemical reactions that can damage the activity of fragile proteins such as BMP-2. The post-loading strategy is facilitated by the formation of poly-ion complexes between charged amino acid residues present in both growth factors and gelatin macromolecules. In addition, GMPs are non-cytotoxic, biodegradable and have already been used in numerous formulations as isolated particles or incorporated as dispersed phase into hydrogels to deliver BMP-2 and other growth factors such as TGF-β1 and bFGF [14,15].

The performance of hydrogels as scaffold materials can be improved by introducing porosity, which lowers the diffusion distance of oxygen and other nutrients to the center of the construct [16]. By applying the bioprinting technology, porosity of hydrogel-based constructs is easily achieved. In addition, the technique of 3D fiber deposition enables production of scaffolds with a defined architecture and regional differences by computer

controlled deposition of the cell- and growth factor laden hydrogel [17]. A well-known hydrogel is alginate, an non-toxic biocompatible anionic polysaccharide polymer, which gelates by addition of divalent cations such as Ca^{2+}, forming reversible ionic bridges between the polymer chains [18]. Alginate is very suitable as a material for 3D printing because it is a viscous, cell-friendly and rapidly crosslinkable hydrogel in which bone formation has been previously reported [19-21].

The present study combined controlled growth factor release with bioprinting technology to enable production of hydrogel scaffolds with properties that can be tuned both in time and space. This study describes bioprinting of hydrogel scaffolds in which controlled release particles containing BMP-2 are included. We investigated whether prolonged BMP-2 presence in scaffolds promotes osteogenic differentiation and bone formation compared to fast growth factor release. Osteogenic differentiation and bone formation in the composite hydrogel scaffolds were observed *in vitro* and *in vivo,* respectively.

MATERIALS AND METHODS

Experimental design

Three experimental groups are investigated in consecutive experimental settings throughout the paper, namely: 1. Control group with empty gelatin microparticles (GMPs) (i.e. PBS-laden), 2. Fast release group with empty GMPs and BMP-2 added directly to the hydrogel, 3. Slow release group with BMP-2-loaded GMPs, dispersed in the hydrogel (Table 1). BMP-2 concentrations were adjusted to the calculated effective dose per experimental setup, based on literature [22-24].

In vitro we investigated release kinetics and bioactivity of BMP-2 from GMPs. Osteogenic differentiation was monitored in bioprinted, cell-laden alginate constructs *in*

Table 1. Experimental groups.

Model	Group	GMPs	[BMP-2]	Method	Hydrogel	Ceramic	Cells
In vitro	1. Control	PBS laden	None	Bioprinted	Alginate	None	gMSCs
	2. Fast	PBS laden	25 ng/ml				
	3. Slow	BMP-2 laden	25 ng/ml				
Mouse	1. Control	PBS laden	None	Bioprinted	Alginate	Granules	gMSCs
	2. Fast	PBS laden	250 ng/ml			106-212 µm	
	3. Slow	BMP-2 laden	250 ng/ml				
Rat	1. Control	PBS laden	None	Cast	Matrigel	Cylinder	None
	2. Fast	PBS laden	100 µg/ml			7mm ∅	
	3. Slow	BMP-2 laden	100 µg/ml			3mm height	

vitro and *in vivo*, after subcutaneous implantation in mice, using flow cytometry and immunohistochemistry. All investigative groups were subsequently combined with ceramic cylinders and implanted subcutaneously in rats to study bone formation using histomorphometry.

Production of gelatin microparticles (GMPs)

We adapted the protocol previously described by Tabata et al. [25,26]. A water in oil emulsion was made using water dissolved gelatin type B (Sigma, St Louis, MO, USA) 10% (w/v) that was added drop wise to refined olive oil (Arcos Organics, NJ, USA) at 60° Celsius. The solution was stirred (350 rpm) for 15 minutes and then rapidly cooled with an ice bath to induce gelation of gelatin droplets. The microparticles were washed with 150 ml of chilled acetone and filtered under pressure (filter paper grade 2, Whatman, Tokyo, Japan). The microparticles were sieved and covalently cross-linked overnight using a 10.6 mM aqueous glutaraldehyde solution (Merck, Darmstadt, Germany) [27,28]. Three washing steps with 100 mM glycine solution (Sigma, St Louis, MO, USA) were applied to remove residual aldehyde groups. Subsequently, the microparticles were washed in deionized water (MilliQ) three times, freeze-dried overnight and kept at 4°C in a vacuum container until use. The microparticles were loaded with the dissolved growth factor by diffusional loading.

Radiolabeling of BMP-2

Human recombinant BMP-2 (InductOS, Wyeth/Pfizer, New York, NY, USA) was labeled with ^{125}I according to the iodogen method [29]. Seventy-five µl of a 0.337 mg/ml BMP-2 solution was pipetted into a 100 µg iodogen coated tube containing 10 µl ^{125}I (radioactivity=1000mCi, Perkin-Elmer, Boston, MA, USA). A 0.5 M phosphate buffer solution with a pH of 7.0 was added to a total volume of 100 µl. This was incubated for 10 minutes at room temperature, then 100 µl of saturated tyrosine solution in PBS was added to react with unbound ^{125}I in the solution. The reaction mixture was filtered over Sephadex G25M column (PD-10, Pharmacia, Uppsala, Sweden) and eluted with 1 mM NaCl with 0.5% BSA (pH 7.0). The fraction with the highest radioactivity was used for the release study. The resulting ^{125}I-BMP-2 solution was diluted to a concentration of 12 µg/ml for further use.

In vitro release of BMP-2 measured by radiolabeling

Microspheres were loaded with ^{125}I-BMP-2 by diffusional loading. 25 µl of a 12 µg/ml ^{125}I-BMP-2 solution was placed on 5 mg microspheres (n=4) and kept at 4°C overnight to allow complete growth factor absorption. These samples, each containing 300 ng ^{125}I-BMP-2, were put in PBS with 400 ng/ml bacterial collagenase type 1A (Sigma, St Louis, MO, USA) and 0.001% (w/v) sodium azide (Wako, Kyoto, Japan) as the release medium.

The release medium was refreshed at multiple time points after centrifuging for 5 minutes at 10,000 rpm to spin down the particles. Release was determined by measuring the residual γ-irradiation in the supernatant using a shielded γ-counter (Wizard, Pharmacia-LKB, Uppsala, Sweden) and corrected for radioactive decay.

In vitro release of BMP-2 measured by ELISA

Microspheres (25 mg) were loaded with 10 µg/ml BMP-2 in PBS /0.5% BSA by diffusional loading overnight at 4°C. Samples were placed into the top compartments of a Transwell system (0.4 µm pores, Corning Sigma, St Louis, MO, USA). The release medium (PBS /0.5% BSA) in the lower compartment was refreshed at multiple time points. Release was determined by measuring the amount of BMP-2 in the release medium samples in duplicate by ELISA (R&D, Minneapolis, MN, USA). Data are expressed as cumulative release in % of total input.

Cell culture

gMSCs were obtained from bone marrow aspiration from iliac wings of adult Dutch milk goats (n=3). This procedure was performed with permission of the local Ethical Committee for Animal Experimentation in compliance with the Institutional Guidelines on the use of laboratory animals. MSCs were isolated by their adherence to plastic tissue culture flasks. They were cultured in expansion medium, consisting of alpha minimum essential medium (α-MEM, Gibco, Breda, The Netherlands) that was supplemented with 15% (v/v) fetal calf serum (Cambrex), 100 U/ml penicillin with 100 µg/ml streptomycin (Gibco), and 2 mM L-glutamine (Glutamax, Gibco). All cells were cultured in a humidified incubator at 37°C and 5% CO_2.

Hydrogel preparation

Alginate powder (IMCD, Amersfoort, the Netherlands) was sterilized by UV-radiation and dissolved at a concentration of 30 mg/ml in α-MEM (Gibco) supplemented with 25 mM $CaCl_2$. This prepolymerised alginate has a suitable viscosity for 3D-printing. gMSCs were added to the gel in a concentration of 10^7 cells/ml, and for the *in vivo* scaffolds 5% (w/v) biphasic calcium phosphate granules (BCP-1150 containing 82% HA and 18%TCP, Xpand, Bilhoven, the Netherlands) with a diameter of 106-212 µm were added to improve scaffold osteoconductivity. Matrigel (growth factor reduced, BD, New Jersey, USA) was thawed overnight at 4°C.

Bioprinting

The Bioscaffolder pneumatic dispensing systems (SYS+ENG, Gladbeck, Germany) was used for bioprinting of the hydrogel scaffolds [17]. Blocks of 20x20x3 mm with vertically connected pores were designed with CAD/CAM software and translated to the NC-code

for layer by layer material deposition (Figure 1). Scaffolds were printed in a laminar flow-cabinet into tissue culture plates. After printing, the scaffolds were crosslinked by adding 100 mM $CaCl_2$ dissolved in MilliQ. After 15 minutes, the $CaCl_2$ solution was removed, the constructs washed with Tris buffered saline (TBS) and cultured in 5 ml culture medium. Directly after printing one sample of each group was processed for paraffin embedding and stained with hematoxylin and eosin to assess the distribution of the different components within the constructs.

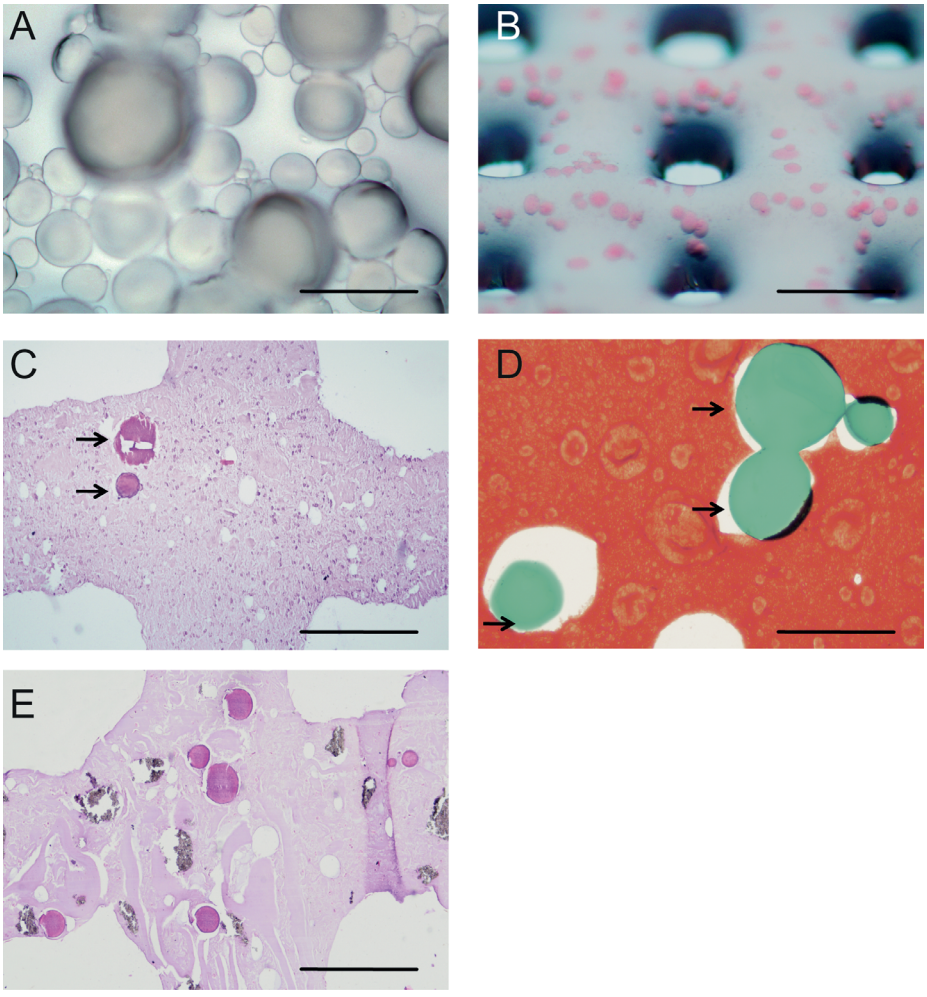

Figure 1. Bioprinted gelatin microparticles.
A. Gelatin microparticles; B. GMPs in alginate, directly after printing, GMPs in pink; C. Section of bioprinted alginate construct, directly after printing (H/E staining). Arrows indicate GMPs; D. Safranin O staining of bioprinted alginate construct, directly after printing. Arrows indicate GMPs; E. Section of bioprinted alginate construct containing BCP, after 3 weeks of culturing (H/E staining). Experiments were performed in triplicate, representative pictures are shown. Scale bars indicate in A: 200 µm, B: 2 mm, C,E: 500 µm, D: 100 µm.

In vitro analysis of osteogenic differentiation

Three groups of constructs with a volume of 600 µl were bioprinted (alginate 3% and 10^7 cells/ml in medium): 1. Control with empty GMPs (PBS laden), 2. Fast release with empty GMPs (PBS laden) and 25 ng/ml BMP-2 in the alginate, 3. Slow release with 25 ng/ml BMP-2 loaded on 2 mg GMPs. BCP granules were omitted from these constructs to allow cell retrieval for FACS analysis (Table 1). Constructs (n=3) were cultured for three weeks in expansion medium in a humidified incubator at 37°C and 5% CO_2. Part of the constructs was paraffin-embedded for histological evaluation, the rest immersed in citrate buffer (150 mM NaCl, 55 mM sodium citrate and 20 mM EDTA in H_2O) for 15 minutes at 37°C to dissolve the alginate. The cell pellet was washed in PBS/BSA 5% (w/v) three times and stained for flow cytometry. This process was repeated with the gMSCs of three different donors.

ALP analysis by FACS staining

Retrieved cells of each group (n=3) were incubated with the monoclonal anti-human alkaline phosphatase (ALP) conjugated with Alexa fluor 647 (clone B4-78, BD Pharmingen, NJ, USA) diluted 1:100 in PBS/1% (v/v) FCS (Cambrex) in the dark for an hour at 4°C. Control stainings were performed using isotype-matched control antibody (IgG_1). After antibody incubation cells were washed and taken up in PBS/FCS and analyzed by FACS Calibur.

Data were analyzed using a one-way ANOVA with Bonferroni correction and expressed as mean ± SD. A value of $p<0.05$ was considered statistically significant.

Bioprinted constructs for *in vivo* analysis of osteogenic differentiation

Three groups of constructs (Table 1) with a volume of 600 µl were bioprinted (20x20x3 mm, alginate 3% and 10^7 cells/ml in medium) as follows: 1. Control with empty GMPs (PBS laden), 2. Fast release with empty GMPs (PBS laden) and 250 ng/ml BMP-2 in the alginate, 3. Slow release with 250 ng/ml BMP-2 loaded on 2 mg GMPs. Constructs were trimmed to a size of 10x5x3 mm and kept in expansion medium overnight before implantation.

BCP cylinders for bone formation analysis

Biphasic calcium phosphate cylinders (BCP-1150 containing 82%HA and 18%TCP, Xpand, Bilhoven, the Netherlands) 7 mm in diameter, 3 mm in height with a porosity of 75±1% were filled with 100 µl Matrigel, supplemented as follows (Table 1): 1. Control with empty GMPs (PBS laden), 2. Fast release with empty GMPs (PBS laden) and 100 µg/ml BMP-2 in 100 µl Matrigel, 3. Slow release with 100 µg/ml BMP-2 loaded on 1 mg GMPs in 100 µl Matrigel.

Ethics Statement

This study was carried out following the Institutional Guidelines under the Dutch Law ("Wet op de dierproeven") on the use of laboratory animals, in accordance with the recommendations in the Guide for the Care and Use of Laboratory Animals of the National Institutes of Health. The study protocol was approved by the Dutch Ethical Committee for Animal Experimentation (Dier Experimentele Commissie, DEC) of the University of Utrecht, the Netherlands (Permit Number: 06/248). All surgery was performed under isoflurane anesthesia, and all efforts were made to minimize suffering.

In vivo implantation

Six female nude mice (Hsd-cbp NMRI-nu, Harlan, Boxmeer, The Netherlands), 6 weeks of age and 10 male Wistar rats (Charles River), 16 weeks of age were housed in standard cages at the Central Laboratory Animal Institute. They were allowed to acclimatize at the institute for at least two weeks prior to surgery. Surgery was performed under inhalation anesthesia of 3% isoflurane. After skin incision subcutaneous pockets were made by blunt dissection. The 3D printed scaffolds were placed in one of the four dorsal pockets in the mice. The BCP cylinders were placed subcutaneously in one of the six dorsal pockets in the rats. All scaffolds were assigned to a subcutaneous pocket by randomization. Pockets were closed using sutures (Vicryl 4.0). Postoperatively the animals were weighed and given a subcutaneous injection of buprenorphin (0.05 mg/kg, Temgesic, Schering-Plough/Merck, Whitehouse station, NJ, USA) every 8 hours (3 times in total).

Sample processing

The mice were terminated by cervical dislocation 6 weeks after implantation. The scaffolds were retrieved to analyze osteogenic differentiation. Samples were fixed overnight in 4% buffered formalin supplemented with 100 mM $CaCl_2$ and further dehydrated for paraffin embedding. The rats were terminated with an injection of Euthanasol. Scaffolds were retrieved and scanned with micro-CT. Subsequently they were fixed in 4% buffered formalin, dehydrated using ethanol series and embedded in polymethylmethacrylate (MMA).

Histology

Hematoxylin/eosin (HE) staining was performed on all paraffin embedded samples to investigate the properties of the 3D printed scaffolds directly after printing, after *in vitro* culturing for 3 weeks and after 6 weeks of *in vivo* implantation.

Safranin O staining was performed to investigate GMP distribution throughout the scaffold directly after printing and to monitor alginate degradation after *in vivo* implantation. Sections were incubated for 5 minutes with Weigert's hematoxylin after deparaffinisation, washed for 5 minutes in running tap water, rinsed in distilled water and coun-

terstained with 5.2 mM Fast Green solution. Sections were then rapidly rinsed 3 times in 166.5 mM acetic acid (Merck) and counterstained again with a freshly prepared 3.56 mM Safranin O staining (Merck). Both cultured and mouse implanted samples were immunostained for osteocalcin, a marker for osteogenic differentiation. The cultured samples were incubated with a mouse-anti-osteocalcin primary antibody (TaKaRa M044, clone OCG4) at 40 µg/ml and a goat-anti-mouse-IgG-HRP (Dako P0447) secondary antibody at 5 µg/ml. The implanted samples were incubated with rabbit-anti-osteocalcin primary antibody (Enzo ALX-210-333-C100) at 4 µg/ml and a goat-anti-rabbit IgG-HRP (Dako P0448) secondary antibody at 3.3 µg/ml. All antibodies were diluted in TBS containing 5% BSA and 100 mM $CaCl_2$, wash buffer consisted of TBS supplemented with 0.1% (v/v) Tween20 (TBST). Stainings were developed with diaminobenzidine (DAB) and Mayer's hematoxylin was used for counterstaining.

Sections of the bioprinted *in vivo* samples were deparaffinised and incubated with Weigert's hematoxylin, followed by Goldner's trichrome to assess collagen deposition. The MMA embedded samples were sawed centrally into 25 µm thick sections using a sawing microtome (Leica, Nussloch, Germany) and were stained with methylene blue and basic fuchsin for histomorphometric analysis. High-resolution digital pictures of the samples were taken using transmitted light microscopy (Olympus-BX50, Olympus, Zoeterwoude, the Netherlands). Bone and scaffold were pseudo-colored red and green using Adobe Photoshop CS5.1 and respective surfaces were measured (Adobe Systems Inc, San Jose, USA). Bone area percentage was calculated as (bone area / (total area - BCP area)*100%.

Micro-CT evaluation

Immediately after explantation of the subcutaneously implanted BCP scaffolds, *ex vivo* micro-CT scans were acquired using a 9 µm-resolution protocol (65 kV, 1320 ms exposure time, 1.0 mm Al filter, 0.32 degree rotation step, 53 min scan). All micro-CT images were reconstructed using volumetric reconstruction software NRecon version 1.5 (Bruker micro-CT). The BCP scaffold material was excluded through segmentation of the greyscale images with a global threshold. Within the remaining pore space, a second global threshold was applied to segment out calcified tissue from non-calcified tissue and noise. Subsequently bone was measured after an extra erosion step was applied to reduce border artifacts caused by the BCP scaffold. All analysis and segmentation was performed by a blinded observer.

Statistics

Histomorphometry data were analyzed by SPSS version 20 software (IBM, Chicago, Illinois, USA). Differences between groups were analyzed with a paired t-Test. *Post hoc* testing was performed using a Bonferroni correction. Significance was assumed when $p<0.05$.

RESULTS

Gelatin microparticles

Particles were uniform in shape when analyzed using light microscopy (Figure 1A). GMPs were selected in the size range between 75-125 µm out of three size ranges (0-50 µm / 50-75 µm / 75-125 µm) since preliminary tests revealed that BMP-2 release from these spheres lasted up to three weeks (data not shown). Smaller particles exhibited a faster growth factor release, whereas release from larger particles was not tested since they could hinder 3D printing with smaller gauged syringes [30].

In vitro release of BMP-2

To investigate whether GMPs could prolong release of BMP-2, several release experiments were performed. After overnight diffusional loading of BMP-2 solution, the amount of BMP-2 that was present in the release medium was measured at multiple time points up to 28 days. In figure 2A the cumulative release profile of loading the microspheres with an ^{125}I-BMP-2 solution in PBS with collagenase A is shown, based on ^{125}I signal in the medium. The reproducibility of the experiment was very high, standard deviations are less than 3% and thus hardly visible in the figure. In figure 2B the release of BMP-2 into PBS without collagenase presence is shown, as measured with ELISA. An initial burst release of about 20-30% of the BMP-2 was observed during the first day, which was followed by a more sustained release for the following four weeks. Without collagenase (Figure 2B), the initial burst of around 10% occurred in the first day, followed by a slow release until day 10 whereafter the growth factor was not further released from the microspheres.

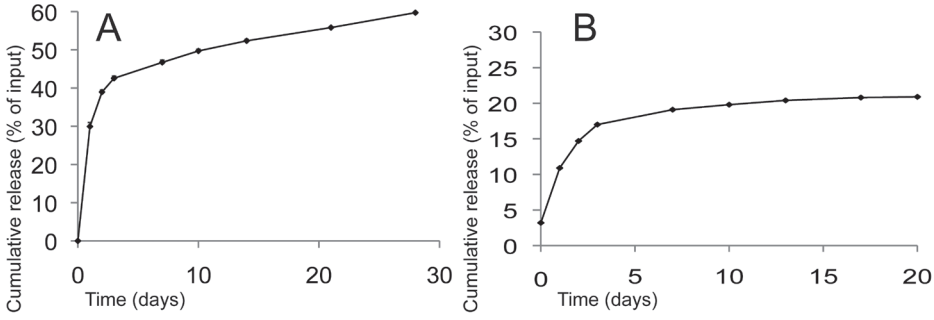

Figure 2. Cumulative release profiles of BMP-2 from gelatin microspheres.
A. Detection of ^{125}I-BMP-2 in PBS supplemented with collagenase, performed in triplicate. Results are presented as mean ± SD (small SDs hardly visible in figure); B. BMP-2 concentrations in PBS without collagenase, as determined by ELISA.

Bioprinting of controlled release particles

The GMPs were embedded in the alginate hydrogel and 3D printed scaffolds were produced. Upon preparation of the 3D printed scaffolds, GMPs were evenly distributed throughout the construct (Figure 1B). Constructs remained intact for at least three weeks *in vitro*. Subsequently, we printed porous constructs containing GMPs (without BMP-2 / fast release / slow release) and gMSCs from 3 different donor goats. One construct from each donor and group was embedded into paraffin directly after printing and stained with HE for gross histological evaluation. We observed that scaffold architecture was well preserved. Note the crossing of two hydrogel strands in the center of the picture (Figure 1C). Two GMPs are in focus (arrows), others were lost during tissue processing and left holes in the material. Staining with Safranin-O was performed to further distinguish the alginate (red) from the gelatin (green) and confirm distribution of the GMPs throughout the scaffold (Figure 1D). The alginate contains regional density differences, presumably caused by uneven degree of crosslinking. The addition of BCP to the constructs did not influence scaffold integrity and the strands were successfully printed and remained intact, shown by HE staining (Figure 1E).

Osteogenic differentiation *in vitro*

The constructs were analyzed for osteogenic differentiation after three weeks of culturing in expansion medium, by both detection of ALP expression using FACS and immunohistochemistry for osteocalcin. After dissolving the scaffold in citrate buffer flow cytometry was performed. The number of ALP positive cells was determined for all three conditions, as shown in Figure 3. Low signal of the isotype matched control antibody group confirms specific binding of the antibody. In one of the donors the number of ALP positive cells increased when BMP-2 was present for a longer period of time, in

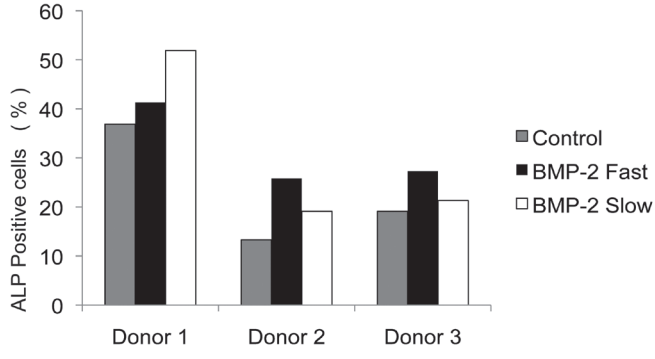

Figure 3. Bioactivity of released BMP-2.
Frequency of ALP positive MSCs after culturing for three weeks without BMP-2 (control), with BMP-2 in the hydrogel (fast release), and with BMP-2 laden GMPs (slow release), determined for 3 individual donors. Statistical analysis performed on mean values per donor.

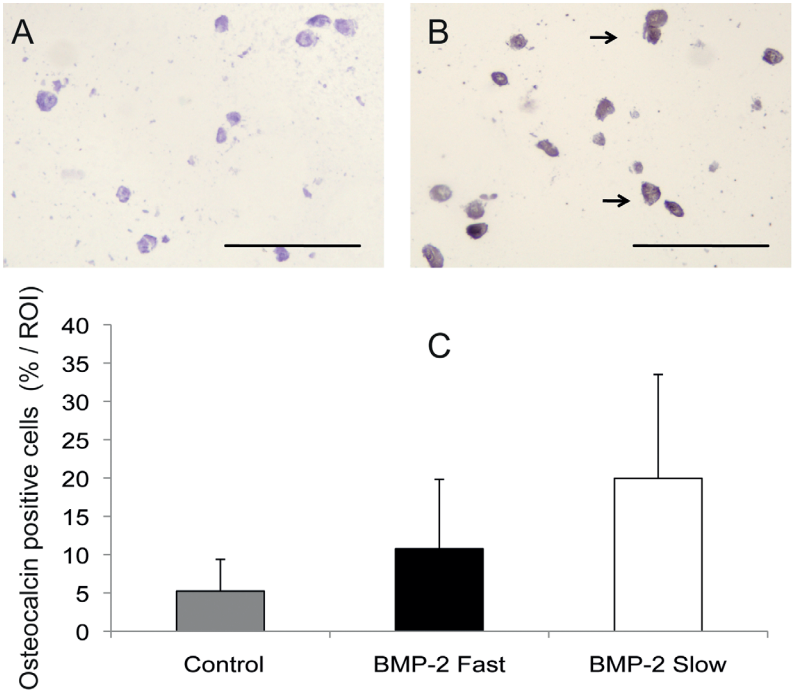

Figure 4. Osteocalcin staining of bioprinted scaffolds after 3 weeks of culturing.
A. Control staining (isotype-matched control antibody); B. Osteocalcin positive cells from a scaffold with slow release of BMP-2. Arrows indicate some of the positively stained cells (brown). Scale bars represent 50 µm; C. Percentage of osteocalcin positive cells per region of interest, no statistically significant differences were found. Results are presented as mean ± SD.

two donors the number of ALP positive cells decreased. A beneficial effect of prolonged protein presence was not seen, as the differences between the experimental groups are not statistically significant. In the immunohistochemical staining for osteocalcin the isotype-matched control staining was negative (Figure 4A). In the control constructs 5.2±4.1% of the cells stained osteocalcin positive. In the fast release group 10.7±9.1% of all cells were expressing osteocalcin. In the slow release group osteogenic differentiation was seen in 19.9±13.6% of the cells (Figure 4B). There was no significant difference between the groups (p=0.2). Arrows indicate positively stained cells.

Osteogenic differentiation in bioprinted scaffolds

After 6 weeks of in vivo implantation in mice the scaffolds were explanted and examined using immunohistochemistry. The alginate scaffolds were degraded to such an extent that scaffold retrieval was challenging, some explants were too small to analyze for osteogenic differentiation. Larger pieces of retrieved scaffolds (all from the fast release group) were suitable for histological analysis (Figure 5).

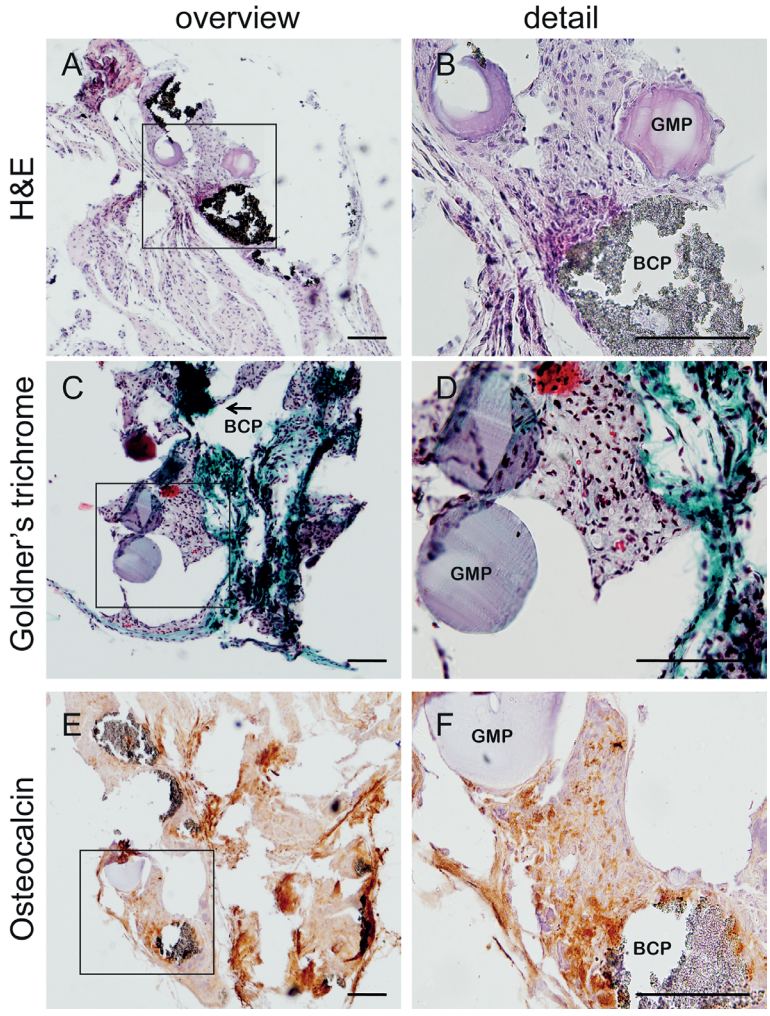

Figure 5. Osteogenic differentiation *in vivo*.
Presence of gelatin microparticles (GMP) and biphasic calcium phosphate granules (BCP) after 6 weeks of subcutaneous implantation in mice as indicated in the pictures. An overview and detail of HE, Goldner's trichrome and osteocalcin stainings are shown. Scale bars represent 100 µm.

In the retrieved scaffolds GMPs and BCP particles were clearly visible on the HE staining. In the Goldner's trichrome staining collagen depositions (in green) were observed. Cells positive for osteocalcin were present in the regions around both BCP and GMPs, which indicates osteogenic differentiation at these locations. No alginate was present in these tissues, as indicated by staining with Safranin-O (data not shown). This indicates that the loss of scaffold integrity occurred rapidly. To further investigate this fast alginate degradation, two alginate/BCP scaffolds were implanted subcutaneously in mice, and already after one week alginate degradation and cell invasion was evident (data not shown).

Bone formation in porous BCP cylinders

To analyze whether BMP-2 release kinetics influenced the extent of bone formation, a second animal study was performed in rats. Porous BCP cylinders (control, fast or slow release) were implanted subcutaneously to ensure scaffold integrity throughout the experiment. Bone formation in BCP cylinders was analyzed using histomorphometry and micro-CT after 12 weeks of subcutaneous implantation (Figure 6). The control group did not form bone (0±0%) in the BCP cylinders, which was significantly lower than the BMP-2 containing groups ($p<0.01$, in both histomorphometry and micro-CT). A bone volume of 5.5±0.9 mm^3 was measured in this group with micro-CT. In the slow release group a bone area of 13.5±8.3% from the histological sections and bone volume of 10.1±4.2

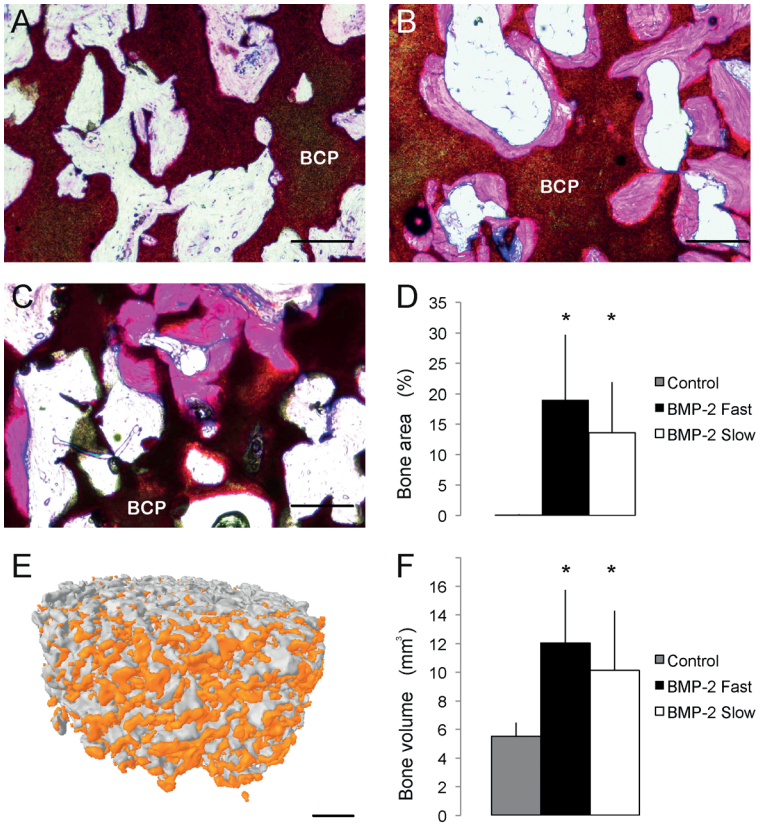

Figure 6. Bone formation after 12 weeks of subcutaneous implantation in rats.
A. Control group; B. Fast release of BMP-2 group; C. Sustained BMP-2 released from GMP group. Section were stained with methylene blue and basic fuchsin. Biphasic calcium phosphate (BCP) is indicated in the pictures. D. Quantification of bone content by histomorphometry, n=10. E. 3D reconstruction of micro-CT showing bone formation (orange) in a scaffold of the BMP-2 fast group. F. Quantification of bone content by micro-CT, n=10. Representative pictures from each group are given. Scale bars represent 100 µm in A-C, 1 mm in E; Results are presented as mean ± SD, * $p<0.01$ compared to control.

mm^3 from the CT data were measured. In the fast release group the average bone area% reached 19±10.7%, and the bone volume 12.1±3.7 mm^3.

DISCUSSION

This study has shown that prolonged presence of BMP-2 in scaffolds can be accomplished by applying controlled delivery microparticles, such as GMPs. It is feasible to incorporate these GMPs into a bioprinted alginate construct containing BCP and gMSCs. The presence of BMP-2 in bioprinted hydrogel constructs has led to osteogenic differentiation *in vitro* and *in vivo*. The ability to place and release growth factors in such a way is novel and offers many possibilities in terms of scaffold architecture and bioactivity.

The 3% pre-crosslinked alginate was printable and could be rapidly crosslinked after printing, but *in vivo* it was degraded very fast, which severely affected scaffold integrity. The hydrogel with incorporated BMP-2, BCP granules and gMSCs probably dispersed through the pocket. The lack of coherence likely explains the absence of bone formation after in vivo implantation, as each of the components has been successfully used in bone tissue engineering approaches in previous experiments by our group [31,32]. The porosity of the constructs may have added to the disintegration effect, as it enlarges the surface to volume ratio of the constructs [33]. It is known that ionically cross-linked alginate loses mechanical properties over time due to an outward flux of ions into surrounding culture medium [34,35]. In the future, other measures need to be taken to be able to make low percentages of alginate printable, or combinations of hydrogels should be used as scaffold material to retain structure until bone starts to form.

Many different biomaterials are suitable for controlled release, gelatin being well-known for its prolonged growth factor delivery, characterized by a small initial burst and showing no tissue damaging residual material. As such, gelatin is used in many FDA-approved devices. The release profile of BMP-2 shown here has two distinct phases, starting with a burst release of about 30% growth factor. It is known from literature on gelatin release kinetics that this burst is due to diffusion from the outer regions of the particles [36]. The second phase, which shows sustained release is suggested to be based on enzymatic degradation of the gelatin, thereby releasing the bound BMP-2. When collagenase was not present in the release medium this second phase hardly occurred. Detection of the released protein was measured using radioactive labeling as well as ELISA, both widely used assays to assess BMP-2 concentrations. Still, these highly quantitative methods do not take into account the loss of protein due to breakdown and surface adhesion.

The *in vitro* release data shown in this article are probably not in accordance with *in vivo* release rates, which can be significantly faster due to higher enzymatic activities.

By using collagenase in the experiments, the *in vivo* degradation was at least partly mimicked, but we expect *in vivo* release to be faster still. Also, a 100% release was not reached after 4 weeks, indicating there was still residual growth factor present in the experimental samples. Give the observation that *in vitro* and *in vivo* release often show different profiles [22], we can only estimate the total dose which has become available in the implanted constructs. Dosage of BMP-2 in the *in vitro* experiments appeared to be sufficient, as prolonged presence of BMP-2 released from GMPs has led to osteogenic differentiation of the cells.

In this study we used goat MSCs as a model system, because this large animal model is widely used in preclinical studies aiming at translation to the clinic and thus in generating cm-scaled bone constructs. The presence of porosity in larger constructs promoted tissue ingrowth and vascularization, which was demonstrated before using the bioprinting technology [37]. When applying the GMPs in bioprinted scaffolds, it appeared that inclusion of BMP-2 through these formulations containing growth factors is feasible. Bone formation by application of BMP-2 laden GMPs was studied, and results were analyzed using both histomorphometry and micro-CT. Although micro-CT analysis poses advantages such as rapid analysis of entire constructs and *in vivo* analysis, there is a discrepancy with histomorphometry measurements, as is illustrated by the control group. We know from histomorphometry that no bone was present in these constructs, yet a considerable signal was detected with micro-CT. This is presumably caused by border-artefacts from the BCP, that has a radiolucency close to to bone. Despite this over-estimation, the relative increase in bone formation between the groups is comparable, which corresponds to literature reporting good correlations between micro-CT and histomorphometry [38]. Histomorphometry however remains the gold standard to analyze bone formation. Growth factor induced bone formation was analyzed, and growth factor presence either by slow or fast release led to a significantly higher bone area % compared to growth factor free formulations in the rat ectopic model. This is in not in accordance with earlier studies in for instance dogs, where the faster BMP-2 release led to higher ectopic bone volume [39]. Apart from location specific differences, also species differences play a role, making clinical translation even more complicated.

CONCLUSION

We conclude from the current investigation that prolonged BMP-2 release can be accomplished by loading the growth factor on GMPs. The BMP-2 released from the GMPs in these scaffolds is biologically active. Presence of BMP-2 in bioprinted hydrogel constructs has led to osteogenic differentiation, from which we conclude that it is feasible to

bioprint a controlled release system. BMP-2 significantly increased bone formation, the release timing did not influence the bone volume within the constructs.

The ability to place and release growth factors in 3D printed constructs is novel and offers many possibilities in terms of scaffold architecture and bioactivity.

ACKNOWLEDGEMENTS

The authors thank Okan Bastian for his assistance with flow cytometry and Jeroen van Bemmel and Kelly van Deventer for their assistance with cell culturing and bioprinting.

REFERENCES

1. Giannoudis PV, Dinopoulos H, Tsiridis E. Bone substitutes: an update. *Injury 2005;36 Suppl 3:S20-7*.
2. Silber JS, Anderson DG, Daffner SD, Brislin BT, Leland JM, Hilibrand AS, Vaccaro AR, Albert TJ. Donor site morbidity after anterior iliac crest bone harvest for single-level anterior cervical discectomy and fusion. *Spine (Phila Pa 1976) 2003;28-2:134-9*.
3. Cross M, Dexter TM. Growth factors in development, transformation, and tumorigenesis. *Cell 1991;64-2:271-80*.
4. Lee K, Silva EA, Mooney DJ. Growth factor delivery-based tissue engineering: general approaches and a review of recent developments. *J R Soc Interface 2011;8-55:153-70*.
5. Rickard DJ, Sullivan TA, Shenker BJ, Leboy PS, Kazhdan I. Induction of rapid osteoblast differentiation in rat bone marrow stromal cell cultures by dexamethasone and BMP-2. *Dev Biol 1994;161-1:218-28*.
6. Garrison KR, Shemilt I, Donell S, Ryder JJ, Mugford M, Harvey I, Song F, Alt V. Bone morphogenetic protein (BMP) for fracture healing in adults. *Cochrane Database Syst Rev 2010-6:CD006950*.
7. Geiger M, Li RH, Friess W. Collagen sponges for bone regeneration with rhBMP-2. *Adv Drug Deliv Rev 2003;55-12:1613-29*.
8. Poynton AR, Lane JM. Safety profile for the clinical use of bone morphogenetic proteins in the spine. *Spine (Phila Pa 1976) 2002;27-16 Suppl 1:S40-8*.
9. Jansen JA, Vehof JW, Ruhe PQ, Kroeze-Deutman H, Kuboki Y, Takita H, Hedberg EL, Mikos AG. Growth factor-loaded scaffolds for bone engineering. *J Control Release 2005;101-1-3:127-36*.
10. Carragee EJ, Hurwitz EL, Weiner BK. A critical review of recombinant human bone morphogenetic protein-2 trials in spinal surgery: emerging safety concerns and lessons learned. *Spine J 2011;11-6:471-91*.
11. Groeneveld EH, Burger EH. Bone morphogenetic proteins in human bone regeneration. *Eur J Endocrinol 2000;142-1:9-21*.
12. Yamamoto M, Takahashi Y, Tabata Y. Controlled release by biodegradable hydrogels enhances the ectopic bone formation of bone morphogenetic protein. *Biomaterials 2003;24-24:4375-83*.
13. Cho TJ, Gerstenfeld LC, Einhorn TA. Differential temporal expression of members of the transforming growth factor beta superfamily during murine fracture healing. *J Bone Miner Res 2002;17-3:513-20*.
14. Ogawa T, Akazawa T, Tabata Y. In vitro proliferation and chondrogenic differentiation of rat bone marrow stem cells cultured with gelatin hydrogel microspheres for TGF-beta1 release. *J Biomater Sci Polym Ed 2010;21-5:609-21*.
15. Habraken WJ, Boerman OC, Wolke JG, Mikos AG, Jansen JA. In vitro growth factor release from injectable calcium phosphate cements containing gelatin microspheres. *J Biomed Mater Res A 2009;91-2:614-22*.
16. Karageorgiou V, Kaplan D. Porosity of 3D biomaterial scaffolds and osteogenesis. *Biomaterials 2005;26-27:5474-91*.
17. Fedorovich NE, Wijnberg HM, Dhert WJ, Alblas J. Distinct tissue formation by heterogeneous printing of osteo- and endothelial progenitor cells. *Tissue Eng Part A 2011;17-15-16:2113-21*.
18. Drury JL, Mooney DJ. Hydrogels for tissue engineering: scaffold design variables and applications. *Biomaterials 2003;24-24:4337-51*.
19. Stevens MM, Marini RP, Schaefer D, Aronson J, Langer R, Shastri VP. In vivo engineering of organs: the bone bioreactor. *Proc Natl Acad Sci U S A 2005;102-32:11450-5*.

20. Augst AD, Kong HJ, Mooney DJ. Alginate hydrogels as biomaterials. *Macromol Biosci 2006;6-8: 623-33*.
21. Wang L, Shelton RM, Cooper PR, Lawson M, Triffitt JT, Barralet JE. Evaluation of sodium alginate for bone marrow cell tissue engineering. *Biomaterials 2003;24-20:3475-81*.
22. Kempen DH, Lu L, Hefferan TE, Creemers LB, Maran A, Classic KL, Dhert WJ, Yaszemski MJ. Retention of in vitro and in vivo BMP-2 bioactivities in sustained delivery vehicles for bone tissue engineering. *Biomaterials 2008;29-22:3245-52*.
23. Boerckel JD, Kolambkar YM, Dupont KM, Uhrig BA, Phelps EA, Stevens HY, Garcia AJ, Guldberg RE. Effects of protein dose and delivery system on BMP-mediated bone regeneration. *Biomaterials 2011*.
24. Angle SR, Sena K, Sumner DR, Virkus WW, Virdi AS. Healing of rat femoral segmental defect with bone morphogenetic protein-2: A dose response study. *J Musculoskelet Neuronal Interact 2012; 12-1:28-37*.
25. Young S, Wong M, Tabata Y, Mikos AG. Gelatin as a delivery vehicle for the controlled release of bioactive molecules. *J Control Release 2005;109-1-3:256-74*.
26. Leeuwenburgh SC, Jo J, Wang H, Yamamoto M, Jansen JA, Tabata Y. Mineralization, biodegradation, and drug release behavior of gelatin/apatite composite microspheres for bone regeneration. *Biomacromolecules 2010;11-10:2653-9*.
27. Patel ZS, Yamamoto M, Ueda H, Tabata Y, Mikos AG. Biodegradable gelatin microparticles as delivery systems for the controlled release of bone morphogenetic protein-2. *Acta Biomater 2008; 4-5:1126-38*.
28. Bigi A, Cojazzi G, Panzavolta S, Rubini K, Roveri N. Mechanical and thermal properties of gelatin films at different degrees of glutaraldehyde crosslinking. *Biomaterials 2001;22-8:763-8*.
29. Fraker PJ, Speck JC, Jr. Protein and cell membrane iodinations with a sparingly soluble chloroamide, 1,3,4,6-tetrachloro-3a,6a-diphrenylglycoluril. *Biochem Biophys Res Commun 1978;80-4: 849-57*.
30. Varde NK, Pack DW. Microspheres for controlled release drug delivery. *Expert Opin Biol Ther 2004; 4-1:35-51*.
31. Wegman F, Bijenhof A, Schuijff L, Oner FC, Dhert WJ, Alblas J. Osteogenic differentiation as a result of BMP-2 plasmid DNA based gene therapy in vitro and in vivo. *Eur Cell Mater 2011;21:230-42; discussion 42*.
32. Wegman F, Geuze RE, van der Helm YJ, Cumhur Oner F, Dhert WJ, Alblas J. Gene delivery of bone morphogenetic protein-2 plasmid DNA promotes bone formation in a large animal model. *J Tissue Eng Regen Med 2012*.
33. Thomson RC, Yaszemski MJ, Powers JM, Mikos AG. Fabrication of biodegradable polymer scaffolds to engineer trabecular bone. *J Biomater Sci Polym Ed 1995;7-1:23-38*.
34. Rowley JA, Madlambayan G, Mooney DJ. Alginate hydrogels as synthetic extracellular matrix materials. *Biomaterials 1999;20-1:45-53*.
35. Shoichet MS, Li RH, White ML, Winn SR. Stability of hydrogels used in cell encapsulation: An in vitro comparison of alginate and agarose. *Biotechnol Bioeng 1996;50-4:374-81*.
36. Ikada Y, Tabata Y. Protein release from gelatin matrices. *Adv Drug Deliv Rev 1998;31-3:287-301*.
37. Fedorovich NE, Kuipers E, Gawlitta D, Dhert WJ, Alblas J. Scaffold Porosity and Oxygenation of Printed Hydrogel Constructs Affect Functionality of Embedded Osteogenic Progenitors. *Tissue Eng Part A 2011*.

38. Gauthier O, Muller R, von Stechow D, Lamy B, Weiss P, Bouler JM, Aguado E, Daculsi G. In vivo bone regeneration with injectable calcium phosphate biomaterial: a three-dimensional micro-computed tomographic, biomechanical and SEM study. *Biomaterials 2005;26-27:5444-53*.
39. Geuze RE, Theyse LF, Kempen DH, Hazewinkel HA, Kraak HY, Oner FC, Dhert WJ, Alblas J. A differential effect of bone morphogenetic protein-2 and vascular endothelial growth factor release timing on osteogenesis at ectopic and orthotopic sites in a large-animal model. *Tissue Eng Part A 2012;18-19-20:2052-62*.

CHAPTER 3

Prolonged presence of VEGF promotes vascularization in 3D bioprinted scaffolds with defined architecture

Michelle Poldervaart
Hendrik Gremmels
Kelly van Deventer
Joost Fledderus
Cumhur Öner
Marianne Verhaar
Wouter Dhert
Jacqueline Alblas

Journal of Controlled Release
2014 Jun 28;184:58-66

ABSTRACT

Timely vascularization is essential for optimal performance of bone regenerative constructs. Vascularization is efficiently stimulated by vascular endothelial growth factor (VEGF), a substance with a short half-life time. This study investigates the controlled release of VEGF from gelatin microparticles (GMPs) as a means to prolong VEGF activity at the preferred location within 3D bioprinted scaffolds, and the effects on subsequent vascularization. Release of VEGF from GMPs was continuous for 3 weeks during *in vitro* studies, and bioactivity was confirmed using human endothelial progenitor cells (EPCs) in migration assays. Traditional and real-time migration assays showed immediate and efficient EPC migration in the presence of GMP-released VEGF, indistinguishable from VEGF-solution that was added to the medium. Matrigel scaffolds containing EPCs and VEGF, which was released either in a fast or sustained fashion by application of GMPs, were investigated for their *in vivo* vasculogenic capacity. Implantation in subcutaneous pockets in nude mice for one week demonstrated that vessel formation was significantly higher in the VEGF sustained-release group compared to the fast release group. In addition, regional differences with respect to VEGF release were introduced in 3D bioprinted EPC-laden scaffolds and their influence on vasculogenesis was investigated *in vivo*. The different regions were retained and vessel formation occurred analogous with the results seen in the Matrigel plugs.

We conclude that GMPs are suitable to generate sustained release profiles of bioactive VEGF, and that they can be used to create defined differentiation regions in 3D bioprinted heterogeneous constructs, allowing a new generation of smart scaffold design. The prolonged presence of VEGF led to a significant increase in scaffold vascularization when applied *in vivo*.

GRAPHICAL ABSTRACT

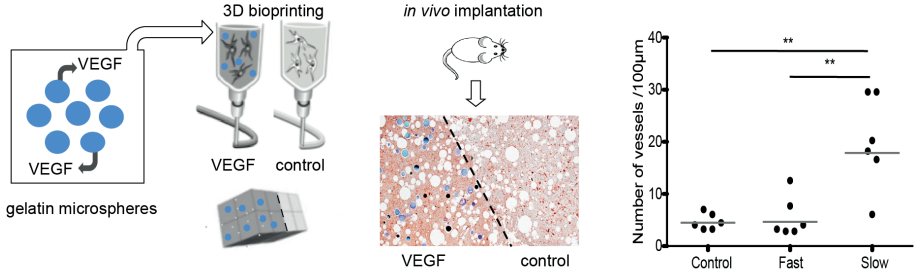

INTRODUCTION

Vascularization of tissue-engineered constructs is an ongoing challenge in regenerative medicine. Without sufficient blood supply, oxygen and metabolic needs are not met, which can lead to central necrosis of constructs. This limits scaffold size to the diffusion distance nutrients can travel in the used material [1,2]. A possible solution to this problem could be to introduce a prevascularization step to stimulate the process of efficient vascularization once the construct is implanted. Grafts with new blood vessels that can connect to the host vasculature could enhance the quantity and quality of newly formed tissues. Endothelial progenitor cells (EPCs) that are present in the circulation play an important role in this process as they can differentiate into endothelial cells that line blood vessels [3]. Late outgrowth EPCs (sometimes referred to as endothelial colony forming cells or ECFCs in literature [4-6]) have a high capacity for proliferation and vessel formation *in vitro* and *in vivo* [7,8]. Vessel formation properties of the EPCs have been studied extensively in established 2D tubulogenesis and 3D vasculogenesis assays, and indicate that they are suitable to prevascularize tissue engineered constructs. A potent angiogenic and vasculogenic growth factor that is often applied in regenerative medicine is vascular endothelial growth factor (VEGF), a heparin-binding, homodimeric glycoprotein of 45 kDa of which $VEGF_{165}$ is the predominant isoform [9]. It is a key regulator of physiological vessel formation during embryogenesis, mainly by preventing apoptosis of endothelial cells [10]. VEGF is degraded rapidly in the bloodstream with a half-life time of less than 1 hour following injection [11,12]. Controlled release of VEGF to accomplish longer growth factor presence at target locations leads to increased vessel formation in scaffolds [13,14]. As a suitable system for growth factor release gelatin or gelatin microparticles (GMP) are often applied. Gelatin is a natural product that is used in many FDA-approved devices. Growth factor encapsulation is based on electrostatic interactions with the gelatin as well as the gelatin degradation rate [15-18]. The main advantages of the GMPs are the diffusional loading of growth factors and the non-covalent nature of the interaction between gelatin and growth factor, thus avoiding chemical reactions that could damage the protein. Furthermore, GMPs are non-cytotoxic, biodegradable and they have previously been used to deliver other growth factors such as BMP-2, TGFβ1 and FGF [19,20]. Intracardial injection of GMPs loaded with VEGF has led to increased neoangiogenesis in a rat myocardial infarct model [21,22]. GMPs can be incorporated into hydrogel plugs or 3D bioprinted constructs [23]. This technique enables production of a new generation of scaffolds with defined architecture and the opportunity to include predefined regions of prevascularization in the scaffold. Furthermore, with 3D bioprinting, scaffold porosity can be introduced, which appears to improve the *in vivo* performance by lowering the diffusion distance for oxygen and nutrients [24].

Based on these considerations the present study aimed to combine controlled VEGF release with 3D bioprinting technology to enable production of novel hydrogel scaffolds with properties that can be tuned both in time and space to optimize vessel formation. Suitability of GMPs for VEGF delivery was first assessed with *in vitro* release studies and real-time EPC migration studies. Subsequently, *in vivo* studies were carried out to investigate whether prolonged VEGF presence in scaffolds would improve the degree of vascularization. The suitability of GMP mediated controlled VEGF release in these novel architectural constructs was studied using the 3D bioprinting technology.

MATERIALS AND METHODS

EPC isolation and culture

Human umbilical cord blood was collected from full term pregnancies, using a protocol approved by the local ethics committee (01/230K, Medisch Ethische Toetsings Commissie (METC), University Medical Center Utrecht). Mononuclear Cells (MNCs) were isolated by density-gradient centrifugation using Ficoll-paque (density 1.077 g/ml). MNCs were subsequently resuspended in Endothelial Growth Medium-2 (EGM-2) containing 10% fetal calf serum (FCS) and EGM-2 SingleQuots (Lonza, Walkersville, MD, USA) and seeded on Collagen I (BD Biosciences, Heidelberg, Germany) coated wells at a density of $2x10^6$ cells per cm^2. Medium was exchanged daily for the first week and three times per week thereafter. Cells were harvested when colonies appeared and expanded for further use. All experiments were conducted with cells at passage 3-5.

Flow cytometric characterization of EPCs

Cells were harvested by trypsinization and labeled with the following antibodies: anti-hVEGFR2-PE (R&D, Minneapolis, MN), anti-hCD34-FITC (BD), anti-hVE-Cadherin-PE, (R&D), anti-CD31-PE (R&D), anti-CD90-PE (R&D), anti-CD105-PE (R&D) anti-CD45-PE (BD), anti-CD14-PE (Biolegend, San Diego, CA). Antibody labeling was performed for 30 minutes at 4°C in the presence of FcR-Blocking reagent (Miltenyi), followed by two washing steps using PBS. Directly before each measurement, Sytox® Blue (Life Technologies, Bleiswijk, The Netherlands) was added in order to assess viability. Flow-cytometric analysis was performed using a Becton Dickinson FACSCanto II. After washing and fixing, at least 10^4 cells were acquired and analyzed.

Immunocytochemistry of EPCs

Cells were grown to confluence on Lab-TekII chamberslides and fixed using 4% paraformaldehyde. Next, cells were permeabilised where appropriate with 0.1% Triton X-100 in PBS and stained with the following antibodies/reagents: anti-CD144 (R&D),

anti-CD31 (R&D), anti vWF (Sigma). Fluorescent second antibody staining was done with Anti-Mouse AlexaFluor 488 and 555 (Molecular Probes) and nuclei were visualized with 4',6-diamidino-2-phenylindole (DAPI). Images were taken with an Olympus BX60 fluorescence microscope.

Production of gelatin microparticles (GMPs)

We adapted the protocol previously described by Tabata et al. [19,25]. A water in oil emulsion was made using water dissolved gelatin type B (Sigma, St Louis, MO, USA) 10% (w/v) that was added drop wise to refined olive oil (Arcos Organics, NJ, USA) at 60°Celsius. The solution was stirred (350 rpm) for 15 minutes and then rapidly cooled with an ice bath to induce gelation of gelatin droplets. The microparticles were washed with 150 ml of chilled acetone and filtered under pressure (filter paper grade 2, Whatman, Tokyo, Japan). The microparticles were sieved and covalently cross-linked overnight using a 10.6 mM aqueous glutaraldehyde solution (Merck, Darmstadt, Germany) [26,27]. Three washing steps with 100 mM glycine solution (Sigma, St Louis, MO, USA) were applied to remove residual aldehyde groups. Subsequently, the microparticles were washed in deionized water (MilliQ) three times, freeze-dried overnight, UV sterilized and kept at 4°C in a vacuum container until use. The GMPs were tested in triplicate for endotoxin content using a chromogenic limulus amebocyte lysate assay (Lonza), according to the manufacturer's protocol. The microparticles were loaded with the dissolved growth factor by diffusional loading.

In vitro release of VEGF measured by ELISA

For slow release GMPs (5 mg) were loaded with 5 µl of a 10 µg/ml VEGF in PBS /0.5% BSA solution by diffusional loading overnight at 4°C, and incorporated into 200 µl Matrigel (growth factor-reduced, BD, New Jersey, USA) plugs (each containing 50 ng VEGF) that were placed in the top compartments of a Transwell system, (0.4 µm pores, Corning Sigma, St Louis, MO, USA). Fast release was also investigated, here the same concentration of VEGF was directly incorporated in the Matrigel plugs. In the lower compartment PBS /0.5% BSA was used as release medium and refreshed at multiple time points. VEGF concentrations in the release medium were determined by ELISA (in duplicate, R&D, Minneapolis, MN, USA). Data are expressed as cumulative release, in mean ± SD.

Transwell migration assay

EPC migration assays were performed using the 24-well Transwell system (10 µm thickness, 8 µm pores, Corning, NY, USA). Microspheres (5 mg) were loaded with 5 µl of PBS, 10 µg/ml or 20 µg/ml VEGF in PBS /0.5% BSA by diffusional loading at 4°C overnight to allow complete growth factor absorption. The GMPs were suspended in 0.5 ml EGM-2 medium, supplemented with 2% FCS and singlequots (without VEGF), and placed in the

lower compartment. For comparison, the same amounts (0, 100 or 200 ng/ml) of VEGF were added directly into the medium (fast release). Medium containing 15% FCS served as a positive control. In the top compartments 10^5 EPCs (serum deprived, cultured overnight in EGM-2 /2% FCS) were seeded. After 24 hours non-migrated cells remaining at the upper side of the membranes were carefully removed with cotton swabs, and migrated cells on the lower side of the membrane were fixed with methanol and stained with hematoxylin. High-resolution pictures of four representative fields were taken using a light microscope, and two observers counted the number of migrated cells per region of interest on blinded samples for 3 EPC donors.

Real-time migration assay

Time-dependent cell migration was measured using the xCELLigence system (Roche, Almere, the Netherlands), a microelectronic biosensor method continuously measuring electrical impedance across integrated electrodes over the membrane of a Transwell chamber setup (CIM-Plate 16 containing wells, inserts and membranes). An increase in impedance correlates with a number of cells migrating through the membrane. The CIM-plate membrane was coated with collagen I for one hour at room temperature and rinsed twice with PBS. Serum-free EGM-2 medium was added to all lower compartments and supplemented with VEGF (ranging from 0-100 ng/ml, fast release) or the same concentrations of VEGF were laden overnight on 5 mg of GMPs (slow release). $4x10^4$ serum-deprived EPCs were resuspended in serum-free EGM-2 and plated into each top compartment. The CIM-plates were assembled and measurements were performed in duplicate following manufacturer's protocol with EPCs from three donors. Impedance was measured twice a minute for 9 hours at 37°C and 5% CO_2, whereafter the results were translated into a cell index signal and normalized to the migration data of the vehicle group.

Matrigel tube formation assay

Matrigel was mixed with alginate 3% ((w/v), IMCD, Amersfoort, the Netherlands), at different ratios and used for EPC tube formation assays. 10^4 EPCs suspended in EGM-2 with 2% FCS were distributed on microwell plates (Ibidi, Martinsried, Germany) coated with alginate, Matrigel or a mixture of these two materials. Cells were allowed to form tubular networks for 24 hours. To visualize tubes and cell viability a LIVE/DEAD viability assay (Molecular Probes, Eugene, USA) was performed according to manufacturer's recommendations. Pictures were taken with a fluorescence microscope (Olympus, BX51, USA), total vascular complex length and branching points were quantified by processing all obtained images with the freeware AngioQuant v1.33 [28].

Dynamic Mechanical Analysis

The hydrogel mixtures that were used for 3D bioprinting were subjected to an unconstrained compression test (2980 DMA, TA Instruments) with a ramp force from 0.1 to 1 N for 10 minutes. The gels were cast into 200 µl discs and tested with and without 100 mM $CaCl_2$ crosslinking for 15 minutes. The compressive modulus was calculated from the slope of the stress-strain curve that was obtained.

3D bioprinting

The Bioscaffolder pneumatic dispensing system (SYS+ENG, Gladbeck, Germany) was used for 3D bioprinting of hydrogel scaffolds (Matrigel/alginate=3/1 mixture) [29].

Scaffold architecture is determined and converted to a computer-aided design (CAD) file and then combined with specific material settings to a numerical control (NC) code, which directs the robotic arm of the 3D printer [30]. One dispensing head contained hydrogel supplemented with $5x10^6$ EPCs/ml, in the second dispensing head GMPs containing 25 µg/ml VEGF were added to the cell-laden hydrogel. Regionally defined hybrid porous scaffolds measuring 10x10x3mm were 3D bioprinted under sterile conditions in a laminar flow-cabinet. After 3D bioprinting the scaffolds were cross-linked by adding 100 mM aqueous $CaCl_2$ for 15 minutes, then washed with Tris buffered saline (TBS) and cultured in EGM-2 medium. Directly after 3D bioprinting one sample was processed for paraffin embedding and stained with HE, Goldner's trichrome and Safranin-O to assess the distribution of the different components within the construct.

Scaffold preparation for *in vivo* implantation

Four groups of constructs were produced (Table 1). Three groups consisted of Matrigel (200 µl) plugs containing $5x10^6$ EPCs/ml, a control group with empty GMPs (PBS laden), a fast release group with empty GMPs (PBS laden) and 25 µg/ml VEGF in the hydrogel, and a slow release group with 25 µg/ml VEGF loaded on 5 mg GMPs. The fourth group consisted of 3D bioprinted Matrigel/alginate=3/1 mixture containing $5x10^6$ EPCs/ml. These hybrid constructs contained two regions, half the construct contained 25 µg/ml VEGF loaded GMPs (slow), and the other half served as control. Constructs were trimmed to a size of 10x5x3mm and kept in EGM-2 medium overnight before implantation.

Table 1. Experimental groups.

Group	Scaffold	Growth factor presence	hEPCs
Control	Matrigel plugs	PBS laden GMPs, no VEGF	$5x10^6$ cells/ml
Fast	Matrigel plugs	PBS laden GMPs, 25 µg/ml VEGF in Matrigel	$5x10^6$ cells/ml
Slow	Matrigel plugs	25 µg/ml VEGF laden GMPs	$5x10^6$ cells/ml
Hybrid	3D bioprinted Matrigel/alginate=3/1	Region 1: no GMPs, no VEGF Region 2: 25 µg/ml VEGF laden	$5x10^6$ cells/ml

In vivo implantation

Surgeries were performed with permission of the local Ethical Committee for Animal Experimentation in compliance with the Institutional Guidelines on the use of laboratory animals. Six female nude mice (Hsd-cbp NMRI-nu, Harlan, Boxmeer, The Netherlands), 10 weeks of age were housed in standard cages at the Central Laboratory Animal Institute. Surgery was performed under inhalation anesthesia of 3% isoflurane. After skin incision, subcutaneous pockets were made by blunt dissection. The scaffolds were placed in one of the four dorsal pockets in the mice in a randomized fashion. Pockets were closed using sutures (Vicryl 4.0). Postoperatively the animals were weighed and given a subcutaneous injection of buprenorphine (0.05 mg/kg, Temgesic, Schering-Plough/ Merck, Whitehouse station, NJ, USA) every 8 hours (3 times in total).

Sample processing and histology

The mice were terminated by cervical dislocation one week after implantation. The scaffolds were retrieved to analyze vessel formation. Samples were fixed overnight in 4% buffered formalin and further dehydrated for paraffin embedding. Hematoxylin/eosin (HE) staining was performed on all samples to investigate the gross morphology of the samples after *in vivo* implantation. Then samples were deparaffinised and incubated with Weigert's hematoxylin followed by Goldner's trichrome to assess vessel formation. The number of erythrocyte-perfused vessels per 100 μm^2 was counted by two independent observers on blinded samples. Subsequently, samples were stained for CD31 (PECAM-1) with rabbit-anti-mouse CD31 primary antibody (cross-reacts with human CD31, B4737, Lifespan, Seattle, WA, USA and 28364, Abcam, Cambridge, UK) at 2 µg/ml, followed by goat-anti-rabbit biotinylated antibody at 5.5 µg/ml (Dako, E0432) and Streptavidin-HRP at 1.4 µg/ ml (Dako, K1016). All antibodies were diluted in PBS containing 5% (w/v) BSA. Staining was developed with diaminobenzidine (DAB) and Mayer's hematoxylin was used for counterstaining. Subsequently anti-goat CD 31 (staining human and mouse CD 31, SC1506, Santa Cruz, Dallas, Tx, USA) and anti-rat CD 31 (staining only mouse CD31, SZ31) stainings were performed, fluorescent secondary antibody staining was done with anti-goat and anti-rabbit AlexaFluor 568 and 594 (Molecular Probes), respectively. Nuclei were visualized with DAPI.

Statistical analysis

Data are represented as mean ± standard deviation, and analyzed using an ANOVA test with *post hoc* Bonferroni correction. Differences were considered statistically significant when $p<0.05$.

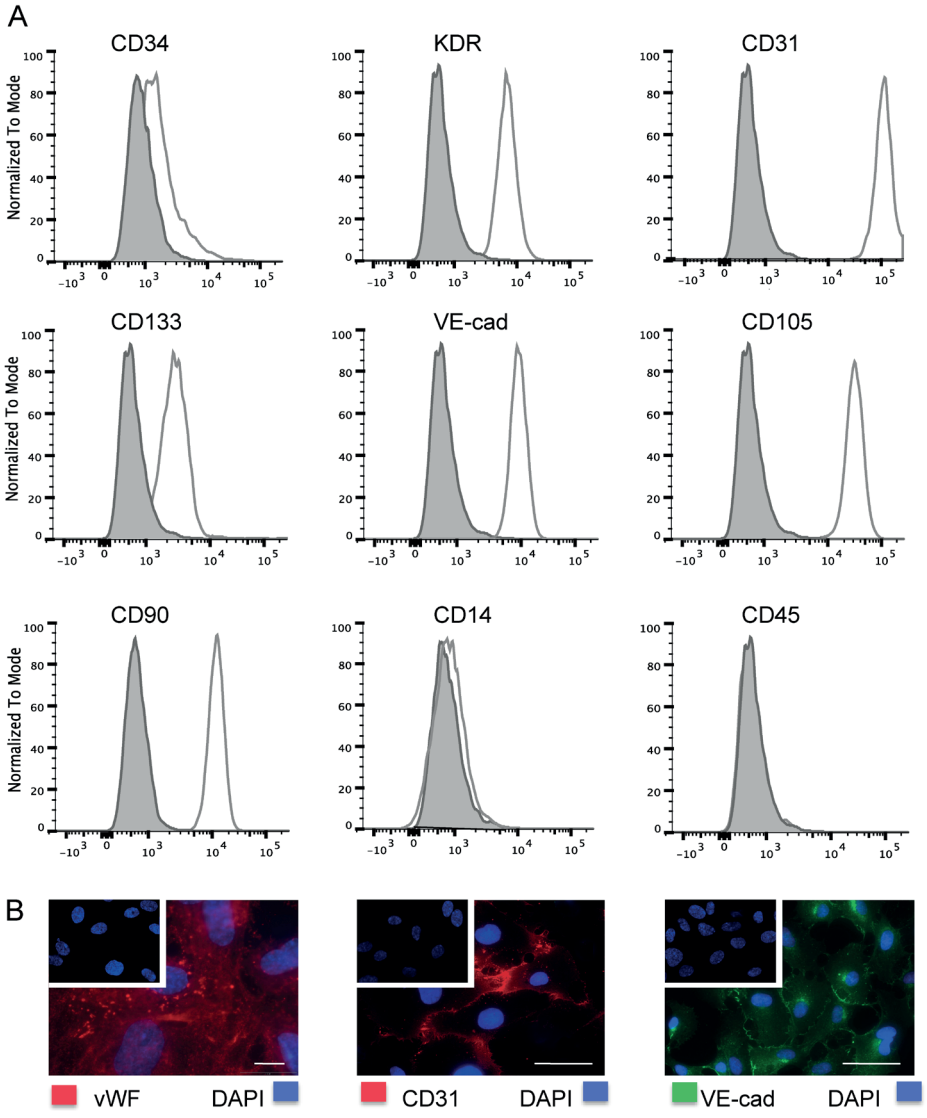

Figure 1. Characterization of human cord blood EPCs.

A: Cytometric analysis of cultured EPCs for markers CD34, KDR (VEGFR-2), CD31, CD133, VE-cadherin (CD144), CD105, CD90, CD14 and CD45. Open histograms represent cells stained with specific antibodies while solid histograms correspond to isotype-matched control antibodies. One representative donor profile of the 3 donors is shown. B: Expression of vWF (red), CD31 (red) and VE-cadherin (green), in confluent monolayers. Immunofluorescence stainings, nuclei stained by DAPI (blue). Insets of isotype-matched control Ab stainings. Scale bars = 50 µm.

RESULTS

Characterization of EPCs from umbilical cord blood (cb-EPCs)

EPCs were isolated from human umbilical cord blood, expanded and characterized as shown in figure 1. Flow cytometric analysis shows that progenitor cell markers CD34, CD105, CD133, and endothelial cell markers CD31, CD144 (VE-cadherin), CD90 and KDR (VEGF-R2) were present and leukocyte marker CD45 and macrophage/monocyte marker CD14 were absent in the cell population. Cells were positive for von Willebrand Factor (vWF), and showed characteristic membrane-bound staining for CD31 and VE-cadherin on immunofluorescence staining. These findings confirm that the cells are late outgrowth EPCs.

VEGF release from GMPs

GMPs were produced in a size range of 75-125 µm, based on release profiles from previous experiments [23]. Using light microscopy it was shown that the macroparticles are uniform in shape. Endotoxin levels were low (0.03±0.02 EU/mg GMP), remaining well under the FDA accepted range. VEGF was incorporated into the Matrigel (fast release) or into the GMPs by diffusional loading which were then dispersed in Matrigel plugs (slow release) and incubated in PBS/ 0.5% BSA for release measurements. PBS/ 0.5% BSA was refreshed at multiple time points and VEGF concentrations (free VEGF, no longer interacting with the GMPs) were determined with ELISA. In figure 2 the cumulative release profiles of slow and fast VEGF groups are shown. VEGF release was prolonged and more gradual in the slow release group compared to the fast release group. VEGF was

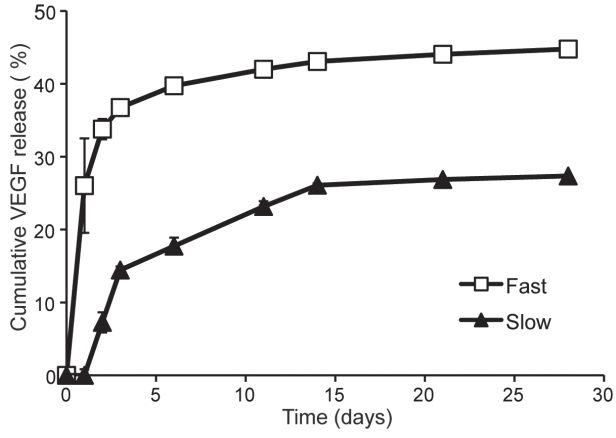

Figure 2. Cumulative release of VEGF.
Fast (directly incorporated in Matrigel) and slow release (application of GMPs) of VEGF measured in PBS /0.5% BSA, analyzed with ELISA. Data represent mean ± SD for n=3.

continuously released for at least 2 weeks at concentrations relevant for vasculogenesis (The ED_{50} of VEGF is typically 1-6 ng/ml) [31]. This indicated that the combined application of GMPs embedded in Matrigel plugs is a suitable system for prolonged VEGF release.

In vitro effectivity of GMP-released VEGF

To establish biological activity of the GMP-released VEGF, migration assays were performed. Migration was assessed using a traditional endpoint measurement chemotaxis set-up and also by real-time migration assays. A statistically significant ($p<0.01$) dose-dependent migration of EPCs towards VEGF is seen in both assays (Fig. 3.), with a peak migration observed at 50 to 100 ng/ml VEGF. Increasing growth factor concentration did not lead to higher cell migration. The VEGF-stimulated migration of EPCs is similar for fast VEGF (added to the medium) and slowly released VEGF (from GMPs). Migration data measured by endpoint cell counting (gold standard) were similar to real-time measurements. Additionally, real-time migration data reveal that EPC migration mainly takes place after 4 to 8 hours of incubation.

3D bioprintable hydrogel selection

To optimize Matrigel for 3D bioprinting applications and accelerate cross-linking after 3D bioprinting, it was supplemented with alginate 3% (w/v) at different ratios. Formation of vascular networks was assessed with EPCs from 4 donors on different hydrogel mixture ratios. Incubation with Matrigel led to formation of vascular complexes throughout the microwell (Figure 4A). When pure alginate was used, large cell aggregates were visible, no vascular complexes were formed (Figure 4C). The addition of alginate to Matrigel reduced the number of vascular complexes and branching points, depending on the alginate concentration (Figure 4D,E). Some complex formation was seen in the hydrogel mixtures, but this was lower compared to Matrigel only. The addition of alginate enhanced the compressive modulus, which enabled 3D bioprinting (Figure 4F-K). To allow both EPC functioning and bioprinting, the mixture with the lowest rate of alginate that was still printable was selected. As a result, the heterogeneous 3D bioprinted scaffolds for the *in vivo* experiment consisted of a mixture of Matrigel/alginate = 3/1.

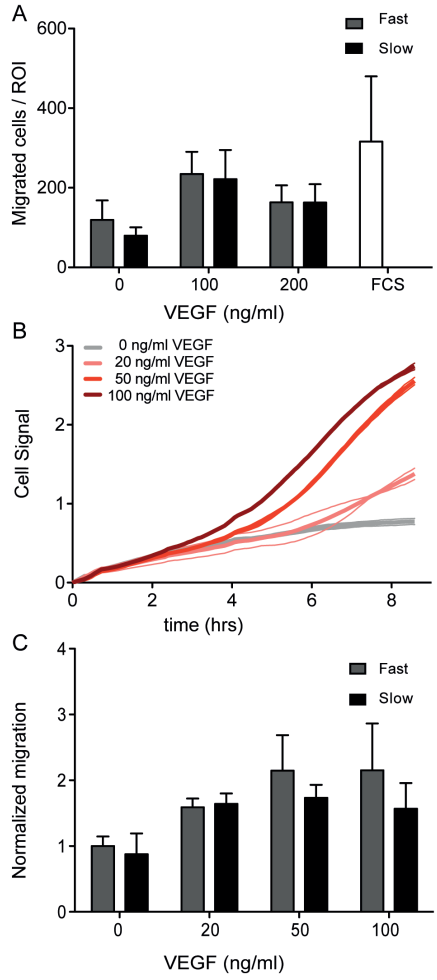

Figure 3. Real-time and conventional migration assays of EPCs towards VEGF.
Cells were seeded in the inserts; VEGF was released from GMPs (slow) or added directly to the wells (fast). Performed in triplicate, data represent mean ± SD for 3 donors. A: Transwell migration assay, the number of migrated cells was assessed after 24 hours of incubation. Migration towards serum (FCS) was included as a positive control. B: Real-time cell index signal (calculated from impedance measurement) depicting time-dependent migration of one EPC donor towards fast released VEGF. C: Concentration effects were statistically significant for both slow and fast groups; cell migration was normalized to migration towards vehicle.

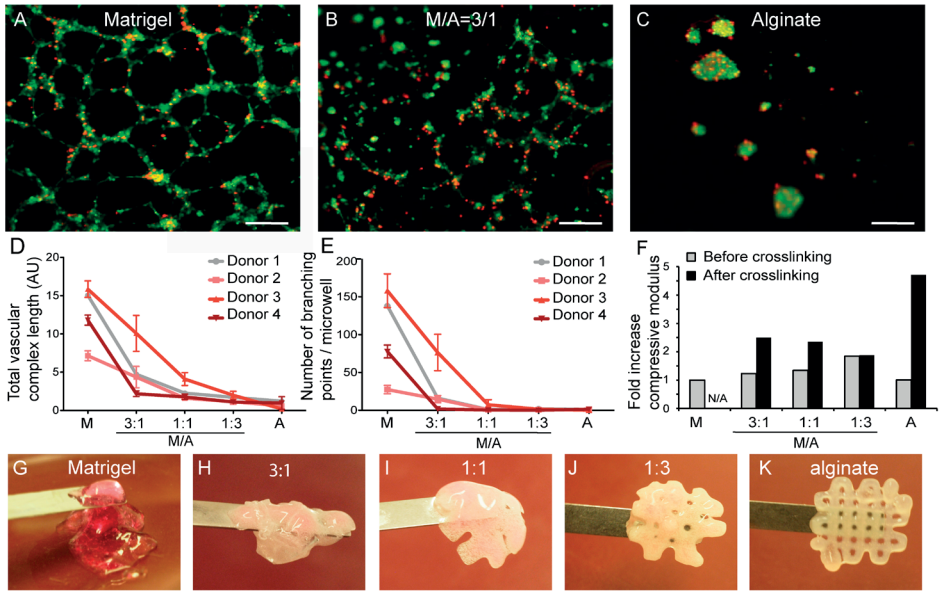

Figure 4. Selection of optimal printable hydrogel mixture by tubulogenesis assay.
A-C: Tubulogenesis of EPCs after 24 hours of incubation on hydrogels, as follows: Matrigel (A), Ratio Matrigel/alginate of 3:1 (B), alginate 3% (C). Scale bar = 200 µm. D: Total vascular complex length for different gel mixture ratios. E: Number of branching points for different gel mixture ratios. Performed in triplicate for donor 2-4, donor 1 performed once, data quantification with Angioquant, presented as mean ± SD. F. Compressive moduli of the gel mixtures, before and after $CaCl_2$-crosslinking. G-K Printability of the hydrogel mixtures showing how the printability increases with the addition of alginate to the Matrigel.

Role of controlled release of VEGF on vessel formation *in vivo*

After selecting the Matrigel/alginate=3/1 hydrogel mixture for 3D bioprinting, scaffolds, as described in M&M were implanted subcutaneously in mice for *in vivo* analysis of vessel formation. After one week of implantation scaffolds were retrieved and paraffin embedded. Presence of GMPs throughout the Matrigel and different amounts of vessel formation were observed in HE stained sections. It was clear that the 3D bioprinted scaffolds were disintegrating faster than the Matrigel plugs, most likely due to the faster dissolving hydrogel mixture combined with scaffold porosity. Cell groups were often seen surrounding the GMPs, which were identified as human EPCs by immunohistochemical staining against CD31. Mouse EPCs were identified by specific anti CD31 staining, mainly surrounding the vessels between the GMPs (Figure 5G,H). αSMA staining on the newly formed vessels remained negative, indicating that the formed vessels are not mature yet (Figure 5I). A Goldner's trichrome staining was performed to localize erythrocytes-perfused vessels. Quantification of the perfused vessels in the different groups revealed that slow release of VEGF led to a significant increase in vessel formation ($p<0.01$, Figure 5) when compared to fast release of VEGF, or the control group without growth factor. In the 3D bioprinted scaffolds disintegration and deformation have hindered the quantita-

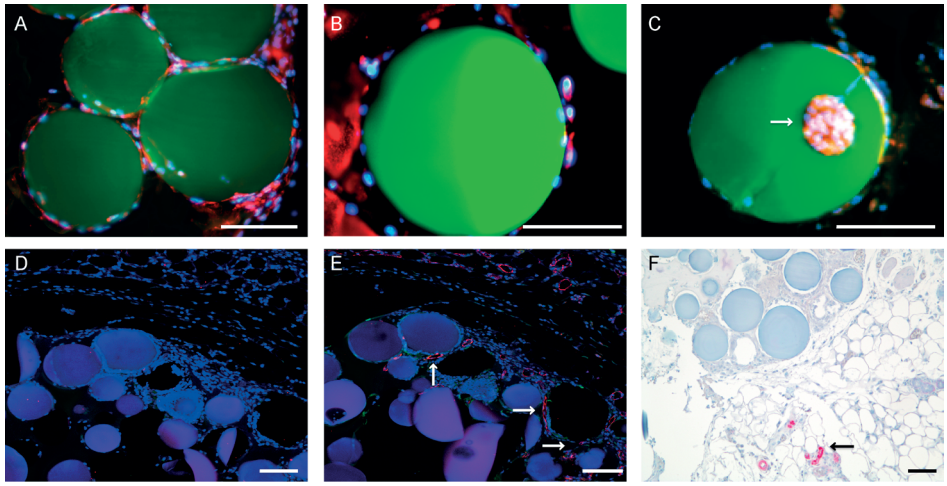

Figure 5. Vessel formation in hEPC seeded scaffolds after a week of subcutaneous implantation in mice.

A: Quantification of vessel formation, number of vessels per 100 μm^2 is depicted. B,C: Goldner's trichrome staining, representative pictures from fast (B) and slow release groups (C) are shown. D-F: CD31 (PECAM-1) staining, human and murine cells stain brown. G. Fluorescent anti human CD31 staining, positive signal in red. H. Fluorescent anti mouse CD31 staining, positive signal in red. I. αSMA staining, only staining mature vessels in subcutaneous tissue (arrow), not the newly formed vessels in the scaffold. Presence of GMPs is indicated with an asterisk in the micrographs. Blood vessels are indicated with arrows. Scale bars = 50 μm.

tive analysis, but the two distinct regions could still be discriminated after explantation. It appears that control regions (without GMP or VEGF) contained hardly any vessels, and in regions of slowly released VEGF, more vessel formation was seen (Figure 6). These findings are in accordance to our observations in the Matrigel plugs. The overall vessel formation is lower in the 3D bioprinted constructs than in the Matrigel plugs, most likely due to alteration of the hydrogel properties that result from alginate addition.

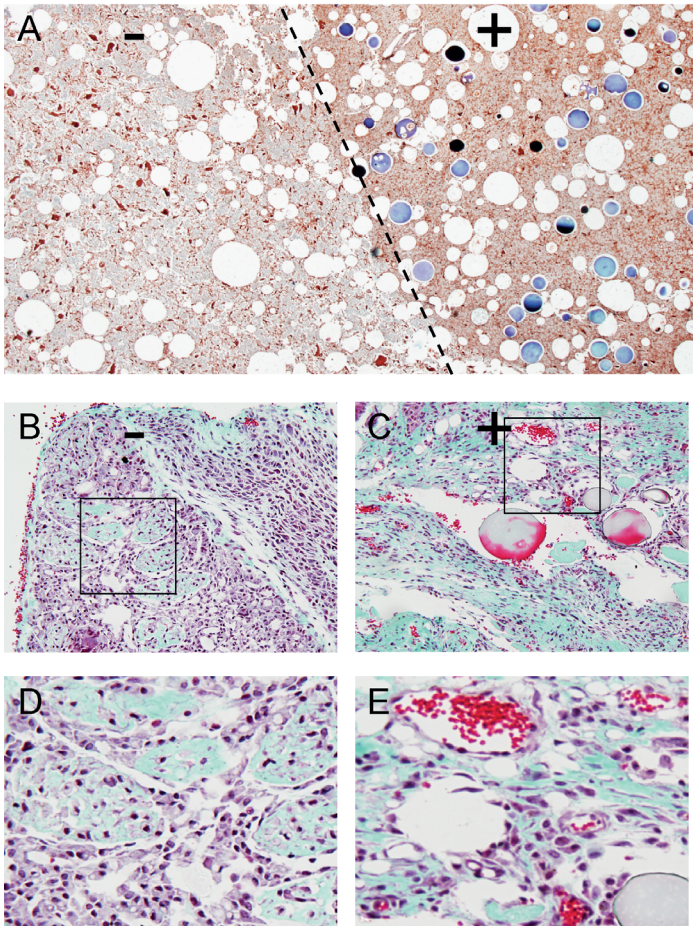

Figure 6. Bioprinted, hEPC-laden, heterogeneous scaffolds.
A. Regionally defined scaffold directly after 3D printing. The two regions (- without VEGF, + VEGF-laden GMPs) are indicated by the dotted line. GMPs stained blue. HE staining, scale bar = 500 µm. B-E: Vessel formation in regionally defined scaffold after one week of *in vivo* implantation, sections stained with Goldner's trichrome. B: No vessel formation in control part of the scaffolds (no VEGF). C: Perfused vessels in region with VEGF from GMP (slow release) part of scaffolds. D, E: details from B and C respectively (inset region). Scale bars = 100 µm.

DISCUSSION

Slow release of VEGF from GMPs led to a significant increase in the number of perfused vessels in a human EPC containing Matrigel plug compared to fast VEGF release or control group in a vascular ingrowth model. When the VEGF-laden GMPs were regionally applied in 3D bioprinted scaffolds with defined architecture this effect was seen locally, more vessels were present in GMP-containing regions.

In this study, umbilical cord EPCs were used to assess the effect of prolonged VEGF presence. From previous studies it is known that without these cells hardly any vessel formation would occur in ectopic constructs. In the formation of new capillaries by endothelial cells VEGF stimulation is necessary and sufficient, through its actions on both endothelial cells and myeloid cells. In this study, with high VEGF concentrations, these vessels will remain leaky and sinusoidal due to negative regulation of pericytes, but they are well perfused. In our GMPs the amount of VEGF is finite (in contrast to for instance VEGF plasmids), once it is exhausted we expect a slow recruitment of pericytes and the formation of a more mature vasculature [32]. EPCs are considered an interesting (autologous) cell source in regenerative medicine [33], as they can be harvested from a patient's peripheral blood. However, ageing effects when culturing EPCs are seen, mainly for EPCs harvested from adults [34]. To avoid loss of vessel formation potency of the EPCs, the current experiment was performed after a minimal number of passages (3-5) [35].

The VEGF release data shown in this article are *in vitro* release data. We know from literature that *in vivo* release rates can be significantly faster than *in vitro* release rates due to higher enzymatic activities [36,37]. We aimed to compensate for faster release by using the GMPs that showed continuous release for three weeks *in vitro*, in an *in vivo* experiment that lasted only one week. After 3 weeks of *in vitro* release, only 50% of the total VEGF that was loaded into the Matrigel plugs was accounted for. It is known from literature that VEGF does not remain stable in solution [11,38]. This protein degradation could explain our low retrieval rate. The amount of released VEGF that was measured by ELISA however is more than the ED_{50}, so it is relevant for vasculogenesis. Furthermore, EPC migration towards the released VEGF took place. Migration assays showed that the biological activity of GMP-released VEGF was intact, which is in accordance to literature on GMPs [16]. Real-time migration measurement has benefits when compared the traditional Transwell chamber, as it provides insight in migration patterns over time [39]. EPC migration towards VEGF already started after a few hours of incubation, therefore, application of GMPs was particularly suitable since diffusion of VEGF out of the GMPs started immediately. Many other release vehicles, such as PLGA, have a shell of material that has to degrade in order for the protein to be released, after which a larger burst release occurs, compared to GMPs [26].

When the EPCs and GMPs were embedded into hydrogel plugs and subsequently implanted subcutaneously in mice, prolonged presence of VEGF led to a significant increase in scaffold vascularization compared to fast release or control groups. This is in accordance with literature regarding VEGF release from other delivery systems such as nanoparticles or PLGA microspheres [14,37,40]. When alginate is added to Matrigel the hydrogel mixture can be bioprinted, and GMPs can be used to generate defined differentiation regions in heterogeneous constructs. Alginate addition led to faster hydrogel degradation, which hindered quantitative analysis of vessel formation in these scaffolds,

but regional differences were clearly visible. Also, the overall number of vessels appeared to decrease when alginate was added, compared to Matrigel alone, implicating that the hydrogel used for bioprinting could be improved with respect to gelation time, cell attachment and degradation speed. Combining bioprinting with controlled growth factor release allows scaffold properties to be fine-tuned in a temporal as well as a spatial manner. This is an important step in smart scaffold design, as it enables researchers to reach a higher level of biomimicry.

CONCLUSION

GMPs are suitable to generate sustained release profiles of bioactive VEGF, and are effectively used to generate defined differentiation regions in 3D bioprinted heterogeneous constructs. The prolonged presence of VEGF led to a significant increase in scaffold vascularization when applied in vivo.

REFERENCES

1. Levenberg S, Rouwkema J, Macdonald M, Garfein ES, Kohane DS, Darland DC, Marini R, van Blitterswijk CA, Mulligan RC, D'Amore PA, Langer R. Engineering vascularized skeletal muscle tissue. *Nat Biotechnol 2005;23-7:879-84*.
2. Laschke MW, Harder Y, Amon M, Martin I, Farhadi J, Ring A, Torio-Padron N, Schramm R, Rucker M, Junker D, Haufel JM, Carvalho C, Heberer M, Germann G, Vollmar B, Menger MD. Angiogenesis in tissue engineering: breathing life into constructed tissue substitutes. *Tissue Eng 2006;12-8: 2093-104*.
3. Asahara T, Takahashi T, Masuda H, Kalka C, Chen D, Iwaguro H, Inai Y, Silver M, Isner JM. VEGF contributes to postnatal neovascularization by mobilizing bone marrow-derived endothelial progenitor cells. *EMBO J 1999;18-14:3964-72*.
4. Ingram DA, Caplice NM, Yoder MC. Unresolved questions, changing definitions, and novel paradigms for defining endothelial progenitor cells. *Blood 2005;106-5:1525-31*.
5. Critser PJ, Yoder MC. Endothelial Colony Forming Cell role in neoangiogenesis and tissue repair. *Curr Opin Organ Transplant 2010;15-1:68-72*.
6. Gremmels H, Fledderus JO, van Balkom BW, Verhaar MC. Transcriptome analysis in endothelial progenitor cell biology. *Antioxid Redox Signal 2011;15-4:1029-42*.
7. Yoder MC, Mead LE, Prater D, Krier TR, Mroueh KN, Li F, Krasich R, Temm CJ, Prchal JT, Ingram DA. Redefining endothelial progenitor cells via clonal analysis and hematopoietic stem/progenitor cell principals. *Blood 2007;109-5:1801-9*.
8. Critser PJ, Yoder MC. Endothelial colony-forming cell role in neoangiogenesis and tissue repair. *Curr Opin Organ Transplant 2010;15-1:68-72*.
9. Santos MI, Reis RL. Vascularization in bone tissue engineering: physiology, current strategies, major hurdles and future challenges. *Macromol Biosci 2010;10-1:12-27*.
10. Ferrara N, Gerber HP, LeCouter J. The biology of VEGF and its receptors. *Nat Med 2003;9-6:669-76*.
11. Eppler SM, Combs DL, Henry TD, Lopez JJ, Ellis SG, Yi JH, Annex BH, McCluskey ER, Zioncheck TF. A target-mediated model to describe the pharmacokinetics and hemodynamic effects of recombinant human vascular endothelial growth factor in humans. *Clin Pharmacol Ther 2002;72-1:20-32*.
12. Stein I, Neeman M, Shweiki D, Itin A, Keshet E. Stabilization of vascular endothelial growth factor mRNA by hypoxia and hypoglycemia and coregulation with other ischemia-induced genes. *Mol Cell Biol 1995;15-10:5363-8*.
13. Kempen DH, Lu L, Heijink A, Hefferan TE, Creemers LB, Maran A, Yaszemski MJ, Dhert WJ. Effect of local sequential VEGF and BMP-2 delivery on ectopic and orthotopic bone regeneration. *Biomaterials 2009;30-14:2816-25*.
14. Formiga FR, Pelacho B, Garbayo E, Abizanda G, Gavira JJ, Simon-Yarza T, Mazo M, Tamayo E, Jauquicoa C, Ortiz-de-Solorzano C, Prosper F, Blanco-Prieto MJ. Sustained release of VEGF through PLGA microparticles improves vasculogenesis and tissue remodeling in an acute myocardial ischemia-reperfusion model. *J Control Release 2010;147-1:30-7*.
15. Ikada Y, Tabata Y. Protein release from gelatin matrices. *Adv Drug Deliv Rev 1998;31-3:287-301*.
16. Patel ZS, Ueda H, Yamamoto M, Tabata Y, Mikos AG. In vitro and in vivo release of vascular endothelial growth factor from gelatin microparticles and biodegradable composite scaffolds. *Pharm Res 2008;25-10:2370-8*.
17. Patel ZS, Young S, Tabata Y, Jansen JA, Wong ME, Mikos AG. Dual delivery of an angiogenic and an osteogenic growth factor for bone regeneration in a critical size defect model. *Bone 2008;43-5: 931-40*.

18. Yamamoto M, Ikada Y, Tabata Y. Controlled release of growth factors based on biodegradation of gelatin hydrogel. *J Biomater Sci Polym Ed 2001;12-1:77-88*.
19. Leeuwenburgh SC, Jo J, Wang H, Yamamoto M, Jansen JA, Tabata Y. Mineralization, biodegradation, and drug release behavior of gelatin/apatite composite microspheres for bone regeneration. *Biomacromolecules 2010;11-10:2653-9*.
20. Yamamoto M, Takahashi Y, Tabata Y. Controlled release by biodegradable hydrogels enhances the ectopic bone formation of bone morphogenetic protein. *Biomaterials 2003;24-24:4375-83*.
21. Cittadini A, Monti MG, Petrillo V, Esposito G, Imparato G, Luciani A, Urciuolo F, Bobbio E, Natale CF, Sacca L, Netti PA. Complementary therapeutic effects of dual delivery of insulin-like growth factor-1 and vascular endothelial growth factor by gelatin microspheres in experimental heart failure. *Eur J Heart Fail 2011;13-12:1264-74*.
22. Liu Q, Zhao SH, Lu MJ, Jiang SL, Yan CW, Zhang Y, Meng L, Tang Y, Meng XM, Wei YJ, Wang LL, Dai HJ, Xu J. [Gelatin microspheres containing vascular endothelial growth factor enhances the efficacy of bone marrow mesenchymal stem cells transplantation in a swine model of myocardial infarction.]. *Zhonghua Xin Xue Guan Bing Za Zhi 2009;37-3:233-9*.
23. Poldervaart MT, Wang H, van der Stok J, Weinans H, Leeuwenburgh SC, Oner FC, Dhert WJ, Alblas J. Sustained Release of BMP-2 in Bioprinted Alginate for Osteogenicity in Mice and Rats. *PLoS ONE 2013;8-8:e72610*.
24. Fedorovich NE, Kuipers E, Gawlitta D, Dhert WJ, Alblas J. Scaffold Porosity and Oxygenation of Printed Hydrogel Constructs Affect Functionality of Embedded Osteogenic Progenitors. *Tissue Eng Part A 2011*.
25. Young S, Wong M, Tabata Y, Mikos AG. Gelatin as a delivery vehicle for the controlled release of bioactive molecules. *J Control Release 2005;109-1-3:256-74*.
26. Patel ZS, Yamamoto M, Ueda H, Tabata Y, Mikos AG. Biodegradable gelatin microparticles as delivery systems for the controlled release of bone morphogenetic protein-2. *Acta Biomater 2008;4-5:1126-38*.
27. Bigi A, Cojazzi G, Panzavolta S, Rubini K, Roveri N. Mechanical and thermal properties of gelatin films at different degrees of glutaraldehyde crosslinking. *Biomaterials 2001;22-8:763-8*.
28. Niemisto A, Dunmire V, Yli-Harja O, Zhang W, Shmulevich I. Robust quantification of in vitro angiogenesis through image analysis. *IEEE Trans Med Imaging 2005;24-4:549-53*.
29. Fedorovich NE, Wijnberg HM, Dhert WJ, Alblas J. Distinct tissue formation by heterogeneous printing of osteo- and endothelial progenitor cells. *Tissue Eng Part A 2011;17-15-16:2113-21*.
30. Schuurman W, Khristov V, Pot MW, van Weeren PR, Dhert WJ, Malda J. Bioprinting of hybrid tissue constructs with tailorable mechanical properties. *Biofabrication 2011;3-2:021001*.
31. Becker PM, Verin AD, Booth MA, Liu F, Birukova A, Garcia JG. Differential regulation of diverse physiological responses to VEGF in pulmonary endothelial cells. *Am J Physiol Lung Cell Mol Physiol 2001;281-6:L1500-11*.
32. Greenberg JI, Cheresh DA. VEGF as an inhibitor of tumor vessel maturation: implications for cancer therapy. *Expert Opin Biol Ther 2009;9-11:1347-56*.
33. Eguchi M, Masuda H, Asahara T. Endothelial progenitor cells for postnatal vasculogenesis. *Clin Exp Nephrol 2007;11-1:18-25*.
34. Ingram DA, Mead LE, Tanaka H, Meade V, Fenoglio A, Mortell K, Pollok K, Ferkowicz MJ, Gilley D, Yoder MC. Identification of a novel hierarchy of endothelial progenitor cells using human peripheral and umbilical cord blood. *Blood 2004;104-9:2752-60*.
35. Melero-Martin JM, Khan ZA, Picard A, Wu X, Paruchuri S, Bischoff J. In vivo vasculogenic potential of human blood-derived endothelial progenitor cells. *Blood 2007;109-11:4761-8*.

36. Kempen DH, Lu L, Hefferan TE, Creemers LB, Maran A, Classic KL, Dhert WJ, Yaszemski MJ. Retention of in vitro and in vivo BMP-2 bioactivities in sustained delivery vehicles for bone tissue engineering. *Biomaterials 2008;29-22:3245-52*.
37. Ennett AB, Kaigler D, Mooney DJ. Temporally regulated delivery of VEGF in vitro and in vivo. *J Biomed Mater Res A 2006;79-1:176-84*.
38. Kleinheinz J, Jung S, Wermker K, Fischer C, Joos U. Release kinetics of VEGF165 from a collagen matrix and structural matrix changes in a circulation model. *Head Face Med 2010;6:17*.
39. Limame R, Wouters A, Pauwels B, Fransen E, Peeters M, Lardon F, De Wever O, Pauwels P. Comparative analysis of dynamic cell viability, migration and invasion assessments by novel real-time technology and classic endpoint assays. *PLoS ONE 2012;7-10:e46536*.
40. des Rieux A, Ucakar B, Mupendwa BP, Colau D, Feron O, Carmeliet P, Preat V. 3D systems delivering VEGF to promote angiogenesis for tissue engineering. *J Control Release 2011;150-3:272-8*.

CHAPTER 4

Combination of bone morphogenetic protein-2 plasmid DNA with chemokine CXCL12 creates an additive effect on bone formation onset and volume

Fiona Wegman
Michelle Poldervaart
Yvonne van der Helm
Cumhur Öner
Wouter Dhert
Jacqueline Alblas

European Cells and Materials (eCM)
2015 Jul 27;30:1-10

ABSTRACT

Bone morphogenetic protein-2 (BMP-2) gene delivery has shown to induce bone formation *in vivo* in cell-based tissue engineering. In addition, the chemoattractant stromal cell-derived factor-1α (SDF-1α, also known as CXCL12) is known to recruit multipotent stromal cells towards its release site where it enhances vascularization and possibly contributes to osteogenic differentiation. To investigate potential cooperative behaviour for bone formation, we investigated combined release of BMP-2 and SDF-1α on ectopic bone formation in mice. Multipotent stromal cell-seeded and cell-free constructs with BMP-2 plasmid DNA and /or SDF-1α loaded onto gelatin microparticles, were implanted subcutaneously in mice for a period of 6 weeks. Histological analysis and histomorphometry revealed that the onset of bone formation and the formed bone volume were both enhanced by the combination of BMP-2 and SDF-1α compared to controls in cell-seeded constructs. Samples without seeded multipotent stromal cells failed to induce any bone formation.

We conclude that the addition of stromal cell-derived factor-1α to a cell-seeded alginate based bone morphogenetic protein-2 plasmid DNA construct has an additive effect on bone formation and can be considered a promising combination for bone regeneration.

INTRODUCTION

Novel strategies are being developed in the field of bone tissue engineering, combining new materials with cell based strategies and growth factor delivery [1,2].

Bone morphogenetic protein-2 (BMP-2) is involved in committing multipotent stromal cells (MSCs) towards the osteogenic lineage and known to induce new bone formation and is therefore considered one of the main growth factors in bone regeneration [3]. In clinical practice large amounts of BMP-2 protein are administered to overcome its fast washout due to degradation by proteinases. These high dosages have recently been under debate due to several serious adverse effects such as vertebral osteolysis, ectopic bone formation, radiculitis and cervical soft tissue swelling [4]. As an alternative for the high dosages of BMP-2 protein, strategies that ensure a prolonged delivery of low, physiological concentrations of BMP-2 are now regarded as favourable. The delivery of growth factors based on plasmid DNA-based (i.e. non-viral) gene therapy is very attractive, as it results in transient expression of the protein, is easy to manipulate and has shown effectivity for bone formation in a number of carriers, known as gene-activated matrices (GAMs). The ideal gene delivery system is biodegradable and non-cytotoxic, and results in a sufficiently high transfection efficiency of the target cells. Recently a focus on several 3D hydrogel matrices, including collagen sponges and polysaccharides has emerged [5], that are suitable for osteogenic differentiation and bone formation. We developed an efficient gene delivery system based on the anionic polysaccharide alginate, which is compatible with simultaneous cell seeding and shows very high transfection efficiencies and effectively induces bone formation when supplemented with BMP-2 plasmid DNA [6]. Combined with other hydrogels or in the form of nanoparticles, alginate has been used to deliver plasmid DNA before [7-9], and was successfully applied in bone tissue engineering applications both *in vitro* and *in vivo* [10,11].

The complexity of bone and its highly vascularized nature demands introduction of multiple biological factors in bone replacement constructs. Besides osteogenic growth factors such as BMP-2, other growth factors such as stromal cell-derived factor-1α (SDF-1α) become increasingly important in the field of bone tissue engineering. SDF-1α is crucial for MSC recruitment to fracture sites and for induction of bone regeneration [12,13]. In addition to homing of cells, SDF-1α has also been shown to induce blood vessel formation *in vitro* as well as *in vivo*, which is crucial in regeneration of bone tissue.

As is known from the literature, the need for construct vascularisation is immediate, and therefore a controlled delivery system such as gelatin microparticles (GMPs) that would release the full amount of SDF-1α in several days is optimal. The main advantage of GMPs is that growth factor can be loaded onto these biocompatible carriers by simple diffusion; no chemical reactions that can damage the fragile growth factor are necessary. Furthermore, the size of the particles combined with the crosslinking density can

tailor the degradation and release rate from the particles [14,15], as shown for SDF-1α [16,17]. In the design of this study, the aim was to prolong the presence of SDF-1α at the scaffold site, but at the same time ensure the presence of biologically relevant concentrations early after implantation, which could be achieved by chosing a particle size that would release the growth factor in a matter of days.

When SDF-1α is combined with BMP-2 protein, a positive effect on bone formation and regeneration has been reported in literature [17-19]. The recruitment of MSCs with SDF-1α or -β towards BMP-2 protein or genetically engineered BMP-2 producing MSCs, induces osteogenic differentiation [20]. When both growth factors are released from a combined construct, a synergistic effect on bone formation has even been reported [17]. The mechanism behind this increased bone formation has been described as a combination of enhanced mobilization and homing of bone marrow-derived osteoprogenitor cells to the implant leading to increased numbers of cells available for bone regeneration at ectopic bone implants [19]. Furthermore, to increase stability and provide a mineralized surface where bone formation can start on, biphasic calcium phosphate (BCP) particles are included in the alginate hydrogel-based ectopic constructs in order to promote efficient bone formation (Fedorovich et al., 2011; Yuan et al., 2010).

This study investigates the ability of SDF-1α protein-loaded gelatin microparticles (G-SDF-1α) to attract MSCs towards the BMP-2 plasmid DNA-laden alginate construct, which could lead to gene expression and subsequent osteogenic differentiation of the cells. Because of the promising results with BMP-2 based gene therapy, and the fact that SDF-1α is a relatively new factor in the field of bone tissue engineering, BMP-2 plasmid DNA is combined with SDF-1α protein.

MATERIALS AND METHODS

Ethics statement

This study was carried out following the Institutional Guidelines under the Dutch Law ("Wet op de dierproeven") on the use of laboratory animals, in accordance with the recommendations in the Guide for the Care and Use of Laboratory Animals of the National Institutes of Health. The study protocol was approved by the Dutch Ethical Committee for Animal Experimentation (Dier Experimentele Commissie, DEC) of the University of Utrecht, the Netherlands (Permit Number: 06/248).

Alginate gel

Autoclaved high-viscosity non-medical-grade alginate powder (International Specialty Products, ISP, Memmingen, Germany) was dissolved at a concentration of 10 mg/ml in alpha minimum essential medium (α-MEM, Gibco, Breda, The Netherlands). The gel was

polymerised by adding an equal volume of 100 mM autoclaved $CaCl_2$ supplemented with 10 mM of 4-(2-hydroxyethyl)-1-piperazineethanesulfonic acid (HEPES) pH 7.4 (Gibco) for 10 minutes. Ca^{2+}-solution was then replaced by expansion medium.

Cell culture

Goat MSCs were isolated from bone marrow (BM), aspirated from the iliac wings of female Dutch milk goats. The MSCs are isolated by adherence to tissue culture plastic and cultured in expansion medium, containing αMEM (Gibco), supplemented with 15% (v/v) fetal calf serum (Cambrex, Charles City, IA, USA), 100 U/ml penicillin, 100 µg/ml streptomycin and 2 mM L-glutamine (Glutamax, Gibco). The cells were maintained at 37°C and 5% CO_2 in a humidified incubator.

Production of gelatin microparticles (GMPs)

Gelatin microparticles (GMPs) were produced using an adapted protocol first described by Y. Tabata et al [21]. In short: hydrated gelatin type B (Sigma, St Louis, MO, USA) was added to refined olive oil (Arcos Organics, NJ, USA) to create a water-in-oil emulsion. The emulsion was stirred, rapidly cooled down, washed with acetone and filtered under pressure. Particles were sieved to obtain a size range of 50-75 µm. Finally the particles were freeze-dried. SDF-1α was dissolved at 200 µg/ml in Tris buffered saline (TBS) supplemented with 1% bovine serum albumin (BSA) and then 10 µl was loaded onto 10 mg microspheres overnight at 4°C by diffusional loading.

Release of SDF-1α from GMPs

SDF-1α release from GMPs was measured after loading 5 µl of SDF-1α-solution (R&D, MN, USA) per sample (n=3) onto 5 mg GMPs to a total amount of SDF-1α (final conc. 100 ng/scaffold). The microspheres were then incorporated into a 100 µl alginate gel (2% w/v) (IMCD, Amersfoort, The Netherlands) that was cross-linked for 5 minutes with 100 mM $CaCl_2$ solution [100 mM aqueous $CaCl_2$ supplemented with 10 mM of 4-(2-hydroxyethyl)-1-piperazineethanesulfonic acid (HEPES) pH 7.4 (Gibco)] to create a plug. $CaCl_2$ was removed and replaced by 1ml TBS/BSA 1% and incubated up to 19 days. At each time point GMPs were centrifuged at 100 g for 5 minutes, supernatant was removed and replaced with 1ml TBS/ BSA 1%. The supernatant was measured using the standard enzyme linked immune sorbent assay (ELISA, R&D) protocol.

Preparation *in vivo* implants

Four different MSC-seeded constructs were made, each consisting of 200 µl alginate (10 mg/ml), 10^7 goat MSCs/ml gel, 20% (w/v) BCP particles (size 106-212 µm) and 10 mg gelatin microparticles (GMPs). The BCP particles consisted of 80%±5% (w/v) hydroxyapatite and 20±5% (w/v) β-tricalcium phosphate, and total porosity was 70±5%, macroporosity

55±5% and microporosity 20±5% (Xpand biotechnology, Bilthoven). The BCP particles were cleaned in an ultrasonic bath and sterilized by autoclave. The BMP-2 plasmid DNA construct contained the full-length human recombinant BMP-2 cDNA, whose expression was driven by the cytomegalovirus promoter in pcDNA3.1 (Invitrogen) [6].

The four different constructs further received: 1) empty GMPs; 2) 10 µg/ml of pBMP-2 and empty GMPs (in short BMP-2); 3) 10 µg/ml of pBMP-2 plus 10 mg GMPs loaded with 2 µg SDF-1α (in short: BMP-2/G-SDF-1α); or 4) 10 mg G-SDF-1α (in short: G-SDF-1α). The alginate constructs were polymerized and implanted the same day. In groups 1 and 2 GMPs were loaded with TBS overnight and added before polymerization, and in group 3 and 4 GMPs were loaded overnight with 10 µl TBS containing 2 µg of SDF-1α, which in literature is considered an optimal dose [19]. All implants were subsequently polymerized with 1 ml of 100 mM autoclaved $CaCl_2$, supplemented with 10 mM of 4-(2-hydroxyethyl)-1-piperazineethanesulfonic acid (HEPES pH 7.4, Gibco), for 10 minutes before implantation. The supernatant was removed and all implants were kept in MSC culture medium until implantation. The four different unseeded constructs were made according to the same protocol except for the addition of goat MSCs.

Animals and implantation

Female nude mice (Hsd-cpb:NMRI-nu, Harlan) were anaesthetized with 1.5% isoflurane, after which 5 separate subcutaneous dorsal pockets per mouse were created. The implants (n=6 per group) were each placed in a pocket with a small surgical spoon and afterwards the skin was sutured back together. The animals were postoperatively treated with the analgesic buprenorphine (0.05 mg/kg, sc; Temgesic, Schering-Plough) and housed together at the Central Laboratory Animal Institute, Utrecht University. Due to ethical reasons female mice were chosen since they can be housed in groups. At 3 weeks after implantation calcein green was administered s.c. (10 mg/kg, Sigma, Zwijndrecht, Netherlands), and at 4 weeks after implantation xylenol orange was administered s.c. (30 mg/kg, Merck, Amsterdam, Netherlands). Six weeks after implantation the animals were terminated by cervical dislocation.

Explantation and embedding

After euthanizing the animals the constructs were retrieved to analyse general morphology, transfection and bone histomorphometry. After a dorsal H-incision samples were clearly visible and dissected from the animals. They were cut in half for processing. One part was fixed overnight in 4% (v/v) formalin containing 100 mM $CaCl_2$ and processed for 5 µm thick decalcified paraffin sections through alcohol dehydration series. The other half was fixed in 4% formalin, dehydrated by ethanol series and embedded in polymethylmethacrylate (MMA), after which 10 µm thick sections were cut from the centre and side of each implant using a sawing microtome (Leica, Nussloch, Germany). These sec-

tions remained unstained for fluorochrome analysis. The presence of each fluorochrome label was scored for all implants.

BMP-2 immunohistochemistry

To detect BMP-2 producing cells in the implants, immunohistochemistry was performed. Sections were permeabilized with Triton X-100 and blocked in 3% H_2O_2 for ten minutes and 5% BSA for 30 min. Sections were washed using Tris buffered saline with 100 mM $CaCl_2$ (TBS/$CaCl_2$). Antigen retrieval was performed using 1 ml Tri Sodium Citrate 2.94g/L which was heated from 37°C – 80°C in 30 min. Cooled down sections were blocked with TBS/$CaCl_2$ with 5% BSA for 30 min at RT. Sections were subsequently incubated with 5 µg/ml rabbit-anti-human BMP2 (LifeSpan Bio, LS-C43125) overnight at 4°C, and as secondary antibody 13 µg/ml goat-anti-rabbit IgG-HRP (Invitrogen, 624320) was incubated for 1 hr at RT. The staining was developed with diaminobenzidine (DAB) and Mayer's hematoxilin was used for counterstaining. All antibodies were diluted in TBS/BSA with $CaCl_2$.

Safranin O staining

Sections were deparaffinised and incubated with hematoxylin (Weigert's) for 5 min. After washing in running tap water, sections were dipped in distilled water and counterstained in 0.4% (w/v) Fast green solution. Sections were rinsed in 0.17 M acetic acid until the colour no longer runs and counterstained again in freshly prepared 0.125% (w/v) Safranin O (Merck) staining dissolved in distilled water. After a short dehydration protocol, sections were mounted in Depex. The staining was performed on duplicate sections. Two independent observers, blinded for the study groups, scored the presence or absence of cartilage.

Bone histomorphometry

High-resolution digital photographs were made from HE stained sections for histomorphometric analysis. From each implant, images from three predefined positions were acquired and analysed in duplicate. Bone and scaffold were pseudo-coloured using Adobe Photoshop CS3, where after histomorphometry was performed using Axiovision software (version 4.8; Zeiss, Nussloch, Germany). A custom macro was used to measure the region of interest, the area of scaffold, and the area of bone. This allowed the quantification of the percentage bone in available space, indicated by bone area% [= (bone area/(total area-scaffold area))*100]. All samples and photographs were analysed blinded by two observers.

Fluorochrome analysis

The fluorochrome markers were analysed from the unstained sections (N=3) using a fluorescence microscope (E600, Nikon) equipped with a quadruple filter block (XF57, dichroic mirror 400, 485, 558, and 640nm, Omega optics, Brattleboro, VT). Fluorochromes incorporated in the newly formed bone were scored for presence/absence. To discriminate between the bone and the underlying scaffold, the fluorescence signal was compared to the bright field signal.

Statistics

The statistical significance of differences between the bone volume percentage of empty GMPs, BMP-2, G-SDF-1α, and BMP-2/ G-SDF-1α groups was assessed using a randomized block design. Multiple comparisons were generated using a LSD post-hoc correction to calculate the p-values. A p-value of < 0.05 was considered significant.

RESULTS

In order to simultaneously deliver the chemokine SDF-1α and the osteogenic stimulus BMP-2, the previously described gene delivery technique where BMP-2 plasmid DNA was incorporated in an alginate hydrogel, which acts as both a transfection agent and controlled release system, was used [6]. This provides a transfection efficiency of around 60% and a long-lasting production and release of BMP-2 up to a period of several weeks. In vivo BCP particles are added as a bone-forming core and in the current study GMPs containing SDF-1α were added to these alginate based BMP-2/BCP containing constructs.

First, the *in vitro* SDF-1α release profile from the alginate plugs was investigated. After 19 days the alginate plugs were still intact and 50% of the loaded protein was gradually released from the plugs (Figure 1).

Subsequently, GMP containing constructs were implanted subcutaneously in mice for 6 weeks to investigate whether host MSCs can be recruited to cell-free constructs via chemokine attraction. These could possibly be transfected with the plasmid DNA, produce BMP-2 as a result of the transfection and eventually induce bone formation. This process might be optimized and accelerated since vascularization, important for bone formation can be stimulated by SDF-1α as well [22].

MSC seeded constructs are also implanted to investigate whether bone formation can be enhanced due to a synergistic effect of the BMP-2/G-SDF-1α combination [17]. After explantation and processing the general morphology of both seeded and unseeded samples was determined by several histological stainings such as hematoxylin/eosin (HE), Safranin O and basic fuchsin/methylene blue. In the unseeded constructs no dif-

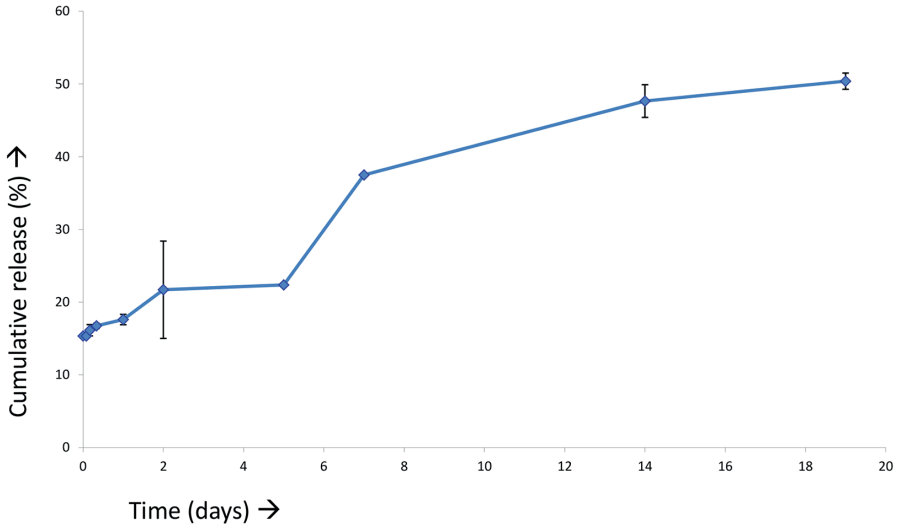

Figure 1. Cumulative release of SDF-1α from GMPs.
Cumulative release of SDF-1α from GMPs in a 200µl alginate plug into TBS/BSA over a period of 19 days. Data are given as mean ± SD for n=3.

ferences could be detected in scoring of vessel-like structures, number of recruited cells or fibrous tissue formed around the BCP particles (Figure 3a, b). All groups, both seeded and unseeded, contained some samples with remnants of the alginate present (Figure 3c, d). However, no presence of the GMPs was detected. Furthermore no signs of an inflammatory response were present. Fibrous capsule formation was hardly present and if detected, presented with a maximum of 5 cell layers thick. In terms of bone formation, all unseeded samples with or without the presence of BMP-2 or SDF-1α lacked any signs of bone formation. The MSC-seeded experimental setup however did result in bone formation. Therefore we will focus on the results from the MSC seeded samples and mainly discuss the results for tissue responses, onset of bone formation and bone histomorphometry in the following paragraphs.

To determine possible differences in bone formation onset, fluorochrome incorporation was analysed. Except for the BMP-2/G-SDF-1α group and one sample in the BMP-2 group, no fluorochromes were detected (Figure 2). Since hardly any of the week 3 and week 4 labels where present in the constructs, the onset of bone formation must have been between week 4 and 6 after implantation in most animals. In the BMP-2/G-SDF-1α group however, 33% of the samples contained the orange label, but not the green 3 week label. This indicates that bone formation occurred between week 3 and week 4 in these samples, which is earlier than the bone onset in the single growth factor groups (Figure 2).

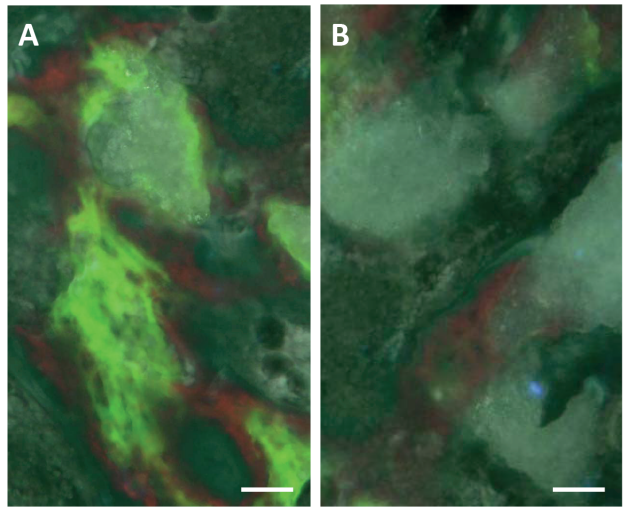

	Week 3	Week 4
Empty GMPs	0	0
BMP-2	0	17
G-SDF-1α	0	0
BMP-2/G-SDF-1α	33	67

Figure 2. Bone onset analysed by fluorochrome analysis.
Detection of Calcein green, administered at week 3 after implantation and Xylenol orange, administered at week 4 after implantation. a) Combined BMP-2/G-SDF-1α sample displaying both the 3 and 4 week label. b) Empty GMP or G-SDF-1α sample, no fluorochromes present. The percentage of samples containing the fluorochrome is listed. Scale bar represents 25 μm.

To investigate not only the onset but also the amount of newly formed bone as a result of combined SDF-1α and BMP-2 release, matrix and bone formation have been analysed by histomorphometry. In contrast to microCT, this allows discrimination between bone and ceramic scaffold. In the BMP-2/G-SDF-1α constructs abundant collagen I staining was seen compared to the empty GMP, BMP-2 or G-SDF-1α samples (Figure 3e, f). Besides collagen, BMP-2 was detected in both the control samples and BMP-2/G-SDF-1α constructs, as a result of antibody cross-species reactivity for BMP-2. Nevertheless a higher intensity of BMP-2 staining was present in the samples with BMP-2 plasmid DNA and SDF-1α loaded GMPs (Fig 5), which corresponds well to the amount of bone that was found in these samples. To indicate bone volume differences in the seeded implants, bone histomorphometry was performed on basic fuchsin/methylene blue stained MMA sections for quantification of bone area%, which by extrapolation are indicative of bone volumes (Figure 3g, h). This revealed that all groups contained several samples showing new bone. In the empty GMP samples however very small volumes were detected. In

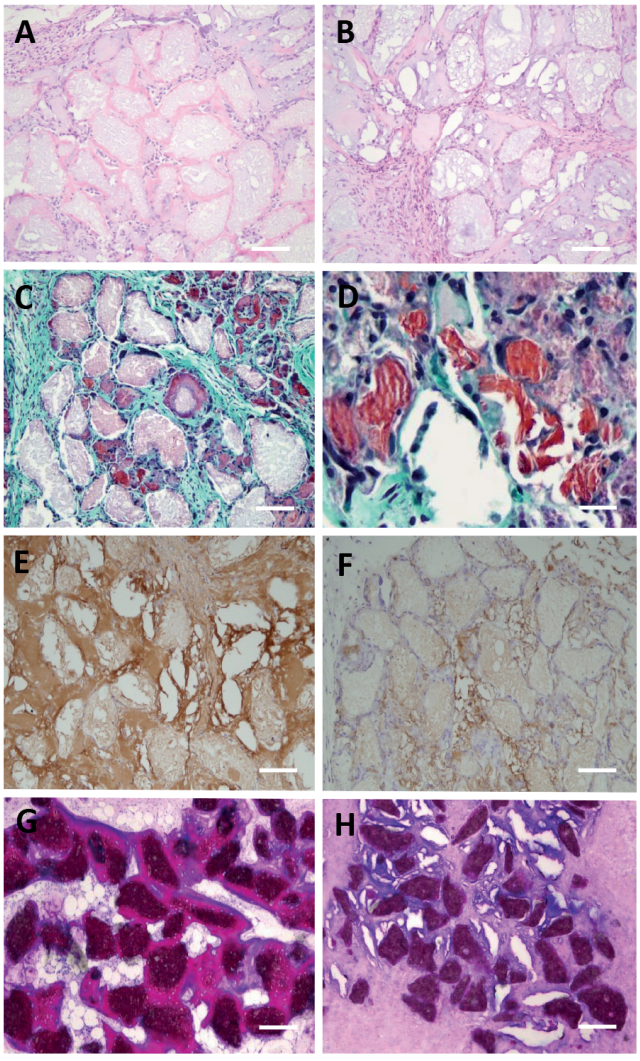

Figure 3. General histology and bone formation of MSC seeded samples.
a, b) HE staining, bone in pink, a)BMP-2/G-SDF-1α sample, b) control sample. c, d) Safranin O staining, fibrous tissue in green, BCP in pink and alginate remains in red. c) representative sample containing alginate remnants, overview. d) representative sample containing alginate remnants, detail. e, f) Collagen I immunocytochemistry (in brown). e) BMP-2/G-SDF-1α sample, f) control sample. g, h) Basic fuchsin/methylene blue staining, bone in pink. g) BMP-2/G-SDF-1α sample, h) control sample. a-c and e-h) Representative samples were chosen for each group, scale bar represents 100 µm, d) scale bar represents 20 µm.

the groups with either BMP-2 or G-SDF-1α bone formation was clearly present. The BMP-2/G-SDF-1α constructs however induced significantly more bone formation compared to the control or single growth factor groups. An average of 6.4 area % was detected (Figure 4).

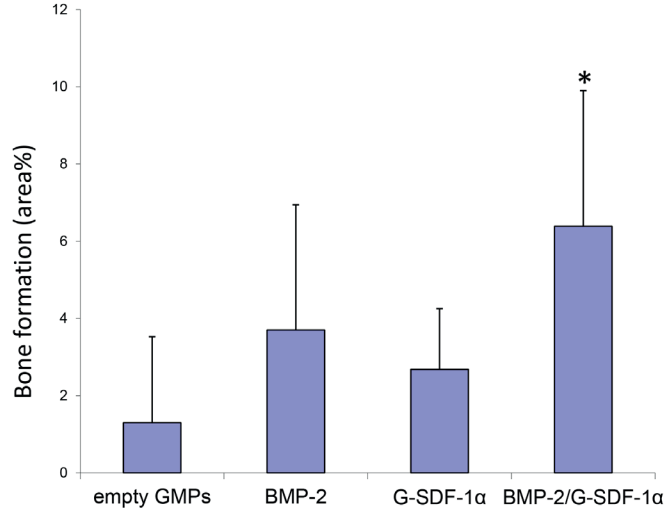

Figure 4. Quantification of bone formation in MSC seeded constructs (3 ROI/ sample, 2 sections per sample, N=6 mice).
Analysis of bone area% (for details see Materials and Methods) after an implantation period of 6 weeks. * = significantly different from control and single growth factor groups, $p<0.05$, data are given as mean ± SD for N=6.

DISCUSSION

This study investigated the use of SDF-1α for bone tissue engineering using alginate/ BMP-2 plasmid DNA laden constructs. Using non-viral plasmid DNA based gene therapy is a promising new strategy to deliver growth factors locally for a longer period of time, without the use of supraphysiological doses [23]. However, most non-viral systems fail to induce high transfection efficiencies. Our previous studies have shown that by using alginate hydrogel, the advantages of using plasmid DNA can be combined with high transfection efficiencies up to 60%. Therefore in this study we investigated the ability of SDF-1α to sufficiently induce the homing of host MSCs towards unseeded BMP-2 plasmid DNA containing alginate constructs. From previous experiments it is known that MSCs are able to take up and express the BMP-2 cDNA, thereby inducing osteogenic differentiation *in vitro* and subsequent bone formation *in vivo*. In this study goat MSCs have been used to be able to proceed to larger animal models such as goats, in order to treat more clinically relevant osteogenic defects in the future. Because immunocompromised mice were chosen, the goat MSCs were not rejected after implantation, and could differentiate towards osteoblasts with subsequent bone formation ectopically. This set-up allows investigating in detail the growth factors (in this case BMP-2 and SDF-1α) that guide bone formation, and perform optimization and feasibility studies before moving to more challenging and costly large animal models.

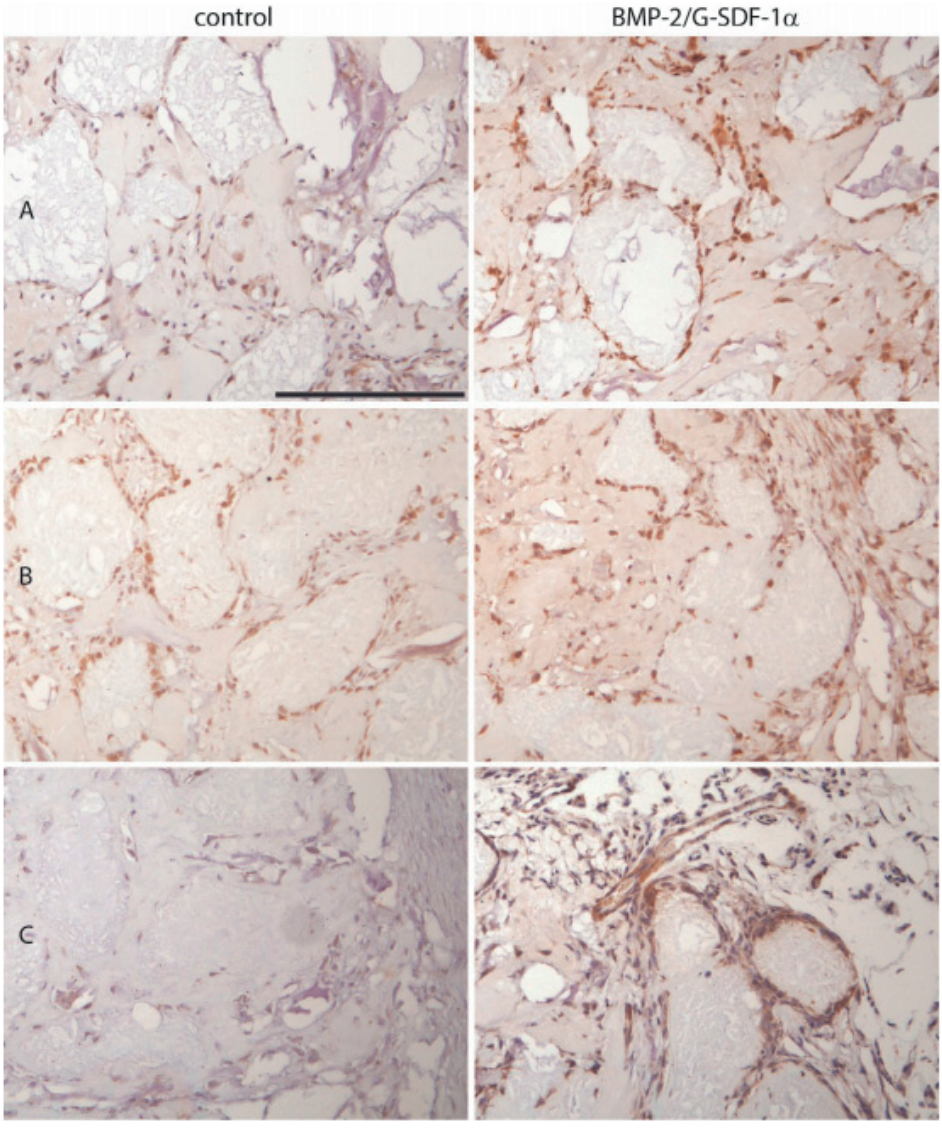

Figure 5. Expression of BMP-2 in MSC seeded constructs.
BMP-2 immunohistochemistry performed on control samples and BMP-2/G-SDF-1α samples after an implantation period of 6 weeks. A,B,C indicate three different mice, scale bar represents 200 μm.

The implanted constructs consisted of alginate plugs combined with BCP particles and GMPs loaded with SDF-1α. The alginate provides the basis of the construct and acts as a transfection agent for BMP-2 plasmid DNA. As known from literature and previous experiments, alginate will degrade within the implantation period of 6 weeks due to an outward flux of the crosslinking ions, allowing a complete growth factor release [24]. The

BCP particles were added to provide a mineralized surface for bone formation to start on. These particles, when combined with MSCs, are known to promote osteogenesis in previous studies [25,26]. The GMPs were chosen as a slow release system for SDF-1α. Microsphere degradation was shown to occur within 28 days *in vitro* when incubated in simulated body fluid (SBF) [27]. When implanted subcutaneously in mice, gelatin microspheres will remain present at least for 4 weeks, during which time they have released the majority of the loaded growth factors [28]. SDF-1α release has been studied *in vivo* before and can be successfully released over a period of 3 weeks from GMPs [16]. Because in this study loaded GMPs are embedded in alginate-based constructs for implantation in mice, release experiments were conducted on these alginate/GMP constructs (Figure 1). Since previous studies showed no influence of BCP on SDF-1α release, this was not included into the experimental setup (data not shown).

After 19 days a sustained release was still apparent. About 50% of all incorporated SDF-1α was released by then (Figure 1). This seems rather slow for a chemokine which is supposed to attract MSCs to the construct directly after implantation. However, *in vivo* release is expected to be faster than *in vitro* release, presumably due to faster degradation of the alginate construct [29]. This is substantiated by the observation that the constructs were completely intact after 19 days of incubation in vitro whereas after in vivo implantation only some fragmented alginate but no GMPs were detected.

In the explanted samples no differences were found in histological scorings of general morphology and immunological processes such as fibrous capsule formation or the presence of multinucleated giant cells (Figure 3a, b). And even though most SDF-1α is thought to be released, no increase in vessel formation was observed in both seeded and unseeded samples at this time point. This finding differs from findings in literature where the presence of SDF-1α increased vessel formation [16,30]. It is possible that the alginate surrounding the GMPs loaded with SDF-1α prevented or delayed vessel ingrowth. Another possibility is that the timeframe of implantation (6 weeks) exceeds the timeframe in which vascular changes can be detected since these are most often seen during early stages of the implantation period. However, the amount of BMP-2 produced by the cells as a result of the addition of BMP-2 plasmid DNA and SDF-1α loaded GMPs appears to be increased. When comparing the results of a BMP-2 immunohistochemistry staining for the control and BMP-2/G-SDF-1α samples (n=3) the staining appears to be darker and present in more cells. Unfortunately it is not possible to discriminate between endogenous BMP-2 and the transgene product, due to cross-species recognition by anti-BMP-2 antibodies. From these results and our previous work ([23,31]) in which we determined BMP-2 production in vitro up to 2 ng/ml, we infer that sufficient amounts of BMP-2 are produced for osteogenicity to occur.

To investigate whether SDF-1α and/or BMP-2 had an effect on the onset of bone formation in cell-seeded constructs, fluorochrome analysis was performed (Figure 2).

Even though we found some bone in the empty GMP and G-SDF-1α laden groups, no fluorochromes were detected with the exception of one sample in the BMP-2 plasmid DNA group, displaying the week 4 label. This indicates that the start of bone formation mainly occurred after the administration of the week 4 fluorochrome but before explantation at week 6. The samples containing both growth factors and expressing the highest amount of bone, showed both the week 3 and week 4 fluorochrome label in several samples. This indicates that the combination of BMP-2 and SDF-1α advances bone onset compared to the other three groups. Bone is first formed sometime around 3 to 4 weeks after implantation. To our knowledge this effect of the combined growth factors has not yet been reported before.

Consistent with the fluorochrome analysis, no bone was present in any of the unseeded constructs. In the in vitro release study we found that SDF-1α was released, however in vivo the constructs contained plasmid DNA as well as BCP granules. It is very unlikely that the presence of BCP affected growth factor release, since the BCP granules had not been soaked in growth factor. Since we know from literature that SDF-1α is able to recruit MSCs [18,22], it is possible that insufficient amounts MSCs have been recruited towards the constructs, and therefore the cell loading limit to obtain bone formation is not reached or the release of SDF-1α exceeded the time frame of implantation [32].

In the MSC-seeded groups, clear differences were observed between all implanted groups. Because BCP particles, known to promote osteogenesis when combined with MSCs, were added to the implanted constructs, some bone had formed in the control samples, which is in accordance with previous results [25,33]. Bone also had formed in the groups containing either BMP-2 plasmid DNA or G-SDF-1α alone, but even though a higher average of bone volume was detected, no significant differences in bone formation occurred compared to the control samples. However, when BMP-2 plasmid DNA and SDF-1α are combined, an in literature described additive effect occurs due to the combination of osteogenic cell recruitment from the circulation with SDF-1α and induction of *in vivo* bone formation in the presence of BMP-2 (Figure 4). This increase in bone formation was consistent with an increase in collagen I (Figure 3e, f). These results confirm previous results describing bone formation as a result of BMP-2 plasmid DNA based bone tissue engineering. BMP-2 is mainly active in the first few weeks of fracture healing, and given the fact that bone formation is induced successfully at an ectopic location, combined with the results of previous in vitro release studies, it is likely that this biological release pattern is approached. SDF-1α is involved in cell recruitment towards an inflammatory site, or the site of release as is the case in this study, and is therefore wanted during the early stages after implantation. SDF-1α could be measured in vitro for a period of at least 19 days, but it is known that *in vivo* growth factor release occurs faster than *in vitro*, due to presence of proteinases [34]. In this experiment we aimed for a presence of SDF-1α during the first 2 weeks after implantation. Based on literature in

which a presence of SDF-1α from a gelatin hydrogel for 21 days *in vivo* has been shown [16], combined to the induced bone formation in our combined growth factor construct we argue that both BMP-2 and SDF-1α have been present for a biologically relevant period of time in this set of experiments.

CONCLUSION

In conclusion, the combination of G-SDF-1α and pBMP-2 plasmid DNA in an alginate based construct induced an additive effect on bone formation, leading to an advanced onset of bone formation and a significantly higher bone volume. This effect was only seen in the presence of seeded MSCs. When SDF-1α was added to cell-free alginate based, BMP-2 plasmid DNA laden construct, osteogenic progenitor cells were not sufficiently recruited from the circulation in order to induce uptake and expression of BMP-2, induce osteogenic differentiation and eventually bone formation in a six weeks implantation period. Therefore we conclude that addition of SDF-1α in the presence of seeded MSCs further optimizes bone regeneration *in vivo* of previously established BMP-2 plasmid DNA-laden alginate constructs.

ACKNOWLEDGEMENTS

Kelly van Deventer is thanked for her contribution to the performed histology.

REFERENCES

1. Asatrian G, Pham D, Hardy WR, James AW, Peault B. Stem cell technology for bone regeneration: current status and potential applications. *Stem Cells Cloning 2015;8:39-48.*
2. Gothard D, Smith EL, Kanczler JM, Rashidi H, Qutachi O, Henstock J, Rotherham M, El Haj A, Shakesheff KM, Oreffo RO. Tissue engineered bone using select growth factors: A comprehensive review of animal studies and clinical translation studies in man. *Eur Cell Mater 2014;28:166-207; discussion -8.*
3. Riley EH, Lane JM, Urist MR, Lyons KM, Lieberman JR. Bone morphogenetic protein-2: biology and applications. *Clin Orthop Relat Res 1996-324:39-46.*
4. Carragee EJ, Hurwitz EL, Weiner BK. A critical review of recombinant human bone morphogenetic protein-2 trials in spinal surgery: emerging safety concerns and lessons learned. *Spine J 2011;11-6: 471-91.*
5. Khan W, Hosseinkhani H, Ickowicz D, Hong PD, Yu DS, Domb AJ. Polysaccharide gene transfection agents. *Acta Biomater 2012;8-12:4224-32.*
6. Wegman F, Bijenhof A, Schuijff L, Oner FC, Dhert WJ, Alblas J. Osteogenic differentiation as a result of BMP-2 plasmid DNA based gene therapy in vitro and in vivo. *Eur Cell Mater 2011;21:230-42; discussion 42.*
7. Krebs MD, Sutter KA, Lin AS, Guldberg RE, Alsberg E. Injectable poly(lactic-co-glycolic) acid scaffolds with in situ pore formation for tissue engineering. *Acta Biomater 2009;5-8:2847-59.*
8. Jain S, Amiji M. Tuftsin-modified alginate nanoparticles as a noncondensing macrophage-targeted DNA delivery system. *Biomacromolecules 2012;13-4:1074-85.*
9. Park DJ, Choi JH, Leong KW, Kwon JW, Eun HS. Tissue-engineered bone formation with gene transfer and mesenchymal stem cells in a minimally invasive technique. *Laryngoscope 2007;117-7:1267-71.*
10. Stevens MM, Marini RP, Schaefer D, Aronson J, Langer R, Shastri VP. In vivo engineering of organs: the bone bioreactor. *Proc Natl Acad Sci U S A 2005;102-32:11450-5.*
11. Hunt NC, Grover LM. Cell encapsulation using biopolymer gels for regenerative medicine. *Biotechnol Lett 2010;32-6:733-42.*
12. Otsuru S, Tamai K, Yamazaki T, Yoshikawa H, Kaneda Y. Circulating bone marrow-derived osteoblast progenitor cells are recruited to the bone-forming site by the CXCR4/stromal cell-derived factor-1 pathway. *Stem Cells 2008;26-1:223-34.*
13. Kitaori T, Ito H, Schwarz EM, Tsutsumi R, Yoshitomi H, Oishi S, Nakano M, Fujii N, Nagasawa T, Nakamura T. Stromal cell-derived factor 1/CXCR4 signaling is critical for the recruitment of mesenchymal stem cells to the fracture site during skeletal repair in a mouse model. *Arthritis Rheum 2009;60-3:813-23.*
14. Berkland C, King M, Cox A, Kim K, Pack DW. Precise control of PLG microsphere size provides enhanced control of drug release rate. *J Control Release 2002;82-1:137-47.*
15. Mladenovska K, Kumbaradzi E, Dodov G, Makraduli L, Goracinova K. Biodegradation and drug release studies of BSA loaded gelatin microspheres. *Int J Pharm 2002;242-1-2:247-9.*
16. Kimura Y, Tabata Y. Controlled release of stromal-cell-derived factor-1 from gelatin hydrogels enhances angiogenesis. *J Biomater Sci Polym Ed 2010;21-1:37-51.*
17. Ratanavaraporn J, Furuya H, Kohara H, Tabata Y. Synergistic effects of the dual release of stromal cell-derived factor-1 and bone morphogenetic protein-2 from hydrogels on bone regeneration. *Biomaterials 2011;32-11:2797-811.*
18. Chim H, Miller E, Gliniak C, Alsberg E. Stromal-cell-derived factor (SDF) 1-alpha in combination with BMP-2 and TGF-beta1 induces site-directed cell homing and osteogenic and chondrogenic

differentiation for tissue engineering without the requirement for cell seeding. *Cell Tissue Res 2012;350-1:89-94*.

19. Higashino K, Viggeswarapu M, Bargouti M, Liu H, Titus L, Boden SD. Stromal cell-derived factor-1 potentiates bone morphogenetic protein-2 induced bone formation. *Tissue Eng Part A 2011;17-3-4:523-30*.
20. Herberg S, Shi X, Johnson MH, Hamrick MW, Isales CM, Hill WD. Stromal cell-derived factor-1beta mediates cell survival through enhancing autophagy in bone marrow-derived mesenchymal stem cells. *PLoS ONE 2013;8-3:e58207*.
21. Young S, Wong M, Tabata Y, Mikos AG. Gelatin as a delivery vehicle for the controlled release of bioactive molecules. *J Control Release 2005;109-1-3:256-74*.
22. Eman RM, Oner FC, Kruyt MMP, Dhert W, Alblas J. Stromal cell-derived factor-1 stimulates cell recruitment, vascularization and osteogenic differentiation. *Tissue Eng Part A 2013*.
23. Wegman F, van der Helm Y, Oner FC, Dhert W, Alblas J. BMP-2 plasmid DNA as a substitute for BMP-2 protein in bone tissue engineering. *Tissue Eng Part A 2013*.
24. Rowley JA, Madlambayan G, Mooney DJ. Alginate hydrogels as synthetic extracellular matrix materials. *Biomaterials 1999;20-1:45-53*.
25. LeGeros RZ, Lin S, Rohanizadeh R, Mijares D, LeGeros JP. Biphasic calcium phosphate bioceramics: preparation, properties and applications. *J Mater Sci Mater Med 2003;14-3:201-9*.
26. Geuze RE, Everts PA, Kruyt MC, Verbout AJ, Alblas J, Dhert WJ. Orthotopic location has limited benefit from allogeneic or autologous multipotent stromal cells seeded on ceramic scaffolds. *Tissue Eng Part A 2009;15-11:3231-9*.
27. Leeuwenburgh SC, Jo J, Wang H, Yamamoto M, Jansen JA, Tabata Y. Mineralization, biodegradation, and drug release behavior of gelatin/apatite composite microspheres for bone regeneration. *Biomacromolecules 2010;11-10:2653-9*.
28. Poldervaart MT, Wang H, van der Stok J, Weinans H, Leeuwenburgh SC, Oner FC, Dhert WJ, Alblas J. Sustained Release of BMP-2 in Bioprinted Alginate for Osteogenicity in Mice and Rats. *PLoS ONE 2013;8-8:e72610*.
29. Kempen DH, Lu L, Heijink A, Hefferan TE, Creemers LB, Maran A, Yaszemski MJ, Dhert WJ. Effect of local sequential VEGF and BMP-2 delivery on ectopic and orthotopic bone regeneration. *Biomaterials 2009;30-14:2816-25*.
30. Jin DK, Shido K, Kopp HG, Petit I, Shmelkov SV, Young LM, Hooper AT, Amano H, Avecilla ST, Heissig B, Hattori K, Zhang F, Hicklin DJ, Wu Y, Zhu Z, Dunn A, Salari H, Werb Z, Hackett NR, Crystal RG, Lyden D, Rafii S. Cytokine-mediated deployment of SDF-1 induces revascularization through recruitment of CXCR4+ hemangiocytes. *Nat Med 2006;12-5:557-67*.
31. Loozen LD, van der Helm YJ, Oner FC, Dhert WJ, Kruyt MC, Alblas J. Bone morphogenetic protein-2 nonviral gene therapy in a goat iliac crest model for bone formation. *Tissue Eng Part A 2015;21-9-10:1672-9*.
32. Wernike E, Montjovent MO, Liu Y, Wismeijer D, Hunziker EB, Siebenrock KA, Hofstetter W, Klenke FM. VEGF incorporated into calcium phosphate ceramics promotes vascularisation and bone formation in vivo. *Eur Cell Mater 2010;19:30-40*.
33. Geuze RE, Wegman F, Oner FC, Dhert WJ, Alblas J. Influence of endothelial progenitor cells and platelet gel on tissue-engineered bone ectopically in goats. *Tissue Eng Part A 2009;15-11:3669-77*.
34. Kempen DH, Lu L, Classic KL, Hefferan TE, Creemers LB, Maran A, Dhert WJ, Yaszemski MJ. Noninvasive screening method for simultaneous evaluation of in vivo growth factor release profiles from multiple ectopic bone tissue engineering implants. *J Control Release 2008;130-1:15-21*.

CHAPTER 5

Growth factor-induced osteogenesis in a novel radiolucent bone chamber

Michelle Poldervaart
Johan van der Stok
Mirthe de Haas
Marieke 't Hart
Cumhur Öner
Wouter Dhert
Harrie Weinans
Jacqueline Alblas

European Cells and Materials (eCM)
2015 Jan 2;29:35-41

ABSTRACT

Treatment of large bone defects is currently performed using mainly autograft or allograft bone. There are important drawbacks to bone grafting such as limited availability, donor site morbidity in the case of autograft and inferior performance of allografts. Therefore, there is a great need for a suitable bone graft substitute. In order to efficiently evaluate newly developed biomaterials and factors intended for orthopedic surgery, the bone chamber is a very suitable model. To allow longitudinal investigation of bone growth with μCT, a new bone chamber made of radiolucent polyether ether ketone (PEEK) was developed and studied for its feasibility. Therefore, PEEK bone chambers were placed on rat tibiae, and filled with vehicle (Matrigel without growth factors, negative controls), with bone morphogenetic protein 2 (BMP-2, positive controls) or a mix of growth factors combining BMP-2, vascular endothelial growth factor (VEGF) and the chemokine stromal cell-derived factor 1α (SDF-1α), all laden on gelatin microspheres (GMP) for controlled release (combined growth factors). Growth factor presence led to a significant increase in bone formation after 8 weeks, which subsided after 12 weeks, underlining the importance of longitudinal analysis. We conclude that the PEEK-bone chamber is a suitable translational animal model to assess orthotopic bone formation in a longitudinal manner.

INTRODUCTION

The majority of large bone defects are currently treated with auto- or allograft bone, which both have important drawbacks such as limited availability of donor bone and donor site morbidity for autograft, whereas allograft bone may lead to inferior performance [1,2]. To reduce the need for auto- or allograft bone, tissue engineered bone constructs have become an important pillar in the field of regenerative medicine. A broad spectrum of biomaterials is currently under investigation in different *in vitro* and *in vivo* models for their suitability to function as a scaffold for bone regeneration [3,4]. One of the *in vivo* models to study a materials' osteopromotive quality is the bone chamber. The main advantages of bone chambers are that they are relatively easy to implant (they are non-weight bearing) and the osteogenicity of biomaterials can be measured as the total amount of bone formed and the bone height reached in the chamber. In the past, many bone chambers were made of titanium [5-8], a very strong and bone-friendly material which however is unsuitable for accurate evaluation of bone formation with micro computed tomography (μCT), as the titanium creates large image artifacts. We developed a new radiolucent bone chamber based on polyether ether ketone (PEEK). PEEK has been used in medical devices and has good mechanical characteristics and biocompatibility [9].

Growth factors are increasingly applied in regenerative medicine to improve construct characteristics. For example, bone morphogenetic protein 2 (BMP-2) is known to induce osteogenesis [10] and can be used in a bone chamber model [11], and application of vascular endothelial growth factor (VEGF) leads to angio- and vasculogenesis [12], whereas the chemokine stromal cell-derived factor 1α (SDF-1α) can attract multipotent stromal cells (MSCs) [13]. Even though SDF-1α is known to play an important role in stem cell homing, its functionality in terms of osteogenic differentiation in tissue engineered constructs *in vivo* is not clear [14]. Some authors have reported a synergistic effect of SDF-1α addition to BMP-2 laden scaffolds [15,16]. These growth factors, that have short half-life times, can be laden on gelatin microspheres (GMP) for controlled release to ensure a prolonged presence [17]. Gelatin is a natural product that is used in many FDA-approved devices. Growth factor encapsulation in GMPs is based on electrostatic interactions with the gelatin as well as the gelatin degradation rate [17-20]. The main advantages of the GMPs are the diffusional loading of growth factors and the non-covalent nature of the interaction between gelatin and growth factor, thus avoiding chemical reactions that could damage the protein. Furthermore, GMPs are non-cytotoxic, biodegradable and they have previously been used to deliver growth factors such as BMP-2, TGFβ1 and FGF [21,22].

The aim of this study was to investigate the applicability and effectivity of the PEEK bone chamber as a model to monitor orthotopic bone formation in a longitudinal manner. To that end, bone chambers were bilaterally implanted in the tibiae of rats, and

growth factor induced bone formation was measured at multiple time points with *in vivo* µCT scans.

MATERIALS AND METHODS

Study design

Objective of this study is to investigate the applicability and effectivity of the PEEK bone chamber model to monitor orthotopic bone formation in a longitudinal manner. To that end, a controlled laboratory experiment was performed. Bone chambers were bilaterally implanted in the tibiae of rats, and growth factor-induced bone formation was measured at multiple time points using *in vivo* µCT. All samples were randomly allocated, and implanted and analyzed by researchers that were blinded for the experimental groups.

Study endpoints and statistical methods were prospectively selected and documented. Sample size was calculated with a power analysis to achieve reliable measurement of the effect, this number did not change in the course of the study. The standard guidelines for humane endpoints in animal experiments were applied, none of the animals met these criteria. All data were included in the analysis, no outliers were detected.

Bone chamber preparations

The experimental design is depicted in Table 1. Bone chambers were placed bilaterally on the tibiae of 10 rats, then filled with 20 µl Matrigel (growth factor-reduced, BD cat no. 354230, New Jersey, USA, negative controls), 20 µl Matrigel with 100 µg/ml BMP-2 (BMP-2, positive controls) or 20 µl Matrigel with 100 µg/ml BMP-2, 25 µg/ml VEGF and 25 µg/ml SDF-1α (combined growth factors), each laden on gelatin microspheres (GMP) for sustained release. Combined growth factor containing chambers (n=10) were implanted in one tibia, and were matched with either a positive (n=5) or negative control (n=5) chamber in the other tibia of the animal to allow paired data analysis.

Production of the bone chambers

The design of the PEEK bone chamber was an adaptation to the titanium bone conduction chamber (BCC) developed by Aspenberg *et al.* [23], that consists of two parts. The inner part is a cylindrical chamber of 7 x 2 mm Ø (≈ 22 mm^3), covered by a cap (Figure 1) to create a confined chamber. Both parts were produced from solid PEEK plates (Vink Kunststoffen, Didam, the Netherlands). The design files of the PEEK bone chambers can be obtained by contacting the corresponding author.

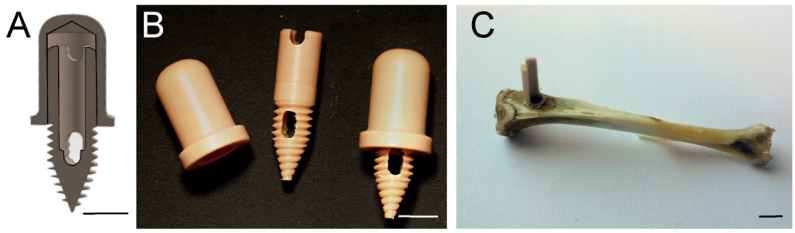

Figure 1. The PEEK bone chamber.
A. Design of the bone chamber. B. PEEK bone chambers, cap, screw and assembled chamber. C. Placement of the bone chamber (cutaway model). Scale bars represent 3 mm.

Surgical technique / animals and operations

Animal experiments were performed with permission of the Animal Ethical Committee of the Erasmus University for Animal Experimentation in compliance with the Institutional Guidelines following the Dutch Law ('Wet op de dierproeven') on the use of laboratory animals. Ten male Wistar rats (Charles River), 16 weeks of age were housed in standard cages at the Laboratory Animal Institute. Prior to surgery, a single dose of antibiotics (enrofloxacin, 5 mg/kg body weight) was administered. Operations were performed aseptically under general anaesthesia (1–3.5% isoflurane).

Implantation of bone chambers

Rats were placed in supine position, both medial knee regions were shaved and disinfected. An elastic band, placed in the groin region, functioned as a tourniquet in order to temporarily reduce blood flow to the operated leg. Subsequently a 1 cm longitudinal incision was made over the medial plane of the proximal tibia. Underlying fascia and muscles were gently pushed to the medial side until the bone was fully exposed. A guiding hole was drilled with a thin bone drill (0.7 mm Ø) approximately 2 mm below the proximal growth plate and 1 mm anterior to the insertion of the semitendinosis and gracilis tendons. The guiding hole was enlarged up to 2 mm Ø by using 1, 1.5, and 2 diameter drill bits. Then the bone chambers were screwed into the hole until the side openings reached the height of the adjacent cortex. After placement the chambers were filled according to a randomized scheme. The cap was placed over the bone chamber before the skin was sutured using Vicryl 4-0. Postoperatively the animals were weighed and given a subcutaneous injection of buprenorphin (0.05 mg/kg, Temgesic, Schering-Plough/Merck, Whitehouse station, NJ, USA) twice a day for the first three days after surgery. Fluorochrome labels were administered at 4 (tetracyclin, 25 mg/kg bodyweight), 8 (calcein, 25 mg/kg body weight), and 11 weeks (xylenol orange, 90 mg/kg body weight) to monitor the onset of bone formation [24]. The 8 week label was not incorporated in any of our samples or control tissue and therefore was excluded from the fluorochrome analysis.

Clinical evaluation of the procedure

All bone chambers performed well, they remained at the correct location during the entire study. The animals rapidly recovered and mobilized, limping was observed the first week after surgery only, and no complications occurred.

µCT evaluation

Immediately after surgery, a baseline *in vivo* µCT scan was acquired of all implanted bone chambers using a SkyScan 1176 scanner (Bruker µCT, Kontich, Belgium) and after 4, 8 and 12 weeks subsequent scans were perfomed. An 18 µm-resolution protocol was used (65 kV, 270 ms exposure time, 1.0 mm Al filter, 0.5 degree rotation step), resulting in a 9 minute scan. After explantation of the subcutaneously implanted BCP scaffolds, *ex vivo* µCT scans were acquired using a 9 µm-resolution protocol (65 kV, 1320 ms exposure time, 1.0 mm Al filter, 0.32 degree rotation step, 53 min scan). All µCT images were reconstructed using volumetric reconstruction software NRecon version 1.5 (Bruker µCT). To measure bone formation inside the bone chamber calcified tissue was distinguished from non-calcified tissue and noise by segmentation. Therefore, grayscale images were reconstructed by an automated algorithm using local thresholds (3D Calculator v0.9 [25]). Subsequently, in the resulting 3D dataset (consisting of stacked black and white cross-sections) bone was measured inside a cylindrical volume of interest capturing the inner volume of the bone chambers using CTAnalyser version 1.11 software (µCT). All analysis and segmentation were performed on blinded data sets.

Histology

The rats were terminated after 12 weeks using an injection of Euthanasol (Virbac, Fort Worth, Tx, USA). Bone chambers were retrieved, fixed in 4% buffered formalin, dehydrated using ethanol series and embedded in polymethylmethacrylate (MMA). Samples were sawed centrally into approximately 25 µm thick sections using a sawing microtome (Leica, Nussloch, Germany) and stained with methylene blue and basic fuchsin for histomorphometric analysis. High-resolution digital pictures of the samples were taken using transmitted light microscopy (Olympus-BX50, Olympus, Zoeterwoude, the Netherlands).

Statistical analysis

Bone formation was analyzed by SPSS version 20 software (IBM, Chicago, Illinois, USA). Combined growth factor filled chambers (n=10) were implanted in one tibia, and were matched with either a positive (n=5) or negative control (n=5) chamber in the other tibia of the animal to allow paired data analysis. Differences between treatments were analyzed with a paired t-Test. Post-hoc testing to correct for the number of tests was performed using a Bonferroni correction. All bars represent mean values, with standard

deviations depicted in the error bars. Significance between treatments was assumed when $p<0.05$.

RESULTS

Assessment of tissue ingrowth and bone formation in the PEEK chambers

Bone formation in the chambers as seen on µCT was confirmed by methylene blue and basic fuchsin staining on the MMA-embedded sections (Figure 2). In the controls

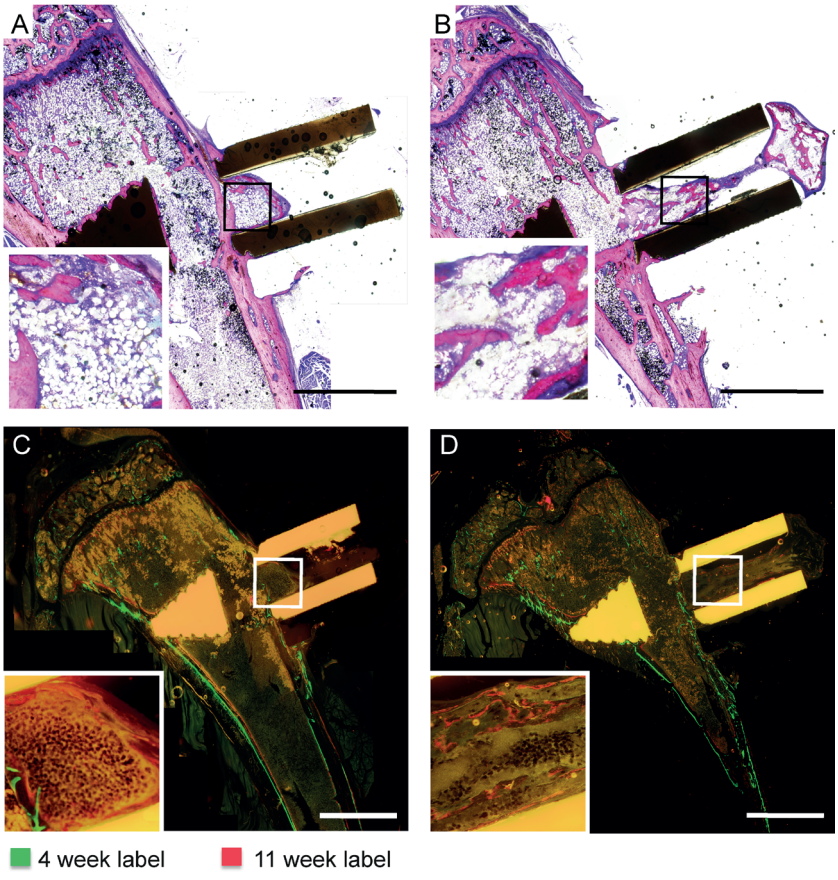

Figure 2. µCT analysis of bone formation in the chambers.
A, B. Bone volume was measured in the bone chambers after 8 and 12 weeks of implantation by µCT. * indicates $p < 0.05$. C, D. Original µCT scan (grey) and segmentations (binary) of bone chambers, with the region of interest for segmentation depicted (blue) for the controls (C) and combined growth factor laden bone chambers (D). E, F. 3D reconstructions of a control (E), and combined growth factor sample (F) µCT scan, from the same animal. Representative pictures with respect to bone volume are shown.

that did not contain growth factors little bone was formed (Figure 2A, C), whereas the chambers were filled with bone that reached to the top of the chamber in the growth factor containing chambers (Figure 2A, D). The 4 week fluorochrome label (green) was not present in the bone in the chambers, the 11 week label (red) was. This confirms late onset of bone formation, which is in accordance with the µCT measurements and previous findings in spinal cassettes [26]. Both labels were present in the cortical bone and epiphysis of the tibia, indicating normal active bone deposition during the entire study period.

The baseline µCT directly after surgery confirmed that no bone fragments were present in the chambers after implantation and that they were correctly placed bicortically on the tibiae. In the µCT scan after 4 weeks of implantation no bone formation was present, but bone ingrowth was clearly visible by µCT from 8 weeks onwards (Figure 3). Quantification of the bone volumes revealed that the chambers that contained the combination of growth factors showed significantly higher bone formation at 8 weeks

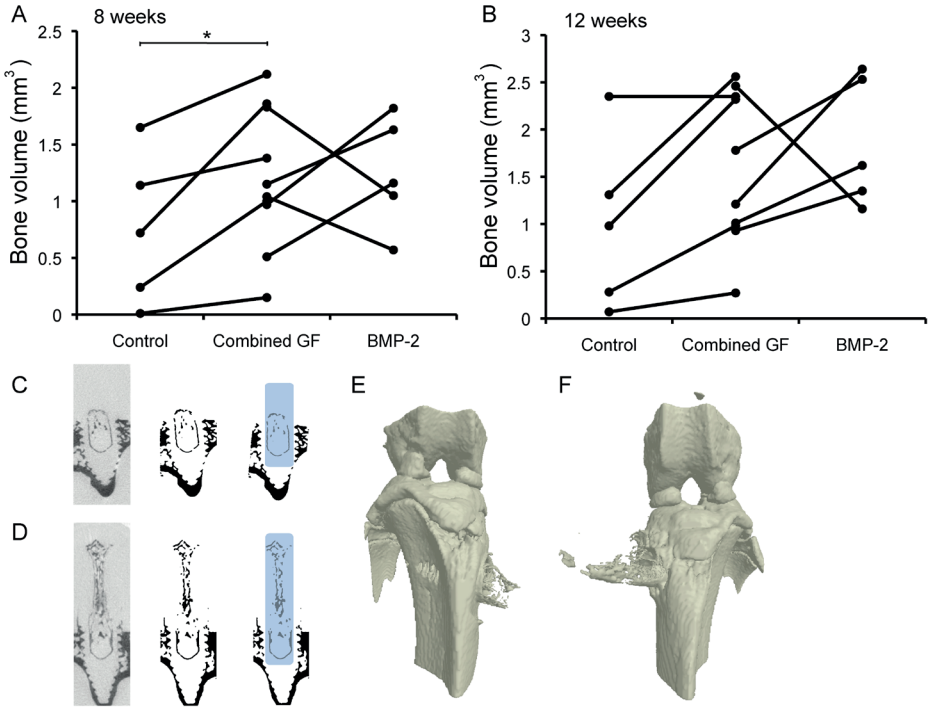

Figure 3. Bone formation in the PEEK chambers.

A-B. Methylene blue and basic fuchsin staining of a control (A) and a combined growth factor (B) bone chamber. C-D. Fluorochrome label incorporation from consecutive unstained sections (compared to A-B) in the bone chambers. In (C) there is no incorporation, in (D) only the red label is present. Insets depict details from the boxed regions. Representative pictures with respect to bone volume are shown, scale bars represent 3 mm.

than the empty chambers (p=0.04). At 12 weeks this difference was no longer statistically significant (p=0.06). Both the BMP-2 and combined growth factor laden chambers contained bone volumes indistinguishable from each other at 8 and 12 weeks.

DISCUSSION

This study showed that the PEEK bone chamber is a suitable model to assess (growth factor induced) orthotopic bone formation. All chambers were easily implanted bicortically (without surgical failures), remained in the correct position and the animal recovered within days after the surgery. The importance of longitudinal analysis of bone formation was underlined by the outcomes of this experiment, namely the significant difference in bone formation between the control and growth factor-laden chambers present at 8 weeks after implantation, which was no longer statistically significant at 12 weeks. We hypothesize that after 8 weeks, remodeling of the newly formed bone started playing a larger role than *de novo* bone formation, lowering the increase in bone volume and leading to larger interindividual variations. Also, due to the small volume of the chamber a plateau-phase was often already reached before 12 weeks of implantation. Longitudinal assessment of bone formation enabled detection of the significant differences in bone volume between the treatments, which would have been missed if only an end point measurement had been performed.

Inclusion of the gold standard treatment for bone augmentation, which is the application of autologous bone was not chosen here, as this would complicate the analysis of new bone ingrowth. Bone induction by BMP-2 in rats is well studied with response to dosage and kinetics, reason why this was taken as positive control. When we compared the BMP-2 laden chambers to the combined growth factor chambers no differences were seen. The BMP-2 that was added to the chambers appeared to induce optimal bone formation in this time frame and setting. Because the necessary cells were most likely able to migrate into the chambers through the openings at cortical level, there may have been a limited need for VEGF and SDF-1α addition. This would mean that in order to assess growth factor synergy the volume of the chambers should be enlarged to a size where vascularization is critical for bone formation. Furthermore, the concentration of BMP-2 was based on findings in literature [27], and was supraphysiological. Together with the confined space offered by the chamber, this may have led to maximal bone induction, hereby masking possible synergistic or additive effects of the other growth factors that are well established for VEGF [28,29], and also reported for SDF-1α [16].

GMPs were applied because of their beneficial effects seen in our previous studies [30]. In this experimental set-up the release of the growth factors was expected to be gradual, also because Matrigel is known to retain growth factors [31]. The use of GMPs is reported

for BMP-2 and VEGF delivery [17], and there is evidence that controlled release of SDF-1α leads to improved angiogenesis [32]. Together, this argues against an insufficient availability of the individual growth factors in the combined growth factor laden chambers.

The limitations of this study are to be optimized further before the PEEK bone chamber can be applied in large animal models and translational research to screen the bone forming capacity of novel materials. First, the size of the bone chambers could be increased to introduce the need for early scaffold vascularization in this model. Then, application of bone chambers at multiple implantation sites could be optimized. In the current setting bone chambers are not weight bearing, resulting in less variation due to implant movement, but also complicating translation to weight bearing orthotopic implantation sites. When these limitations are addressed and the model is further optimized, implant components such as matrices and biologicals can be screened in small and large animal models, which is an important step to translate *in vitro* findings to clinical applications.

CONCLUSION

The PEEK bone chamber proved to be a suitable model to investigate orthotopic bone formation in a longitudinal manner. Our results showed that in all growth factor-laden chambers bone formation increased significantly compared to control.

REFERENCES

1. Silber JS, Anderson DG, Daffner SD, Brislin BT, Leland JM, Hilibrand AS, Vaccaro AR, Albert TJ. Donor site morbidity after anterior iliac crest bone harvest for single-level anterior cervical discectomy and fusion. *Spine (Phila Pa 1976) 2003;28-2:134-9*.
2. Khan SN, Cammisa FP, Jr., Sandhu HS, Diwan AD, Girardi FP, Lane JM. The biology of bone grafting. *J Am Acad Orthop Surg 2005;13-1:77-86*.
3. Barradas AM, Yuan H, van Blitterswijk CA, Habibovic P. Osteoinductive biomaterials: current knowledge of properties, experimental models and biological mechanisms. *Eur Cell Mater 2011; 21:407-29; discussion 29*.
4. Van der Stok J, Van Lieshout EM, El-Massoudi Y, Van Kralingen GH, Patka P. Bone substitutes in the Netherlands - a systematic literature review. *Acta Biomater 2011;7-2:739-50*.
5. Belfrage O, Isaksson H, Tagil M. Local treatment of a bone graft by soaking in zoledronic acid inhibits bone resorption and bone formation. A bone chamber study in rats. *BMC Musculoskelet Disord 2012;13:240*.
6. Hannink G, Aspenberg P, Schreurs BW, Buma P. Development of a large titanium bone chamber to study in vivo bone ingrowth. *Biomaterials 2006;27-9:1810-6*.
7. Mathijssen NM, Hannink G, Pilot P, Schreurs BW, Bloem RM, Buma P. Impregnation of bone chips with alendronate and cefazolin, combined with demineralized bone matrix: a bone chamber study in goats. *BMC Musculoskelet Disord 2012;13:44*.
8. Wang JS, Aspenberg P. Basic fibroblast growth factor increases allograft incorporation. Bone chamber study in rats. *Acta Orthop Scand 1994;65-1:27-31*.
9. Toth JM, Wang M, Estes BT, Scifert JL, Seim HB, 3rd, Turner AS. Polyetheretherketone as a biomaterial for spinal applications. *Biomaterials 2006;27-3:324-34*.
10. Garrison KR, Shemilt I, Donell S, Ryder JJ, Mugford M, Harvey I, Song F, Alt V. Bone morphogenetic protein (BMP) for fracture healing in adults. *Cochrane Database Syst Rev 2010-6:CD006950*.
11. Jeppsson C, Bostrom M, Aspenberg P. Intraosseous BMP implants in rabbits. Inhibitory effect on bone formation. *Acta Orthop Scand 1999;70-1:77-83*.
12. Ferrara N, Gerber HP, LeCouter J. The biology of VEGF and its receptors. *Nat Med 2003;9-6:669-76*.
13. Hattori K, Heissig B, Tashiro K, Honjo T, Tateno M, Shieh JH, Hackett NR, Quitoriano MS, Crystal RG, Rafii S, Moore MA. Plasma elevation of stromal cell-derived factor-1 induces mobilization of mature and immature hematopoietic progenitor and stem cells. *Blood 2001;97-11:3354-60*.
14. Eman RM, Oner FC, Kruyt MMP, Dhert W, Alblas J. Stromal cell-derived factor-1 stimulates cell recruitment, vascularization and osteogenic differentiation. *Tissue Eng Part A 2013*.
15. Liu X, Zhou C, Li Y, Ji Y, Xu G, Wang X, Yan J. SDF-1 promotes endochondral bone repair during fracture healing at the traumatic brain injury condition. *PLoS ONE 2013;8-1:e54077*.
16. Ratanavaraporn J, Furuya H, Kohara H, Tabata Y. Synergistic effects of the dual release of stromal cell-derived factor-1 and bone morphogenetic protein-2 from hydrogels on bone regeneration. *Biomaterials 2011;32-11:2797-811*.
17. Patel ZS, Young S, Tabata Y, Jansen JA, Wong ME, Mikos AG. Dual delivery of an angiogenic and an osteogenic growth factor for bone regeneration in a critical size defect model. *Bone 2008;43-5: 931-40*.
18. Ikada Y, Tabata Y. Protein release from gelatin matrices. *Adv Drug Deliv Rev 1998;31-3:287-301*.
19. Yamamoto M, Ikada Y, Tabata Y. Controlled release of growth factors based on biodegradation of gelatin hydrogel. *J Biomater Sci Polym Ed 2001;12-1:77-88*.

20. Patel ZS, Ueda H, Yamamoto M, Tabata Y, Mikos AG. In vitro and in vivo release of vascular endothelial growth factor from gelatin microparticles and biodegradable composite scaffolds. *Pharm Res 2008;25-10:2370-8*.
21. Leeuwenburgh SC, Jo J, Wang H, Yamamoto M, Jansen JA, Tabata Y. Mineralization, biodegradation, and drug release behavior of gelatin/apatite composite microspheres for bone regeneration. *Biomacromolecules 2010;11-10:2653-9*.
22. Yamamoto M, Takahashi Y, Tabata Y. Controlled release by biodegradable hydrogels enhances the ectopic bone formation of bone morphogenetic protein. *Biomaterials 2003;24-24:4375-83*.
23. van der Donk S, Buma P, Aspenberg P, Schreurs BW. Similarity of bone ingrowth in rats and goats: a bone chamber study. *Comp Med 2001;51-4:336-40*.
24. van Gaalen SM, Kruyt MC, Geuze RE, de Bruijn JD, Alblas J, Dhert WJ. Use of fluorochrome labels in in vivo bone tissue engineering research. *Tissue Eng Part B Rev 2010;16-2:209-17*.
25. Waarsing JH, Day JS, van der Linden JC, Ederveen AG, Spanjers C, De Clerck N, Sasov A, Verhaar JA, Weinans H. Detecting and tracking local changes in the tibiae of individual rats: a novel method to analyse longitudinal in vivo micro-CT data. *Bone 2004;34-1:163-9*.
26. Geuze RE, Theyse LF, Kempen DH, Hazewinkel HA, Kraak HY, Oner FC, Dhert WJ, Alblas J. A differential effect of bone morphogenetic protein-2 and vascular endothelial growth factor release timing on osteogenesis at ectopic and orthotopic sites in a large-animal model. *Tissue Eng Part A 2012;18-19-20:2052-62*.
27. Jang JW, Yun JH, Lee KI, Jung UW, Kim CS, Choi SH, Cho KS. Osteoinductive activity of biphasic calcium phosphate with different rhBMP-2 doses in rats. *Oral Surg Oral Med Oral Pathol Oral Radiol 2012;113-4:480-7*.
28. Kanczler JM, Ginty PJ, White L, Clarke NM, Howdle SM, Shakesheff KM, Oreffo RO. The effect of the delivery of vascular endothelial growth factor and bone morphogenic protein-2 to osteoprogenitor cell populations on bone formation. *Biomaterials 2010;31-6:1242-50*.
29. Kempen DH, Lu L, Heijink A, Hefferan TE, Creemers LB, Maran A, Yaszemski MJ, Dhert WJ. Effect of local sequential VEGF and BMP-2 delivery on ectopic and orthotopic bone regeneration. *Biomaterials 2009;30-14:2816-25*.
30. Kempen DH, Lu L, Hefferan TE, Creemers LB, Maran A, Classic KL, Dhert WJ, Yaszemski MJ. Retention of in vitro and in vivo BMP-2 bioactivities in sustained delivery vehicles for bone tissue engineering. *Biomaterials 2008;29-22:3245-52*.
31. Gao Y, Zhu S, Luo E, Li J, Feng G, Hu J. Basic fibroblast growth factor suspended in Matrigel improves titanium implant fixation in ovariectomized rats. *J Control Release 2009;139-1:15-21*.
32. Kimura Y, Tabata Y. Controlled release of stromal-cell-derived factor-1 from gelatin hydrogels enhances angiogenesis. *J Biomater Sci Polym Ed 2010;21-1:37-51*.

CHAPTER 6

3D bioprinting of methacrylated hyaluronic acid (MeHA) hydrogel with intrinsic osteogenicity

Michelle Poldervaart
Birgit Goversen
Mylene de Ruijter
Anna Abbadessa
Ferry Melchels
Cumhur Öner
Wouter Dhert
Tina Vermonden
Jacqueline Alblas

PLoS One.
2017 Jun 6;12(6):e0177628.

ABSTRACT

In bone regenerative medicine there is a need for suitable bone substitutes. Hydrogels have excellent biocompatible and biodegradable characteristics, but their visco-elastic properties limit their applicability, especially with respect to 3D bioprinting. In this study, we modified the naturally occurring extracellular matrix glycosaminoglycan hyaluronic acid (HA), in order to yield photo-crosslinkable hydrogels with increased mechanical stiffness and long-term stability, and with minimal decrease in cytocompatibility. Application of these tailor-made methacrylated hyaluronic acid (MeHA) gels for bone tissue engineering and 3D bioprinting was the subject of investigation. Visco-elastic properties of MeHA gels, measured by rheology and dynamic mechanical analysis, showed that irradiation of the hydrogels with UV light led to increased storage moduli and elastic moduli, indicating increasing gel rigidity. Subsequently, human bone marrow derived mesenchymal stromal cells (MSCs) were incorporated into MeHA hydrogels, and cell viability remained 64.4% after 21 days of culture. Osteogenic differentiation of MSCs occurred spontaneously in hydrogels with high concentrations of MeHA polymer, in absence of additional osteogenic stimuli. Addition of bone morphogenetic protein-2 (BMP-2) to the culture medium further increased osteogenic differentiation, as evidenced by increased matrix mineralisation. MeHA hydrogels demonstrated to be suitable for 3D bioprinting, and were printed into porous and anatomically shaped scaffolds. Taken together, photosensitive MeHA-based hydrogels fulfilled our criteria for cellular bioprinted bone constructs within a narrow window of concentration.

INTRODUCTION

Natural hydrogels are increasingly applied in regenerative medicine, as they can provide scaffolds with unique biocompatible and biodegradable properties [1]. Many of the materials used can be tailored to accommodate various shapes and sizes and functional groups can be incorporated to introduce specific desirable physical and chemical characteristics [2,3]. Due to these properties, hydrogels can be employed as cell-friendly materials that can present signals to guide cellular processes and release proteins or drugs in a controlled fashion [4]. Altogether, this makes hydrogel scaffolds very suitable for tissue engineering purposes, the reason why worldwide research is increasingly focusing on the manufacturing and optimization of hydrogels [5-7].

In order to present cell laden hydrogel scaffolds with a desired shape for tissue engineering, several technologies have been applied, such as molding [8,9], lithography [10], and 3D bioprinting [11]. 3D bioprinting offers the advantage of creating porous constructs with predefined complex architecture, allowing deposition of specific cell types, signaling molecules or biomaterials at predefined regions [12]. This technique allows better mimicry of native tissue organization compared to the other deposition methods mentioned above, for example by addition of specific and predefined vasculature stimulating regions to a bone promoting scaffold.

Hyaluronic acid (HA), [α-1,4-D-glucuronic acid-β-1,3-*N*-acetyl-D-glucosamine]$_n$ is a naturally occurring high molecular weight hydrophilic glycosaminoglycan. It is an abundant polymer present in the extracellular matrix where it gives mechanical support [13]. The chemical structure of HA allows easy modification of the (primary) hydroxyl-groups by esterification. Modification with methacrylate groups, followed by addition of a photo initiator leads to polymerization upon UV-exposure, resulting in network formation. Methacrylated HA (MeHA) hydrogels have shown increased rigidity and are more resistant to degradation, compared to non-derivatized HA hydrogels, while maintaining good biocompatibility [14]. Gel stiffness after methacrylation is highly dependent on the degree of substitution (DS, defined as the number of methacrylate groups per 100 disaccharide units), and may be used to steer differentiation of incorporated cells [15]. Methacrylation allows hydrogels to be 3D printed, as scaffolds can be crosslinked with UV light directly after gel deposition to fixate their shape [16]. Osteogenic differentiation of mesenchymal stromal cells (MSCs) was observed during their incorporation in photocrosslinked low molecular weight HA [17]. This finding is promising for the application of 3D printed MeHA scaffolds for the purpose of bone tissue engineering.

MeHA can be obtained using different protocols, with reaction taking place either in organic solvents or aqueous environment [18], yielding various degrees of substitution. Control over the degree of substitution is of major importance to obtain materials with

tuneable mechanical properties in a reproducible manner [19]. Therefore, in this study, we apply a protocol that utilizes a mixture of water and *N,N*-dimethylformamide (DMF) [20].

The aim of this study was to select a MeHA hydrogel composition for the development of 3D printable scaffolds supporting bone-like tissue formation. Gel properties such as visco-elastic behaviour, swelling and degradability *in vitro*, viability and osteogenic differentiation of encapsulated primary cells, as well as 3D bioprintability of the gel were the main subjects of investigation.

MATERIALS AND METHODS

Synthesis of MeHA

Hyaluronic acid sodium salt (HA, M_W=~1.7*10^6 g/mol, from *Strept. Equi*, Sigma-Aldrich, Zwijndrecht, the Netherlands) was methacrylated following an adapted protocol by Hachet et al [20]. In short, 2.0 g HA (corresponding to 5.0 mmol of disaccharide units) was dissolved in 150 ml of reverse osmosis (RO) water and stirred overnight at RT for complete dissolution. Subsequently, DMF (Biosolve, Valkenswaard, the Netherlands) was added drop wise to obtain a water/DMF ratio of 3/2 (v/v). Methacrylic anhydride (MA, Sigma-Aldrich) was added using a molar ratio HA disaccharide unit/MA ranging from 1/1.5 to 1/3, while maintaining the pH at 8 to 9 using 0.5 M NaOH. After overnight stirring, the mixture was diluted with RO-water (final water/DMF ratio of 10/1 (v/v)) and sodium chloride (NaCl, Merck, Darmstadt, Germany) was added to achieve a final concentration of 0.5 M. After this, the solution was transferred to a dialysis membrane (M_W 12-14 kDa cut-off, Medicell, London, UK) and dialyzed for 5 days at 4°C against RO water. The remaining HA solution was lyophilized overnight and kept at −20°C until characterization and use.

High Performance Liquid Chromatography (HPLC) and Nuclear Magnetic Resonance (NMR)

For ^{1}H-NMR, a solution was prepared (6% (w/w)) of MeHA polymer in D_2O and analyzed on a 300 mHz Gemini Spectrometer (Varian, Palo Alto, CA). All samples were measured with a relaxation delay of 0.6 seconds for 512 scans. The degree of methacrylate substitution was calculated by comparing the integrals of the peaks of the methacrylate groups at 1.9, 5.7 and 6.1 ppm relative to the integrals originating from the protons of HA.

For the HPLC measurements, 15 mg of MeHA was dissolved in 10 ml of 0.02 M NaOH solution, and incubated at 37°C for 30 minutes to ensure complete hydrolysis of the ester bonds. After that, 2 ml of 2 M acetic acid (Merck) was added to acidify the solution. Samples were filtered over 0.2 µm filters and injected onto a Sunfire RP-18 column (Lichrospher, Darmstadt, Germany). Samples were analyzed using a HPLC Waters 2695

system equipped with an UV detector model 2487 (λ=210 nm, Waters Inc., Dublin, Ireland). The mobile phase consisted of a mixture of acetonitrile (Actu-All Chemicals, Oss, the Netherlands) and water (ratio: 15/85) adjusted to pH 2 with perchloric acid ($HClO_4$, 70%, Sigma-Aldrich) and a flow rate of 1 ml/min was used. A calibration curve was obtained by injection of methacrylic acid solutions in eluent with a concentration range of 0 to 160 µg/ml. Empower Pro software (Waters) was used to calculate the concentration of methacrylic acid.

Experimental design

MeHA was dissolved in a concentration range in alpha minimum essential medium (α-MEM, Gibco, Breda, The Netherlands), and stirred overnight. A 1% (w/v) stock solution of photoinitiator (Irgacure 2959, Ciba Specialty Chemicals, Basel, Switzerland) was prepared at 90°C, cooled down and then added to the polymer solution in order to achieve a final concentration of 0.1%. The resulting polymer concentrations ranged from 1% to 3% (w/v). The polymer solutions and their UV-crosslinked products were analyzed in terms of mechanical strength, biodegradability, biocompatibility, 3D printability and the ability of MSCs to differentiate when incorporated into the gels.

Hydrogel swelling and degradation

Polymer solutions (1-3% (w/v)) were photopolymerized for 10 minutes at 365 nm and 3 mW/cm^2 (1800 mJ/cm^2) in a UVP CL-1000L crosslinker (UVP, Upland, Ca, USA) using custom made Teflon moulds (50x4x2 mm), then cut and transferred to pre-weighed microtubes and weighed (W_0). The gels were then immersed in 5 ml PBS (n=5) or PBS supplemented with 2.6 U/ml hyaluronidase (type II, H2126, Sigma) (n=5) in accordance to endogenous enzymatic circumstances [21]. The buffer was discarded at multiple time points, and gels were weighed (W_{wet}), lyophilized and weighed again (W_{dry}). Swelling was calculated as W_{wet}/W_0, degradation as W_{dry}/W_0.

Rheological analysis

Rheological analysis of the MeHA hydrogels was performed on an ARG2 rheometer with UV curing accessory (TA Instruments, Etten-Leur) using a 20 mm parallel plate UHP steel. 120 µl of gel was placed between the two plates and analysed at 37°C under oscillation mode using 1% strain and a frequency of 1 Hz. Exposure to UV-light (365 nm) occurred after 5 minutes using a bluepoint 4 UV-lamp (Honle UV technology) at 40 mW/cm^2 (1200 mJ/cm^2) and lasted for 5 minutes. G' (storage modulus) and G" (loss modulus) were monitored at RT for 15 minutes. Moduli and tan delta were calculated as the mean of values measured after a plateau level was achieved.

Dynamic Mechanical Analysis

Hydrogel discs of 200 µl were obtained (1-3% (w/v)) using a syringe with a diameter of 8 mm and a height of ± 3 mm as a mould, by UV-photopolymerization for 10 minutes at 6 mW/cm^2. Compression tests were performed in triplicate on a 2980 DMA (TA Instruments) with a ramp force from 0.1-1 N for 10 minutes. The elastic modulus was calculated as the slope of the stress-strain curve that was obtained from the compression test.

Mesenchymal stromal cells (MSC)

Human bone marrow-derived MSCs were isolated from bone marrow aspirates, acquired during orthopedic surgery of patients after written informed consent. Acquiring the bone marrow was approved by the Institutional Medical Ethical Review Committee (METC, approval number 08-001K).

The mononuclear fraction was isolated using Ficoll density gradient centrifugation. The MSCs were isolated by their adherence to tissue culture plastic, and expanded in αMEM, supplemented with 10% (v/v) fetal calf serum (Cambrex, Charles City, IA, USA), 100 U/ml penicillin, 100 µg/ml streptomycin, 0.2 mM L-ascorbic acid-2-phosphate (AsAP, Sigma-Aldrich) and 1 ng/ml basic fibroblast growth factor (bFGF, R &D Systems, Minneapolis, MN, USA). Cells were cultured in a humidified incubator at 37°C and 5% CO_2.

MSC survival in MeHA hydrogels

Human bone marrow-derived MSCs were incorporated into 1-3% (w/v) MeHA hydrogels at a density of 2x10^6 cells/ml, and photopolymerized in UV mold chambers at 1800 mJ/cm^2 (10 minutes, 3 mW/cm^2). The cell-laden gels were subsequently cultured in expansion medium (control) or expansion medium supplemented with 1 µg/ml bone morphogenetic protein 2 (BMP-2) until analysis. To quantify MSC viability, a LIVE/DEAD Viability Assay (Molecular ProbesMP03224, Eugene, Oregon, USA) was performed according to the manufacturer's protocol. Samples were examined in triplicate using an Olympus BX51 light microscope with excitation/emission filters set at 488/530 nm to observe living (green) cells and at 530/580 nm to detect dead (red) cells. Three pictures were taken at random locations throughout each sample. Live and dead cells were counted automatically using Image J software [22] with identical settings after 1 and 21 days of culture in MSC expansion medium.

MSC osteogenic differentiation in MeHA hydrogels

Human bone marrow-derived MSCs were incorporated into 1-3% (w/v) MeHA hydrogels at a density of 2.0x10^6 cells/ml, photopolymerized in UV mold chambers at 1800 mJ/cm^2. The cell-laden gels were subsequently cultured in expansion medium (control) or expansion medium supplemented with BMP-2 until analysis. After 21 days, osteogenic differentiation was quantified using a calcium assay kit (DICA-500, QuantiChrom, BioAs-

say Systems, Hayward, CA, USA) measuring calcium deposition by the MSCs per mg of scaffold. Additionally, Alizarin red staining was performed on these scaffolds to visualize scaffold calcification. For this, a 2% Alizarin Red S (Fluka 5600) solution in water was used, with the pH set to 4.7 by addition of 0.5% ammonium hydroxide (NH_4OH in H_2O, Merck). The gels were soaked in this solution for 1 minute and then thoroughly washed with demi water.

3D bioprinting

MeHA was dissolved in α-MEM as described above to yield 1 - 3% (w/v) hydrogels, including 0.1% photoinitiator Irgacure 2959. Subsequently, these hydrogels were 3D bioprinted using the Bioscaffolder dispensing system (SYS+ENG, Gladbeck, Germany) [23]. Scaffold architecture was designed as either porous cube or non-porous human L3 vertebrae shapes (acquired from a CT scan) and converted to computer-aided design (CAD) files. CAD files were then combined with specific material settings to a numerical control (NC) code, which directs XYZ controller of the 3D printer [24]. Porous scaffolds measuring 20x20x3 mm, and lumbar scaffolds measuring 20x25x1 mm were 3D bioprinted under sterile conditions in a laminar flow-cabinet, using a 25 G needle, with a strand thickness of 0.2 mm and strand distances of 1 mm (porous), or 0.2 mm (non-porous). After 3D bioprinting, the scaffolds were UV irradiated with a Superlite S-UV 2001 AV lamp (Lumatec, Munchen, Germany) at 1800 mJ/cm^2 to ensure crosslinking.

Statistical analysis

Data are represented as mean ± standard deviation, and analyzed using an ANOVA test with post hoc Bonferroni correction. Differences were considered statistically significant when $p<0.05$.

RESULTS

Synthesis and characterization of MeHA

MeHA was acquired by methacrylation of HA (Figure 1A). Methacrylation was visible in NMR with peaks at 1.9, 5.7 and 6.1 ppm, but accurate quantification was difficult due to overlapping peaks. Therefore, HPLC of degraded samples at high pH was performed to quantify hydrolysed methacrylic acid. Variations in HA disaccharide unit/MA ratios and batch sizes led to DS values of 6.3 ± 2.8. Polymer batches with a DS between 5 and 7% were selected for further experiments, since these yielded hydrogels with visco-elastic properties that allow handling with a pipette, a necessity for the experiments that involve cell-incorporation, moulding and 3D bioprinting (Figure 1B).

A

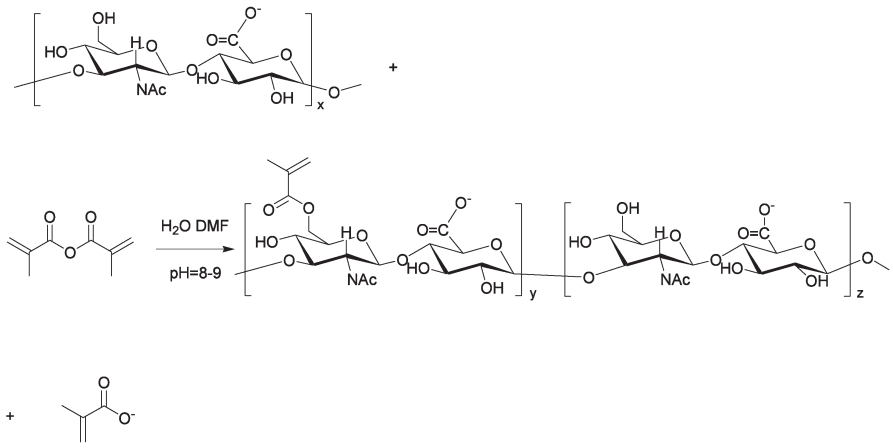

B

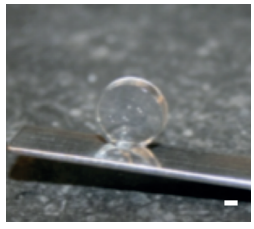

Figure 1. Schematic representation for the methacrylation reaction of HA and photograph of crosslinked MeHA gel.

A. HA reacted with methacrylic anhydride in an aqueous environment in presence of DMF, yielding the photo-crosslinkable MeHA. B. Hydrogel disc prepared from 3% MeHA (DS = 5%). Scale bar represents 1 mm.

Effectivity of UV-induced MeHA crosslinking over time was assessed by rheometry. After UV exposure, a sharp increase in storage modulus was observed at all polymer concentrations tested, and this increased with higher concentrations of MeHA polymer within the hydrogel (Table 1). This increased storage modulus indicated effective intermolecular crosslink formation by photopolymerization of HA chains. The loss modulus (viscosity) increased negligibly during this time. Tan delta values indicated that after gelation the MeHA hydrogels were more elastic than viscous (Tan δ <1). Subsequently, mechanical properties of the hydrogels were measured by dynamic mechanical analysis (DMA). Elastic moduli increased with increasing concentrations, indicating higher material stiffness (Table 1).

Table 1. MeHA hydrogel characteristics before and after application of UV irradiation.

(w/v) %	Storage modulus[a] G′ (Pa) before UV	Storage modulus[a] G′(Pa) after UV	Loss modulus[a] G″ (Pa) after UV	Elastic modulus E[b] (kPa) after UV
1	5 ± 0.5	170 ± 63	7 ± 2	1.3 ± 0.1
1.5	15 ± 2	205 ± 66	7 ± 6	4.1 ± 0.5
2	26 ± 9	374 ± 197	8 ± 4	6.3 ± 1.2
2.5	66 ± 4	766 ± 150	11 ± 2	6.8 ± 1.2
3	200 ± 15	2602 ± 199	22 ± 4	10.6 ± 0.1

[a] Measured with rheometry, [b] measured with dynamic mechanical analysis (DMA). Data are represented as mean ± SD of n=3.

Hydrogel swelling and degradation

The wet weight increase of hydrogels as function of time is presented in Figure 2A. The swelling (wet weight increase) in the initial 24 hours was largest for the lowest concentration hydrogel (1% w/v) and decreased in the more concentrated hydrogels. Degradation of the gels occurred fastest in the lower percentage gels, hereby lowering their ability retain water, reflected in their decreasing wet weight. In PBS without enzymatic supplements, the dry weight loss became evident after 14 days in a similar way for almost all the gels tested (Figure 2B). When hyaluronidase was added at physiological concentrations, the 1 and 1.5% (w/v) gels disintegrated within 24 hours. The more concentrated gels lasted longer. All gels enzymatically degraded within 2 weeks of incubation (Figure 2C).

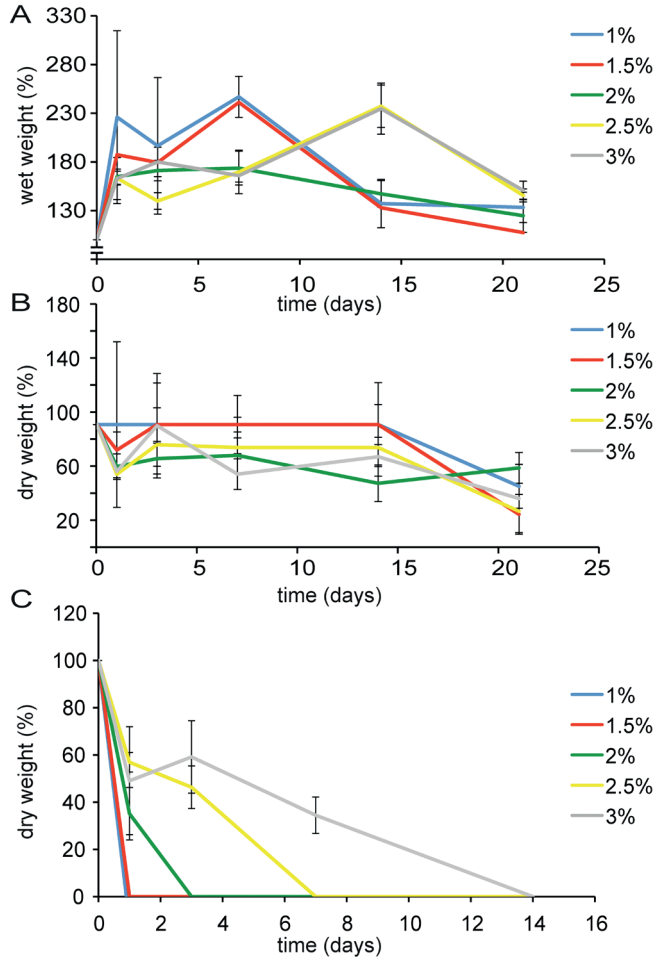

Figure 2. MeHA hydrogel swelling and degradation as a function of gel concentration.
A. Increase of hydrogel wet weight (swelling) during 3 weeks incubation at 37°C, which was most pronounced at lower MeHA concentrations. B. Decrease of hydrogel dry weight during incubation. C. Decrease of hydrogel dry weight followed in time in the presence of hyaluronidase. Gel degradation was slower with increasing MeHA concentration. Data presented as mean ± SD, n=5 for all measurements.

MSC survival in MeHA hydrogels

Survival of human bone marrow derived MSCs in MeHA hydrogels is presented in Figure 3. Average survival of MSCs in MeHA hydrogels after 1 day of gel encapsulation was 73.6±6.4%. When the live/dead analysis was repeated after 21 days of culturing, average MSC survival was still 64.4±12.2% (Figure 3A). The 1% (w/v) hydrogels disintegrated during culture in approximately 14 days; therefore data for day 21 are absent (N/A). Cell survival was significantly lower in the 2.5% (w/v) MeHA hydrogels compared to 2% (w/v) after 1 day. After 21 days of incubation cell survival in the 2.5% (w/v) gel was significantly

lower compared to all other hydrogel concentrations. Also differences in cell morphology were observed: in the lower percentage (1.5 - 2% (w/v)) gels, many cells showed an elongated morphology within the gel (Figure 3B). At higher MeHA concentrations (2.5 - 3% (w/v)) gels, cells were only present in a round morphology.

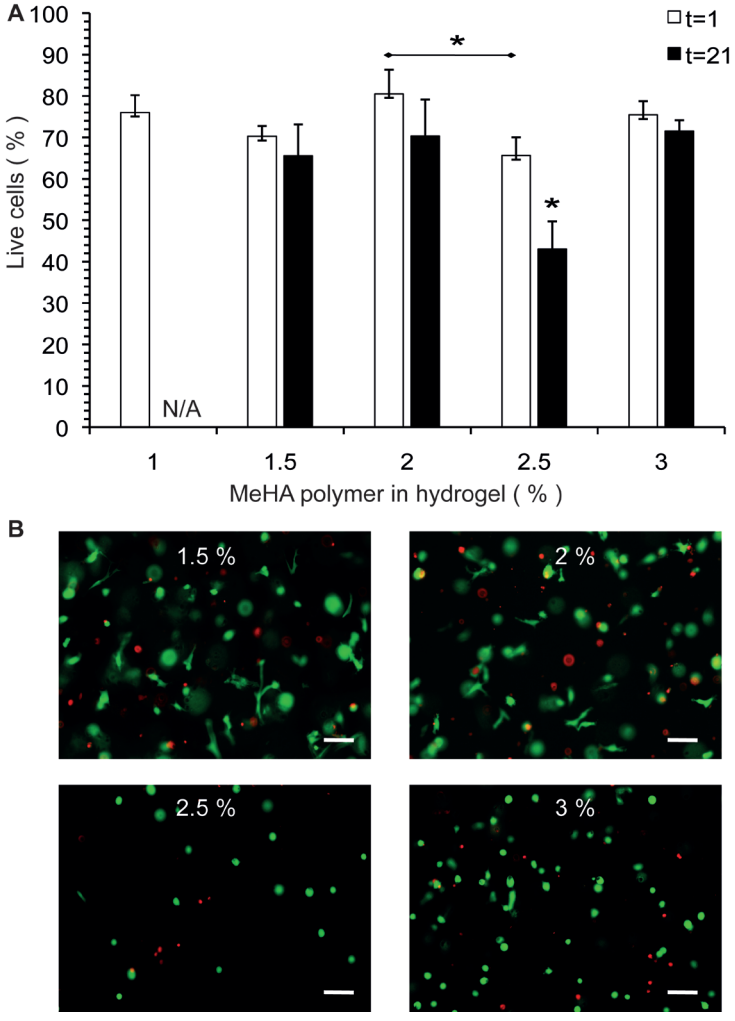

Figure 3. MSC survival and morphology in MeHA hydrogels.
A. Survival of human MSCs after 1 and 21 days of MeHA hydrogel encapsulation. N/A: The 1% (w/v) hydrogels disintegrated before day 21. B. Cell morphology in the MeHA hydrogels after 21 days of culturing. Representative pictures are shown. Scale bars = 100 µm. * Represents $p<0.05$.

Osteogenic differentiation of MSCs in MeHA hydrogels

Osteogenic differentiation, measured by quantification of calcium deposition by MSCs is depicted in Figure 4. In hydrogels that did not receive an external osteogenic stimulus

(BMP-2), increasing the MeHA polymer concentration led to significantly higher calcium precipitate formation (in 2.5-3% (w/v)) compared to 1.5% (w/v). Mineralization increased further when BMP-2 was added. Only in the 3% (w/v) group addition of BMP-2 did not lead to increased calcium deposition compared to control. Calcium deposition in the 2.5% (w/v) gel that received BMP-2 was significantly higher than in all other BMP-2 supplemented groups. Alizarin red staining confirmed the findings of the quantitative calcium assay, showing increased staining at higher polymer concentrations, which further increased when BMP-2 was added. The highest amount of mineralization was seen in the 2.5% (w/v) gels.

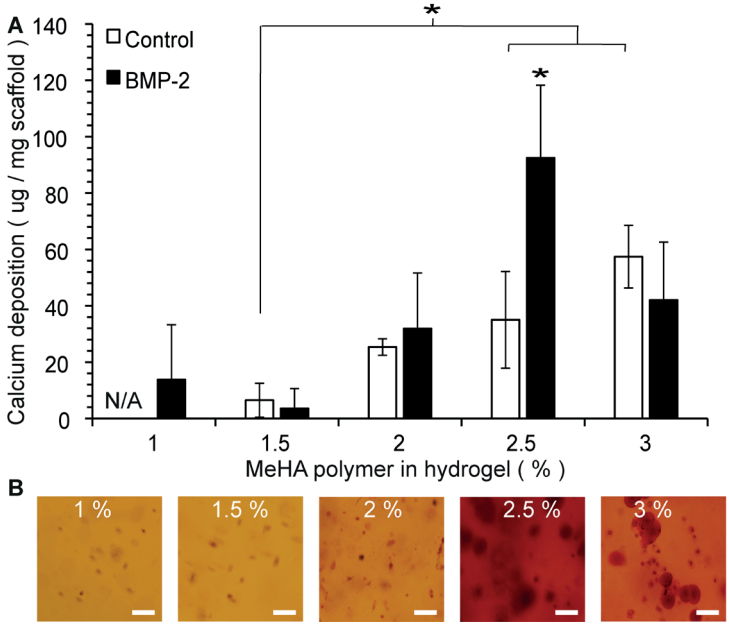

Figure 4. Osteogenic differentiation of MSCs in MeHA hydrogels.

A. Calcium mineralization per mg of hydrogel scaffold after 21 days of culturing in αMEM (control, white bars) or αMEM supplemented with BMP-2 (black bars). Experiments performed in duplicate and replicated with 3 MSC donors. Data shown as mean ± SD. N/A: The 1% (w/v) hydrogels without BMP-2 disintegrated before the day 21 time point. * Represents $p<0.05$.

B. Whole-mount Alizarin red staining of the MeHA hydrogels after 21 days of incubation in the presence of BMP-2. At lower MeHA concentration (1 - 1.5% (w/v)) gels, only some cells stained red. When the gel's MeHA polymer concentration was increased, larger areas around the cells stained red, indicating calcium deposition into the surrounding matrix. Most intense staining is seen in the 2.5% (w/v) gels. Representative pictures are shown. Scale bars = 100 µm.

3D printability of MeHA hydrogels

In order to assess the MeHA gel printability, two distinct designs were 3D printed, photocrosslinked and the resulting scaffolds were subsequently tested for handling with a spatula. (Figure 5). Hydrogels were printed in the form of a porous cube, and as a solid

human lumbar vertebra (L3, scaled 1:10). In order to maintain porosity in scaffolds, 3% (w/v) MeHA was the only hydrogel rigid enough to enable crosslinking before collapsing under its own weight. In case of a solid scaffold design, the desired shape could be reached with gels ≥2% (w/v) and they could be handled well after crosslinking, indicating adequate network formation. In accordance to the results in the porous cubes, the 'vertebral channel' remained best intact in the 3% (w/v) gel, indicating that hydrogel rigidity also played a role in shape maintenance of these scaffolds. In order to maintain designed porosity at least 3% (w/v) hydrogel was needed, in non-porous structures scaffolds printed from ≥ 2% (w/v) hydrogels were functional.

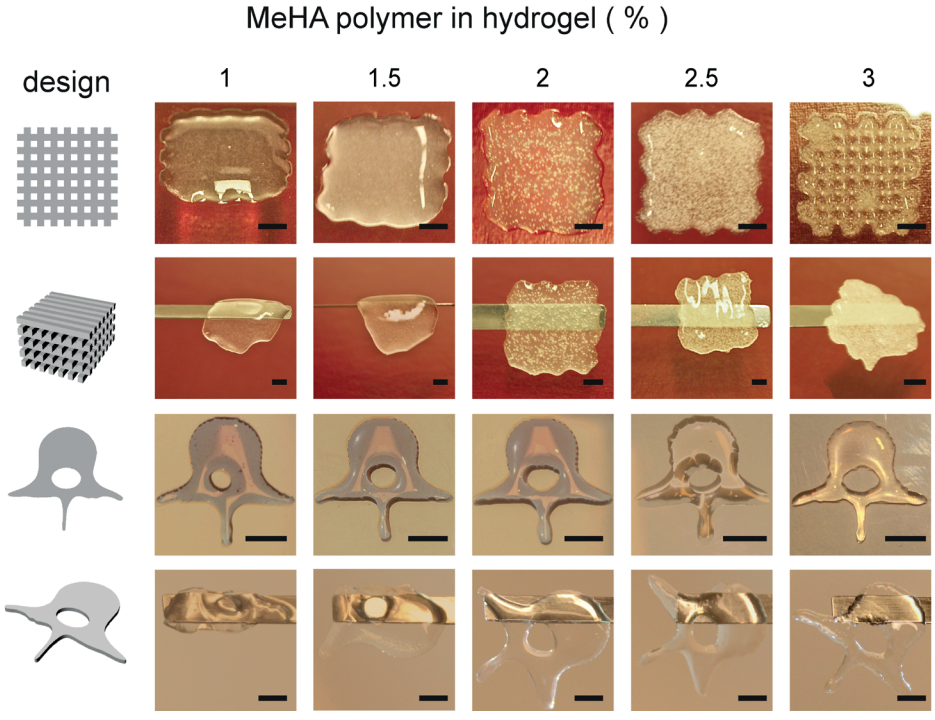

Figure 5. MeHA printability.
Porous cubes (upper rows) and non-porous human L3 vertebrae shapes (lower rows) were 3D bioprinted, using the designs shown in the left column, and subsequently UV irradiated. After crosslinking, scaffolds were lifted using a spatula (horizontal bar) to test handling. Scale bars = 500 µm.

Overall assessment of optimal MeHA hydrogel properties

Taking together elastic properties, primary cell survival, MSC osteogenic differentiation and 3D bioprinting properties of the MeHA-polymer based hydrogels, the most suitable hydrogel concentration for different purposes in regenerative medicine could be defined. These properties are depicted in Figure 6, combining cell survival after 21 days of culture and osteogenic differentiation (mineralization), as a function of percentage

of polymer dissolved, also indicating boundaries for 3D bioprinting requirements (both solid and porous). Based on these data, it becomes apparent that selection of the ideal hydrogel in this polymer concentration range, is highly dependent on the purpose of application in further experiments. The best suitable hydrogel for 3D bioprinting for bone applications is the 2.5% MeHA polymer.

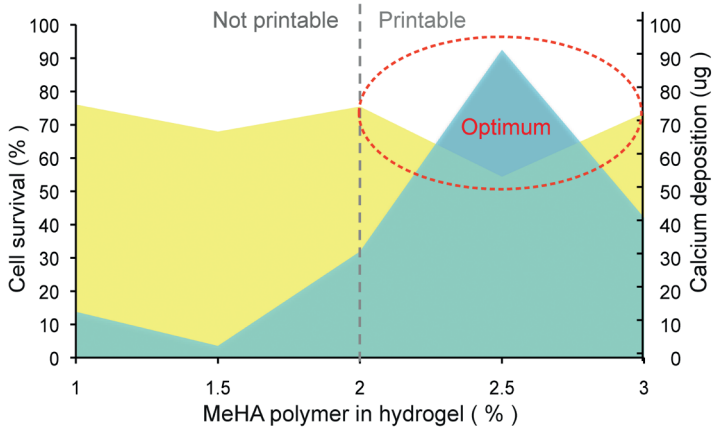

Figure 6. Optimal MeHA hydrogel selection.
Combining MSC survival (yellow), osteogenic differentiation (green) and 3D printability (dotted grey line) data, reveals the boundary conditions for selection of optimal MeHA gel composition (dotted red line) for bone tissue engineering.

DISCUSSION

In this study, high molecular weight hyaluronic acid was successfully methacrylated, thereby attaining photocrosslinking properties [25-27]. Methacrylation increased the final mechanical strength and this resulted in hyaluronic acid-based hydrogels that could be 3D bioprinted. Methacrylation has been applied in literature mainly on low molecular weight HA (<500 kDa) [28-30], that has less favorable biological properties [31]. Introduction of DMF as co-solvent in an aqueous reaction mixture, firstly described by Hachet *et al*. for HA with a molecular weight of 100 kDa [20], led to more efficient substitution than reactions performed in purely aqueous environment in their study. Following this approach, it was possible to obtain controlled DS on high molecular weight HA. The use of photopolymerizable methacrylate groups allowed mixing in of biological components (cells, bioactive molecules, etcetera [32]) at low rigidity, after which exposure at the appropriate wavelength of UV light led to rapid polymerization, causing minimal cell damage [17].

Hydrogels of different polymer concentrations were prepared and gel properties such as swelling, degradation rate and elastic moduli were dependent on the polymer

concentration, and thereby tunable. MeHA gels showed good primary cell (human MSC) survival, for an extensive culture period of 3 weeks. When we compare this cell survival to survival in other hydrogels with tunable mechanical properties, such as polyethylene glycol (PEG), we observed much higher viability [33], and in contrast to the PEG, MeHA did not need addition of functional peptides (such as RGD) to enhance gel performance [34].

Most interestingly, the photopolymerized HA gel showed intrinsic osteogenicity depending on the gel concentration, even when no additional osteogenic stimulus was given in the medium. When gel rigidity increased, cell morphology changed from elongated to round cells, and although overall cell survival decreased, more osteogenic differentiation of MSCs was observed. This intrinsic osteogenicity of surviving cells has, to our knowledge, not been reported in literature. Changes in viscoelastic properties of MeHA gels have directly led to altered differentiation patterns of neural progenitor cells as reported in literature [35], indicating that mechanical properties of the material influence cell fate [36,37], which is in agreement with our findings. When an osteogenic stimulus (BMP-2) was added to the hydrogel with intrinsic osteogenicity, a synergistic pattern of increased mineralization was observed. These data indicate that the MeHA hydrogels can function as suitable scaffold material for bone regeneration purposes in regenerative medicine, when the appropriate hydrogel concentration and with this, visco-elastic properties are selected [38].

Printability of the MeHA hydrogels was thoroughly investigated, in a porous and non-porous (anatomical) scaffold design. 3D printability of a material allows smart scaffold design, for example, with 3D bioprinting specific deposition of (multiple) cell types, (local) presence of bioactive molecules, pore size and distribution, complex geometries and customized 3D shapes, according to individual needs [39] can be accomplished. Scaffold porosity is considered beneficial for bone regeneration as it lowers the diffusion distance within the constructs, allowing rapid tissue ingrowth and vascularization [40]. We have shown that 3D bioprinting applying a hydrogel with a relatively low elastic modulus is possible when solid bioprinting of the anatomically shaped scaffolds is needed. The open structure of the MeHA hydrogel together with its excellent biocompatibility result in good cell performance and may be favorable for various cell types.

We were, to our knowledge, the first to introduce primary cells to the resulting high molecular weight MeHA, induce (intrinsic) differentiation and apply this material in 3D bioprinted scaffolds. The high levels of cell survival and intrinsic osteogenic differentiation in a 3D bioprintable hydrogel are very promising for future applications of this material in regenerative medicine.

CONCLUSION

By methacrylation of high molecular weight hyaluronic acid, 3D printable hydrogels were acquired. These hydrogels showed good primary cell survival and excellent spontaneous osteogenic differentiation *in vitro*. We defined boundary conditions for optimization of 3D bioprinted hydrogel based scaffolds for bone regeneration. MeHA-based hydrogels with intrinsic osteogenicity are promising scaffold materials for application in 3D printed, tissue engineered bone substitutes.

REFERENCES

1. Slaughter BV, Khurshid SS, Fisher OZ, Khademhosseini A, Peppas NA. Hydrogels in regenerative medicine. *Adv Mater 2009;21-32-33:3307-29.*
2. Bulpitt P, Aeschlimann D. New strategy for chemical modification of hyaluronic acid: preparation of functionalized derivatives and their use in the formation of novel biocompatible hydrogels. *J Biomed Mater Res 1999;47-2:152-69.*
3. Rowley JA, Madlambayan G, Mooney DJ. Alginate hydrogels as synthetic extracellular matrix materials. *Biomaterials 1999;20-1:45-53.*
4. Benoit DS, Schwartz MP, Durney AR, Anseth KS. Small functional groups for controlled differentiation of hydrogel-encapsulated human mesenchymal stem cells. *Nat Mater 2008;7-10:816-23.*
5. Munarin F, Petrini P, Bozzini S, Tanzi MC. New perspectives in cell delivery systems for tissue regeneration: natural-derived injectable hydrogels. *J Appl Biomater Funct Mater 2012;10-2:67-81.*
6. Malafaya PB, Silva GA, Reis RL. Natural-origin polymers as carriers and scaffolds for biomolecules and cell delivery in tissue engineering applications. *Adv Drug Deliv Rev 2007;59-4-5:207-33.*
7. Annabi N, Tamayol A, Uquillas JA, Akbari M, Bertassoni LE, Cha C, Camci-Unal G, Dokmeci MR, Peppas NA, Khademhosseini A. 25th anniversary article: Rational design and applications of hydrogels in regenerative medicine. *Adv Mater 2014;26-1:85-123.*
8. Burdick JA, Anseth KS. Photoencapsulation of osteoblasts in injectable RGD-modified PEG hydrogels for bone tissue engineering. *Biomaterials 2002;23-22:4315-23.*
9. Hirama H, Odera T, Torii T, Moriguchi H. A lithography-free procedure for fabricating three-dimensional microchannels using hydrogel molds. *Biomed Microdevices 2012;14-4:689-97.*
10. Arcaute K, Mann BK, Wicker RB. Fabrication of Off-the-Shelf Multilumen Poly(Ethylene Glycol) Nerve Guidance Conduits Using Stereolithography. *Tissue Eng Part C Methods 2010.*
11. Gaetani R, Doevendans PA, Metz CH, Alblas J, Messina E, Giacomello A, Sluijter JP. Cardiac tissue engineering using tissue printing technology and human cardiac progenitor cells. *Biomaterials 2012;33-6:1782-90.*
12. Fedorovich N, Schuurman W, Wijnberg H, Prins HJ, van Weeren R, Malda J, Alblas J, Dhert W. Biofabrication of osteochondral tissue equivalents by printing topologically defined, cell-laden hydrogel scaffolds. *Tissue Eng Part C Methods 2011.*
13. Fraser JR, Laurent TC, Laurent UB. Hyaluronan: its nature, distribution, functions and turnover. *J Intern Med 1997;242-1:27-33.*
14. Burdick JA, Chung C, Jia X, Randolph MA, Langer R. Controlled degradation and mechanical behavior of photopolymerized hyaluronic acid networks. *Biomacromolecules 2005;6-1:386-91.*
15. Engler AJ, Sen S, Sweeney HL, Discher DE. Matrix elasticity directs stem cell lineage specification. *Cell 2006;126-4:677-89.*
16. Billiet T, Gevaert E, De Schryver T, Cornelissen M, Dubruel P. The 3D printing of gelatin methacrylamide cell-laden tissue-engineered constructs with high cell viability. *Biomaterials 2014;35-1:49-62.*
17. Fedorovich NE, Oudshoorn MH, van Geemen D, Hennink WE, Alblas J, Dhert WJ. The effect of photopolymerization on stem cells embedded in hydrogels. *Biomaterials 2009;30-3:344-53.*
18. Oudshoorn MHM RR, Bouwstra JA, Hennink WE. Synthesis of methacrylated hyaluronic acid with tailored degree of substitution. *Polymer 2007;48-7:1915-20.*
19. Hayami JWS, Waldman, S.D., Amsden, B.G. Photo-Cross-Linked Methacrylated Polysaccharide Solution Blends With High Chondrocyte Viability, Minimal Swelling, and Moduli Similar to Load Bearing Soft Tissues. *European Polymer Journal 2015.*

20. Hachet E, Van Den Berghe H, Bayma E, Block MR, Auzely-Velty R. Design of biomimetic cell-interactive substrates using hyaluronic acid hydrogels with tunable mechanical properties. *Biomacromolecules 2012;13-6:1818-27*.
21. Delpech B, Bertrand P, Chauzy C. An indirect enzymoimmunological assay for hyaluronidase. *J Immunol Methods 1987;104-1-2:223-9*.
22. Egan KP, Brennan TA, Pignolo RJ. Bone histomorphometry using free and commonly available software. *Histopathology 2012;61-6:1168-73*.
23. Fedorovich NE, Wijnberg HM, Dhert WJ, Alblas J. Distinct tissue formation by heterogeneous printing of osteo- and endothelial progenitor cells. *Tissue Eng Part A 2011;17-15-16:2113-21*.
24. Schuurman W, Khristov V, Pot MW, van Weeren PR, Dhert WJ, Malda J. Bioprinting of hybrid tissue constructs with tailorable mechanical properties. *Biofabrication 2011;3-2:021001*.
25. Smeds KA, Pfister-Serres A, Miki D, Dastgheib K, Inoue M, Hatchell DL, Grinstaff MW. Photocrosslinkable polysaccharides for in situ hydrogel formation. *J Biomed Mater Res 2001;54-1:115-21*.
26. Baier Leach J, Bivens KA, Patrick CW, Jr., Schmidt CE. Photocrosslinked hyaluronic acid hydrogels: natural, biodegradable tissue engineering scaffolds. *Biotechnol Bioeng 2003;82-5:578-89*.
27. Trudel J, Massia SP. Assessment of the cytotoxicity of photocrosslinked dextran and hyaluronan-based hydrogels to vascular smooth muscle cells. *Biomaterials 2002;23-16:3299-307*.
28. Patterson J, Siew R, Herring SW, Lin AS, Guldberg R, Stayton PS. Hyaluronic acid hydrogels with controlled degradation properties for oriented bone regeneration. *Biomaterials 2010;31-26: 6772-81*.
29. Yoon HY, Koo H, Choi KY, Chan Kwon I, Choi K, Park JH, Kim K. Photo-crosslinked hyaluronic acid nanoparticles with improved stability for in vivo tumor-targeted drug delivery. *Biomaterials 2013; 34-21:5273-80*.
30. Khademhosseini A, Eng G, Yeh J, Fukuda J, Blumling J, 3rd, Langer R, Burdick JA. Micromolding of photocrosslinkable hyaluronic acid for cell encapsulation and entrapment. *J Biomed Mater Res A 2006;79-3:522-32*.
31. Yang C, Cao M, Liu H, He Y, Xu J, Du Y, Liu Y, Wang W, Cui L, Hu J, Gao F. The high and low molecular weight forms of hyaluronan have distinct effects on CD44 clustering. *J Biol Chem 2012;287-51: 43094-107*.
32. Bae MS, Yang DH, Lee JB, Heo DN, Kwon YD, Youn IC, Choi K, Hong JH, Kim GT, Choi YS, Hwang EH, Kwon IK. Photo-cured hyaluronic acid-based hydrogels containing simvastatin as a bone tissue regeneration scaffold. *Biomaterials 2011;32-32:8161-71*.
33. Salinas CN, Cole BB, Kasko AM, Anseth KS. Chondrogenic differentiation potential of human mesenchymal stem cells photoencapsulated within poly(ethylene glycol)-arginine-glycine-aspartic acid-serine thiol-methacrylate mixed-mode networks. *Tissue Eng 2007;13-5:1025-34*.
34. Nuttelman CR, Tripodi MC, Anseth KS. Synthetic hydrogel niches that promote hMSC viability. *Matrix Biol 2005;24-3:208-18*.
35. Seidlits SK, Khaing ZZ, Petersen RR, Nickels JD, Vanscoy JE, Shear JB, Schmidt CE. The effects of hyaluronic acid hydrogels with tunable mechanical properties on neural progenitor cell differentiation. *Biomaterials 2010;31-14:3930-40*.
36. Xue R, Li JY, Yeh Y, Yang L, Chien S. Effects of matrix elasticity and cell density on human mesenchymal stem cells differentiation. *J Orthop Res 2013;31-9:1360-5*.
37. Hu X, Park SH, Gil ES, Xia XX, Weiss AS, Kaplan DL. The influence of elasticity and surface roughness on myogenic and osteogenic-differentiation of cells on silk-elastin biomaterials. *Biomaterials 2011;32-34:8979-89*.

38. Nam J, Johnson J, Lannutti JJ, Agarwal S. Modulation of embryonic mesenchymal progenitor cell differentiation via control over pure mechanical modulus in electrospun nanofibers. *Acta Biomater 2011;7-4:1516-24*.
39. Peltola SM, Melchels FP, Grijpma DW, Kellomaki M. A review of rapid prototyping techniques for tissue engineering purposes. *Ann Med 2008;40-4:268-80*.
40. Fedorovich NE, Kuipers E, Gawlitta D, Dhert WJ, Alblas J. Scaffold Porosity and Oxygenation of Printed Hydrogel Constructs Affect Functionality of Embedded Osteogenic Progenitors. *Tissue Eng Part A 2011*.

CHAPTER 7

Micro-computed tomography analysis to quantify growth factor-induced bone formation in ceramic scaffolds

Michelle Poldervaart
Johan van der Stok
Marieke 't Hart
Cumhur Öner
Wouter Dhert
Harrie Weinans
Jacqueline Alblas

Manuscript in preparation

ABSTRACT

Large bone defects are currently treated by application of bone grafts, however bone grafts are associated with important drawbacks such as limited availability, donor site morbidity and inferior performance. Together, this creates a great need for development of a suitable bone graft substitute, which involves testing performance in laboratory settings, preclinical animal tests and clinical trials. The gold standard to quantify bone formation is bone histomorphometry, a time consuming method, which is performed *ex vivo*. In order to longitudinally monitor bone formation micro-CT (μCT) is promising. In the presence of ceramics, μCT analysis of new bone formation is complicated, since the density of this material is similar to that of bone. Depending on the defect location, growth factors are effective in inducing bone formation in bone replacement constructs. In this study, bone morphogenetic protein 2 (BMP-2), vascular endothelial growth factor (VEGF) and the chemokine stromal cell derived factor 1α (SDF1-α), were laden on gelatin microspheres (GMP) for controlled release in ceramic ectopic scaffolds. Analysis of bone formation by μ-CT as well as histomorphometry indicated that growth factor combinations induced significantly more bone than control scaffolds. Addition of VEGF or SDF1-α did not increase bone formation compared to BMP-2 laden scaffolds, but addition of SDF1-α was significantly more effective than addition of VEGF. To analyze bone formation, histomorphometry was performed, and μCT analysis was validated, and proved to be a reliable method, even in the presence of radio opaque ceramic scaffold materials.

INTRODUCTION

Treatment of extensive bone defects poses a challenge in orthopedic surgery. Large bone defects rely on the suppletion of bone tissue in order to heal, they are currently treated with auto- or allograft bone. Autograft bone has important drawbacks, namely limited availability of donor bone and donor site morbidity [1,2]. Allograft bone is also scarce, and subject to necessary tissue processing steps, such as freeze-drying, in order to eliminate pathogens and create surgically applicable materials, which may lead to inferior performance [3]. To provide a safe and effective alternative to bone grafts, tissue engineered bone constructs have become an important subject of research in the field of regenerative medicine [4]. A broad spectrum of biomaterials is currently under investigation in different *in vitro* and *in vivo* models for their suitability to function as a scaffold for bone regeneration [5,6]. To this purpose, calcium phosphate scaffolds are applied as bone substitute materials, for example in dental implants, and they are mainly of interest due to their chemical similarity to the mineral composition of bone. Ceramic scaffolds are biocompatible, osteoconductive, and their degradation is tailorable. However, the lack of vascularization and osteoblast colonization renders it impossible to repair large osseous defects. In order to improve vascularization and osteoblast colonization, growth factors are increasingly applied in regenerative medicine [7]. Growth factors such as vascular endothelial growth factor (VEGF) can be utilized to achieve angio- and vasculogenesis [8,9], and the chemokine stromal cell-derived factor 1α (SDF1-α) is known to play an important role in stem cell homing, and can recruit multipotent stromal cells (MSCs) towards tissue engineered constructs [10]. Even though the effects of SDF1-α on osteogenic differentiation in tissue engineered constructs *in vivo* is not clear [11], synergistic effects of SDF1-α addition to bone morphogenetic protein 2 (BMP-2) laden scaffolds have been reported [12,13]. BMP-2 is a clinically applied growth factor, used for vertebral fusion, that induces osteogenic differentiation of MSCs *in vitro* [14], stimulates bone formation *in vivo*, and plays an important role in fracture healing [15].

Growth factors have short half-life times *in vivo*, and in order to achieve optimal results of their application, prolonged growth factor presence, for example by the means of a controlled release system, is believed to be favorable [16]. Gelatin microparticles (GMP) are a biocompatible, easily tailorable release vehicle, in which growth factor encapsulation is based on non-covalent, electrostatic interactions between the growth factor and the gelatin [17-19]. One of the main advantages of GMPs is that growth factor loading is based on diffusion, hereby avoiding protein damage that is associated with chemical cross-linking. GMPs degrade after several weeks *in vivo*, they are not cytotoxic, and have previously been used to deliver various growth factors [20,21].

Osteogenesis of different growth factor-laded ceramic scaffolds is currently mainly analyzed by bone histomorphometry, a time consuming and laborious method, per-

formed *ex vivo*. Compared to histomorphometery, analyzing bone formation using micro computed tomography (μCT) offers the advantages of being a non-invasive technique that allows longitudinal data gathering. Unfortunately, μCT detection of bone in the presence of the ceramics poses major challenges, since their structure and radio-opaque properties are very similar. However, new and improved scanning systems and optimal scanning parameters might make it possible to discriminate bone and ceramic tissue more easily. Here μCT and histomorphometric analysis of growth factor-laden ceramics implanted at an ectopic site in rats were compared, and the validity of μCT analysis in ceramic scaffolds was determined. The potential added effects of growth factor combinations by means of endogenous cell attraction, provision of an osteogenic stimulus, and stimulation of vascularization was investigated. Bone formation was explored by using the single and combined application of BMP-2, SDF1-α and VEGF.

MATERIALS AND METHODS

Scaffold preparation and study design

Biphasic calcium phosphate cylinders (BCP-1150 containing 82% hydroxyapatite and 18% tricalcium phosphate, Xpand, Bilhoven, the Netherlands) 7 mm in diameter, 3 mm in height with a porosity of 75±1% were cast-filled with 100 μl Matrigel (354230, growth factor-reduced, BD, New Jersey, USA, negative control group), or supplemented with single addition of 100 μg/ml BMP-2, or 100 μg/ml BMP-2 combined with 25 μg/ml VEGF, or with 25 μg/ml SDF1-α or all three factors. All growth factors were separately laden on gelatin microspheres (GMP) for sustained release before inclusion in the Matrigel. The experimental groups are depicted in table 1.

Table 1. Experimental groups.

Group	Control	BMP-2	BMP-2 VEGF	BMP-2 SDF1-α	Combined growth factors
BMP-2 [100 μg/ml]	-	✓	✓	✓	✓
VEGF [25 μg/ml]	-	-	✓	-	✓
SDF1-α [25 μg/ml]	-	-	-	✓	✓

Surgical technique / animals and operations

Animal experiments were performed with permission of the Animal Ethical Committee of the Erasmus University for Animal Experimentation in compliance with the Institutional Guidelines following the Dutch Law ('Wet op de dierproeven') on the use of laboratory animals. Ten male Wistar rats (Charles River), 16 weeks of age were housed in standard

cages at the Laboratory Animal Institute. Prior to surgery, a single dose of antibiotics (enrofloxacin, 5 mg/kg body weight) was administered. Operations were performed aseptically under general anesthesia (1-3.5% isoflurane).

Dorsal subcutaneous pockets were created bilaterally by blunt dissection. The BCP cylinders were assigned to a pocket by randomization (each animal received all treatment groups). Pockets were closed using sutures (Vicryl 4.0). The animals also received bilateral femoral bone chambers, that were reported on elsewhere [22]. Postoperatively the animals were weighed and given a subcutaneous injection of buprenorphin (0.05 mg/kg, Temgesic, Schering-Plough/Merck, Whitehouse station, NJ, USA) twice a day for the first three days after surgery.

Fluorochrome labels were administered at 4 (tetracyclin, 25 mg/kg bodyweight), 8 (calcein, 25 mg/kg body weight), and 11 weeks (xylenol orange, 90 mg/kg body weight) to monitor the onset of bone formation [23]. The 8 week label was not incorporated in any of the samples or bone tissue and, therefore it was not included in the fluorochrome analysis.

The rats were terminated after 12 weeks using an injection of Euthanasol (Virbac, Fort Worth, Tx, USA).

µCT evaluation

After explantation of the subcutaneously implanted BCP scaffolds, *ex vivo* µCT scans were acquired using a SkyScan 1176 scanner (Bruker µCT, Kontich, Belgium) and a 9 µm-resolution protocol was applied (65 kV, 1320 ms exposure time, 1.0 mm Al filter, 0.32 degree rotation step, 53 min scan). All µCT images were reconstructed using volumetric reconstruction software NRecon version 1.5 (Bruker µCT).

Bone formation was measured after exclusion of the BCP scaffold, which was achieved through segmentation of the greyscale images with a global threshold (CTAnalyser version 1.11 software). Within the remaining pore space, another global threshold was applied to segment calcified tissue from non-calcified tissue and noise. To reduce border artifacts caused by the BCP, an extra erosion step was applied after which bone volume was quantified. An observer that was blinded for the research groups performed all analyses and segmentations.

Histology and histomorphometry

The BCP scaffolds were fixed in 4% buffered formalin, dehydrated using ethanol series and embedded in polymethylmethacrylate (MMA). All samples were sawed centrally into approximately 25 µm thick sections using a sawing microtome (Leica, Nussloch, Germany) and stained with methylene blue and basic fuchsin for histomorphometric analysis. High-resolution digital pictures of the samples were taken using transmitted light microscopy (Olympus-BX50, Olympus, Zoeterwoude, the Netherlands). Bone and

scaffold were pseudo-colored on blinded samples using Adobe Photoshop CS5.1 and respective surfaces were measured (Adobe Systems Inc, San Jose, USA). Bone area percentage was calculated as (bone area / (total area - BCP area))*100%.

Statistical analysis

Study endpoints and statistical methods were prospectively selected and documented. Sample size (n=10) was calculated with a power analysis to achieve reliable measurement of the effect, this number did not change in the course of the study. All data were included in the analysis and no outliers were detected. All samples were randomly allocated, and implanted and analyzed by researchers who were blinded for the experimental groups.

Histomorphometry data were analyzed by SPSS version 20 software (IBM, Chicago, Illinois, USA). Differences between groups were analyzed with a paired t-test. Post-hoc testing was performed using a Bonferroni correction. All bars represent mean values, with standard deviations depicted in the error bars. The correlation between µCT measurements and histomorphometric data in presence of BCP was assessed with a Pearson Correlation. Significance was assumed when $p<0.05$.

RESULTS

Growth factor induced bone formation

Bone formation after 12 weeks of implantation was evident in the growth factor containing groups (Figure 1), which all showed a significant increase compared to the control group, in which bone was not formed. Addition of VEGF or SDF1-α to BMP-2 laden scaffolds did not increase bone formation compared to scaffolds loaded with BMP-2 alone, but the addition of SDF1-α to a BMP-2 laden scaffold performed better than VEGF addition, resulting in a significantly higher bone area%. Furthermore, when SDF1-α and VEGF were both added (the combined growth factor group) this led to a significant increase in bone area % compared to the BMP-2/VEGF group. In the scaffolds that contained bone, the earliest given fluorochrome (the week 4 label) was present, indicating that bone formation started before week 4 and was continuous. No significant differences in onset of bone formation were observed between the groups (Figure 2).

Validation of µCT analysis for bone formation in presence of ceramics

The BCP cylinders were excluded from the *ex vivo* µCT volume determination by segmentation, and bone volumes were calculated. In the control group without growth factors some signal was apparent after 12 weeks of implantation, indicating that not all border artifacts could be excluded. Similar to histomorphometry, in all other experimen-

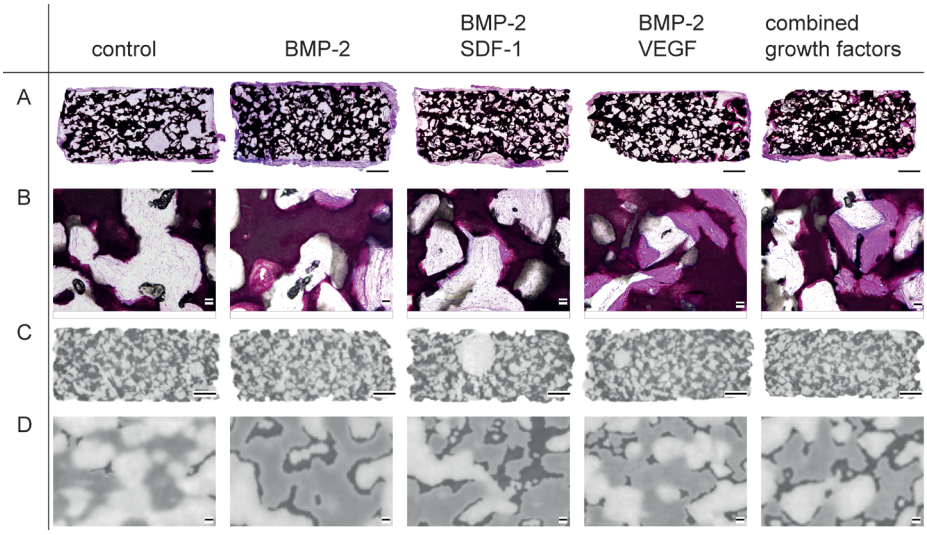

Figure 1. Bone formation in ectopic scaffolds.
A-B. Histological overview **(A)** and detail magnification **(B)** of the research groups. Bone stained bright pink using basic fuchsin eosin staining. **C-D**. µCT scan of the samples, showing total, unsegmented overview **(C)**, and segmented detail images **(D)**. After segmentation scaffold is depicted in light grey, bone in dark grey. Scale bars represent 1mm. Representative pictures are shown.

tal groups significantly more bone was measured than in the control group (Figure 3A). Comparison between histological and µCT assessment of the bone formation revealed a significant correlation, indicating that both methods can be reliably applied, even in the presence of BCP (Figure 3B).

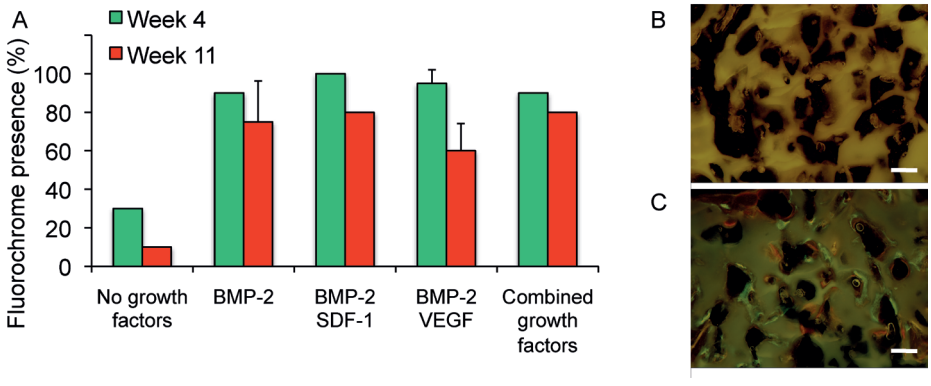

Figure 2. Onset of bone formation
(A) Green bars depict incorporation of week 4 label, red bars depict incorporation of the week 11 label. **(B)** Construct without fluorochrome incorporation (control group) and **(C)** construct that incorporated both fluorochrome labels (combined growth factor group, bottom), representative images are shown. Scale bars represent 500 µm.

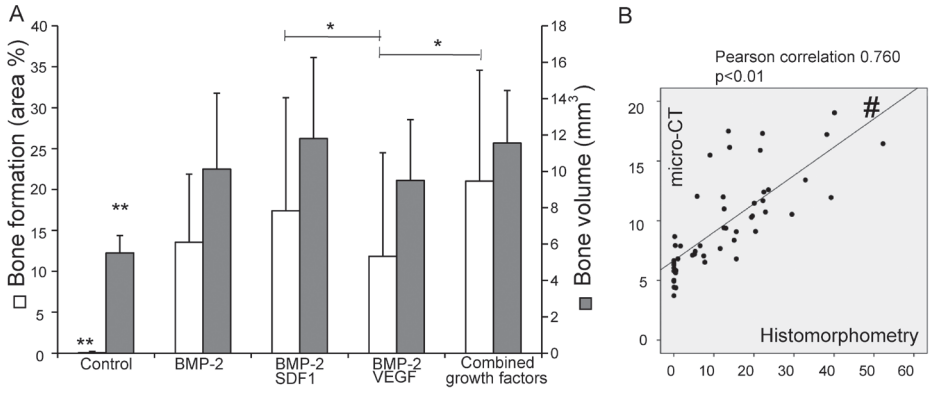

Figure 3. Quantification of bone formation.
(**A**) The bone area % as measured by histomorphometry is depicted in white bars, grey bars represent bone volume in mm^3, measured by ex-vivo µCT. **Significantly different from all other groups ($p<0.01$), *Significant differences between BMP-2/VEGF group compared to BMP-2/SDF-1α and combined growth factor groups ($p<0.05$). (**B**) Scatter plot of correlation between µCT and histomorphometric measurements. # indicates a significant correlation ($p<0.01$).

DISCUSSION

In this study, application of growth factor led to increased bone formation, and results obtained from histology and µCT were significantly correlated, even in the presence of a radio-opaque ceramic.

Hardly any differences in bone formation were observed for the various growth factor containing groups based on the µCT data, after 12 weeks of implantation. An earlier end-point could possibly have elucidated more pronounced differences between the research groups, as it became apparent in the simultaneously implanted bone chambers that bone formation was most pronounced after 8 weeks of implantation [22]. Addition of VEGF or SDF1-α to BMP-2 laden scaffolds did not increase ectopic bone formation. Nevertheless, presence of SDF1-α in BMP-2 based scaffolds was more effective in stimulating bone formation than VEGF combined with BMP-2. Overall, high ectopic bone formation occurred in groups where SDF1-α was present, which could indicate an effect of the chemokine on MSC recruitment towards the BMP-2 laden constructs, or increased vascularization induced by SDF1-α. In this particular model, BMP-2 alone showed a strong bone inducing potential at the ectopic location; the combination of three growth factors did not show a synergistic effect as expected. This could be related to the applied concentration of BMP-2, which was supraphysiological based on findings in literature [24]. This may have led to optimal bone induction, hereby masking possible synergistic or additive effects of the other growth factors that are well established for VEGF [9,25], and also reported for SDF1-α [13].

GMPs were applied because of their beneficial effects on growth factor delivery seen in our previous studies [26,27]. In this experimental set-up the release of the growth factors was expected to be gradual, also because Matrigel is known to retain growth factors efficiently [28]. The use of GMPs is reported for BMP-2 and VEGF delivery, both single and combined [16], and there is evidence that controlled release of SDF1-α leads to improved angiogenesis [29]. Together, these findings argue against insufficient presence of the individual growth factors due to combined release systems.

To analyze bone formation in this study, histomorphometry as well as μCT scans were performed. Histomorphometry is considered the gold standard in the assessment of bone formation. A good correlation between histomorphometric and μCT acquired data in cortical bone has been established in the literature [30,31], but this correlation is highly dependent on the opacity of materials present in the implants [32]. Bone volume determination in the context of BCP is known to pose a problem in the analysis of μCT data, as bone and BCP are very similar in radio-opacity [33]. This is seen for instance in the control group of the ectopic implants, where histomorphometry consistently showed that no bone was formed. However, when this group was analyzed by μCT a sizable volume was measured. From this we conclude that despite vigorous segmentation, the μCT analysis still identified a substantial signal, measuring up to 10.5% of the total BCP volume in the bone-defined grayscale. These volumes are per definition an overestimation, which could possibly be improved by acquiring higher resolution μCT scans and more precise scanning settings. Despite this overestimation, the results from the two methods were significantly correlated, leading us to conclude that differences between the experimental groups were detectable and valid. This offers the advantage of longitudinal, non-invasive monitoring of bone formation. More advanced scanning protocols may lead to *in vivo* monitoring of bone formation. To our knowledge, the use of μCT for BCP-based scaffolds has not been previously validated.

CONCLUSION

Taken together, we conclude that μCT analysis is a suitable method to detect growth factor induced bone formation, even in the presence of ceramic scaffolds. Application of μCT analysis in this fashion allows longitudinal, non-invasive investigation of bone formation.

REFERENCES

1. Silber JS, Anderson DG, Daffner SD, Brislin BT, Leland JM, Hilibrand AS, Vaccaro AR, Albert TJ. Donor site morbidity after anterior iliac crest bone harvest for single-level anterior cervical discectomy and fusion. *Spine (Phila Pa 1976) 2003;28-2:134-9*.
2. Khan SN, Cammisa FP, Jr., Sandhu HS, Diwan AD, Girardi FP, Lane JM. The biology of bone grafting. *J Am Acad Orthop Surg 2005;13-1:77-86*.
3. Finkemeier CG. Bone-grafting and bone-graft substitutes. *J Bone Joint Surg Am 2002;84-A-3: 454-64*.
4. Hutmacher DW. Scaffolds in tissue engineering bone and cartilage. *Biomaterials 2000;21-24: 2529-43*.
5. Barradas AM, Yuan H, van Blitterswijk CA, Habibovic P. Osteoinductive biomaterials: current knowledge of properties, experimental models and biological mechanisms. *Eur Cell Mater 2011; 21:407-29; discussion 29*.
6. Van der Stok J, Van Lieshout EM, El-Massoudi Y, Van Kralingen GH, Patka P. Bone substitutes in the Netherlands - a systematic literature review. *Acta Biomater 2011;7-2:739-50*.
7. Lee K, Silva EA, Mooney DJ. Growth factor delivery-based tissue engineering: general approaches and a review of recent developments. *J R Soc Interface 2011;8-55:153-70*.
8. Ferrara N, Gerber HP, LeCouter J. The biology of VEGF and its receptors. *Nat Med 2003;9-6:669-76*.
9. Kanczler JM, Ginty PJ, White L, Clarke NM, Howdle SM, Shakesheff KM, Oreffo RO. The effect of the delivery of vascular endothelial growth factor and bone morphogenic protein-2 to osteoprogenitor cell populations on bone formation. *Biomaterials 2010;31-6:1242-50*.
10. Hattori K, Heissig B, Tashiro K, Honjo T, Tateno M, Shieh JH, Hackett NR, Quitoriano MS, Crystal RG, Rafii S, Moore MA. Plasma elevation of stromal cell-derived factor-1 induces mobilization of mature and immature hematopoietic progenitor and stem cells. *Blood 2001;97-11:3354-60*.
11. Eman RM, Oner FC, Kruyt MMP, Dhert W, Alblas J. Stromal cell-derived factor-1 stimulates cell recruitment, vascularization and osteogenic differentiation. *Tissue Eng Part A 2013*.
12. Liu X, Zhou C, Li Y, Ji Y, Xu G, Wang X, Yan J. SDF-1 promotes endochondral bone repair during fracture healing at the traumatic brain injury condition. *PLoS ONE 2013;8-1:e54077*.
13. Ratanavaraporn J, Furuya H, Kohara H, Tabata Y. Synergistic effects of the dual release of stromal cell-derived factor-1 and bone morphogenetic protein-2 from hydrogels on bone regeneration. *Biomaterials 2011;32-11:2797-811*.
14. Poldervaart MT, Wang H, van der Stok J, Weinans H, Leeuwenburgh SC, Oner FC, Dhert WJ, Alblas J. Sustained Release of BMP-2 in Bioprinted Alginate for Osteogenicity in Mice and Rats. *PLoS ONE 2013;8-8:e72610*.
15. Garrison KR, Shemilt I, Donell S, Ryder JJ, Mugford M, Harvey I, Song F, Alt V. Bone morphogenetic protein (BMP) for fracture healing in adults. *Cochrane Database Syst Rev 2010-6:CD006950*.
16. Patel ZS, Young S, Tabata Y, Jansen JA, Wong ME, Mikos AG. Dual delivery of an angiogenic and an osteogenic growth factor for bone regeneration in a critical size defect model. *Bone 2008;43-5: 931-40*.
17. Ikada Y, Tabata Y. Protein release from gelatin matrices. *Adv Drug Deliv Rev 1998;31-3:287-301*.
18. Yamamoto M, Ikada Y, Tabata Y. Controlled release of growth factors based on biodegradation of gelatin hydrogel. *J Biomater Sci Polym Ed 2001;12-1:77-88*.
19. Patel ZS, Ueda H, Yamamoto M, Tabata Y, Mikos AG. In vitro and in vivo release of vascular endothelial growth factor from gelatin microparticles and biodegradable composite scaffolds. *Pharm Res 2008;25-10:2370-8*.

20. Leeuwenburgh SC, Jo J, Wang H, Yamamoto M, Jansen JA, Tabata Y. Mineralization, biodegradation, and drug release behavior of gelatin/apatite composite microspheres for bone regeneration. *Biomacromolecules 2010;11-10:2653-9*.
21. Yamamoto M, Takahashi Y, Tabata Y. Controlled release by biodegradable hydrogels enhances the ectopic bone formation of bone morphogenetic protein. *Biomaterials 2003;24-24:4375-83*.
22. Poldervaart MT, van der Stok J, de Haas MF, t Hart MC, Oner FC, Dhert WJ, Weinans H, Alblas J. Growth factor-induced osteogenesis in a novel radiolucent bone chamber. *Eur Cell Mater 2015;29: 35-41; discussion*
23. van Gaalen SM, Kruyt MC, Geuze RE, de Bruijn JD, Alblas J, Dhert WJ. Use of fluorochrome labels in in vivo bone tissue engineering research. *Tissue Eng Part B Rev 2010;16-2:209-17*.
24. Jang JW, Yun JH, Lee KI, Jung UW, Kim CS, Choi SH, Cho KS. Osteoinductive activity of biphasic calcium phosphate with different rhBMP-2 doses in rats. *Oral Surg Oral Med Oral Pathol Oral Radiol 2012;113-4:480-7*.
25. Kempen DH, Lu L, Heijink A, Hefferan TE, Creemers LB, Maran A, Yaszemski MJ, Dhert WJ. Effect of local sequential VEGF and BMP-2 delivery on ectopic and orthotopic bone regeneration. *Biomaterials 2009;30-14:2816-25*.
26. Kempen DH, Lu L, Hefferan TE, Creemers LB, Maran A, Classic KL, Dhert WJ, Yaszemski MJ. Retention of in vitro and in vivo BMP-2 bioactivities in sustained delivery vehicles for bone tissue engineering. *Biomaterials 2008;29-22:3245-52*.
27. Poldervaart MT, Gremmels H, van Deventer K, Fledderus JO, Oner FC, Verhaar MC, Dhert WJ, Alblas J. Prolonged presence of VEGF promotes vascularization in 3D bioprinted scaffolds with defined architecture. *J Control Release 2014;184:58-66*.
28. Gao Y, Zhu S, Luo E, Li J, Feng G, Hu J. Basic fibroblast growth factor suspended in Matrigel improves titanium implant fixation in ovariectomized rats. *J Control Release 2009;139-1:15-21*.
29. Kimura Y, Tabata Y. Controlled release of stromal-cell-derived factor-1 from gelatin hydrogels enhances angiogenesis. *J Biomater Sci Polym Ed 2010;21-1:37-51*.
30. Schouten C, Meijer GJ, van den Beucken JJ, Spauwen PH, Jansen JA. The quantitative assessment of peri-implant bone responses using histomorphometry and micro-computed tomography. *Biomaterials 2009;30-27:4539-49*.
31. Muller R, Van Campenhout H, Van Damme B, Van Der Perre G, Dequeker J, Hildebrand T, Ruegsegger P. Morphometric analysis of human bone biopsies: a quantitative structural comparison of histological sections and micro-computed tomography. *Bone 1998;23-1:59-66*.
32. Vandeweghe S, Coelho PG, Vanhove C, Wennerberg A, Jimbo R. Utilizing micro-computed tomography to evaluate bone structure surrounding dental implants: A comparison with histomorphometry. *J Biomed Mater Res B Appl Biomater 2013;101-7:1259-66*.
33. Gauthier O, Muller R, von Stechow D, Lamy B, Weiss P, Bouler JM, Aguado E, Daculsi G. In vivo bone regeneration with injectable calcium phosphate biomaterial: a three-dimensional micro-computed tomographic, biomechanical and SEM study. *Biomaterials 2005;26-27:5444-53*.

CHAPTER 8

General discussion and summary

Bone tissue engineering has been investigated for decades, and has shown to be an effective method to induce ectopic bone formation in numerous animal models. The translation to, and application in clinical practice is an ongoing challenge, and as a result, tissue engineered bone grafts are not used routinely. The overall aim of this thesis was to improve scaffold architecture and functionality for tissue engineering of bone. The resulting scaffolds can be applied as a model to answer basic scientific questions as well as an important step towards future application of regenerative techniques in clinical practice.

APPLICATION OF CELLS IN BONE TISSUE ENGINEERING

Mesenchymal stromal cells in bone tissue engineering

In animal models, application of mesenchymal stromal cells (MSCs) has led to very promising results, often inducing ectopic bone formation in cell-seeded scaffolds [1-3]. MSCs from various sources are used, from both autologous and allogeneic origin [4]. The common goal of researchers is to create a bone graft substitute that can replace autologous and allogeneic bone grafts in clinical practice. Cell based bone graft substitutes are very successful in small animal models [5-7], however in larger animal models the results are less favorable [8-10]. In humans, only a limited amount of cell based bone tissue engineered constructs have been reported, with inconclusive outcomes [11-13].

Alternatively, MSCs comprise a very important model in *in vitro* work. MSC survival and differentiation resulting from new bioactive molecules or materials are often the first steps towards translation to animal models. In this thesis, MSCs were applied *in vitro* (chapter 2) as a model to compare BMP-2 induced osteogenic differentiation in 3D bioprinted alginate scaffolds. The *in vivo* application of the MSCs was performed in an ectopic location, in this case dorsal pockets, where no osteoblasts are present, so that bone formation could be fully attributed to MSC differentiation[14].

In our mice study presence of MSCs was pivotal for ectopic bone formation; and the strategy to attract endogenous MSCs to our scaffolds using SDF1-α was found to be insufficient (chapter 4), despite earlier encouraging results in our group [15]. In contrast, in our rat model, no MSCs were necessary to induce ectopic bone formation, growth factor presence on ceramic scaffolds provided sufficient osteoinductivity (chapter 5). In these cases the experimental setup was different in regards to scaffold material, growth factor concentrations and release profiles. Also, in order to allow the use of xenograft cells, it was necessary to employ immuno-deficient mice. The role of the immune system in bone formation is increasingly researched and found to be important[16]. Species-dependent findings underline the difficulty interpreting the outcomes of animal models and clinical trials. This is further complicated by the variety of methods that are applied

in numerous models, the lack of comparability of outcome measures and the impact of donor-dependent differences [17-19]. Cell free approaches are as a result increasingly applied, eliminating the need for immuno-deficient animal models and donor-variable difficulties, facilitating the translation to clinical practice.

Prevascularization strategies

A crucial step for survival of bone tissue engineered grafts is vascularization. Bone is a highly vascularized tissue. After implantation of a bone graft, host vessel in-growth takes time, limiting nutrient supply and waste removal to diffusion in the first implantation phase. In the absence of sufficient vascularization central necrosis appears beyond the critical diffusion distance[20]. Different approaches are known to facilitate rapid vasculogenesis *in vivo*, ideally, novel networks anastomose with pre-existing blood vessels, which infiltrate the defect site from its periphery. One of the possible approaches is the application of umbilical cord epithelial progenitor cells (EPCs) in scaffold materials, since they can form *de novo* blood vessels[21,22]. Another approach is angiogenic growth factor application, for example by using vascular endothelial growth factor (VEGF) or stromal-cell derived factor 1α (SDF1-α). These growth factors can induce vasculogenesis, vasculogenesis and attract host cells towards constructs in order to improve scaffold survival, and later these early vascular structures are known to adapt and remodel over time in response to functional demands [23].

In this thesis, prolonged presence of VEGF, released from gelatin microspheres, led to an increased number of perfused vessels in EPC containing Matrigel plugs compared to regular VEGF application (chapter three). Umbilical cord EPCs were used to assess the effect of prolonged VEGF presence. From previous studies it is known that without these cells hardly any vessel formation would occur in ectopic constructs, but better control over growth factor release and timing, combined with endogenous EPC recruitment could mean important progress in achieving cell free, well-vascularized constructs. This is a fundamental step for *in vivo* survival of clinically relevant sized tissue engineered bone grafts.

IMPROVING SCAFFOLD MATERIALS FOR BONE TISSUE ENGINEERING

Scaffolds as bone regeneration matrices

A large variety in scaffold materials for bone tissue engineering is currently under investigation, ranging from polymers, bioglass, titanium to ceramics and hydrogels. Ideally, a scaffold should be highly porous with an interconnected pore network enabling vascularization for transport of nutrients and metabolic waste.

Scaffolds should be biocompatible, minimizing the host response to the graft and be bioresorbable, ideally at the rate the new tissue grows in. Mechanical properties should match the demands of the implantation site, for example the need for weight baring, and the material should have a suitable surface for cell interaction, allowing osteoconduction and osteoinduction[24]. Futhermore they should be shaped to fit clinical applications, safe, off the shelf available and easy to prepare for application. The mentioned (bio) materials have their own advantages and disadvantages (as detailed for each biomaterial mentioned below); combined application of scaffold materials allows for combining and optimizing scaffold properties. In this thesis a palet of materials was used, to allow bioprinting, cell encapsulation, survival and differentiation and implement growth factor incorporation.

Hydrogels

Hydrogels, the main scaffold materials in this thesis, were applied in plugs, in bone chambers and were bioprinted. Hydrogels do not possess the mechanical strength that bone has, however hydrogels allow cell and growth factor incorporation, making the resulting scaffolds highly bioactive, enabling fast integration with host tissues. Enforcing a hydrogel by adding stiffer materials, by post-processing or for example by applying the gel in a cage or capsule or a non-weightbaring location compensates for the lack of mechanical strength[25].

In chapter 2 and 4, alginate was used to bioprint BMP-2 and MSC laden scaffolds, incorporate SDF1-α and transfect cells, respectively. It could be rapidly crosslinked after cell and growth factor incorporation or bioprinting. Bioprinted alginate was degraded very fast *in vivo*, and this severely affected tissue ingrowth and the availability of signals leading to osteogenesis. The lack of coherence likely explained the absence of bone formation after in vivo implantation, as each of the components has been successfully used in bone tissue engineering approaches in previous experiments by our group [26,27]. The porosity of the constructs may have added to the disintegration effect, as it enlarges the surface to volume ratio of the constructs [28]. Alginate has proven to be a very promising scaffold material and transfection agent [29]. For bioprinting of porous constructs alginate needs further functionalization to control cross-linking density [30].

In chapter 3 and 5 Matrigel was applied, as it is a hydrogel that mimics extracellular matrix such that many cell types, and especially EPCs, perform optimally. In order to avoid by-stander effects with the many growth factors abundant in the gel, we applied the growth factor reduced variant [31]. The gel polymerizes at room temperature, but is unable to retain its bioprinted shape. Therefore, copolymers with alginate were made to include bioprinted porous scaffolds in this study. This addition directly diminished cell survival and differentiation. In an attempt to identify optimal conditions for a bioprintable hydrogel methacrylated hyaluronic acid was investigated in detail in chapter 6.

Several authors have previously published on the promising characteristics of the material [32-34]. The hydrogel density had significant effects on cell survival, differentiation and printability. Most striking was that at certain densities an intrinsic osteogenecity could be observed, underlining the pivotal importance of hydrogel selection.

Ceramics

When we consider the main components that comprise human bone tissue, it is not surprising that ceramics are a widely used bone substitute material. Ceramics in the form of carbonated apatite are by far the main component of the non organic matrix (69%)[35]. The organic matrix (22%) consists mainly of collagen type I, enriched with proteoglycans, lipids and osteogenic factors. The remaining 9% is comprised by water.

Calcium phosphate ceramics show remarkable biocompatibility and tailorable bioresorbability when applied as a scaffold material [36]. Though osteoconductive (guiding reparative bone growth), calcium phosphate scaffolds are not osteoinductive (stimulating bone growth by activating osteoblasts) *per se* but only in the context of binding tissue factors. Since it has been shown that combining the biomaterial with cells or bioactive factors can induce this property, both were applied in this thesis [37]. Biphasic calcium phosphates (BCP) are known to increase scaffold mechanical strength, but in this thesis adding BCP granules to bioprinted hydrogel scaffolds didn't perform as expected as many scaffolds were degraded at explantation, without formation of bone. When BCP was applied in the form of porous cylinders as a carrier of hydrogel and growth factors, bone was formed and the scaffolds remained intact. In this application however, no bioprinted architecture can be used. For future research, the use of BCP granules in a bioprinted, stiffer hydrogel can be a promising approach [34].

APPLICATION OF 3D BIOPRINTING TO INTRODUCE COMPLEX SCAFFOLD ARCHITECTURE IN BONE TISSUE ENGINEERING

Previous work from our research group emphasized the importance of scaffold porosity to allow ingrowth of host cells and tissue [38], in accordance with many international authors [39]. Also, it has been hypothesized that biomimicking of scaffolds, with architectonic similarity to the aimed host tissues could outperform randomly mixed materials as seen for example in casted scaffolds [39]. The 3D bioprinting technology makes it possible to investigate the role of regional complexity in tissue engineered constructs.

In order to introduce both macroporosity and regional subdifferentiation, various hydrogels were 3D bioprinted using fibre deposition. The aim of subdifferentiation was to design scaffolds with predefined regions for vessel formation and zonal bone formation (locally applying appropriate cells and bioactive factors). Hydrogels, and more

specifically natural hydrogels, are a highly favorable printing material due their intrinsic bioactivity and the possibility of cell encapsulation during the printing process with high cell survival. Hydrogels have not yet been ideally tailored to allow for the demands of the bioprinting process; there is a major gap between properties that provide for cell- and printing performance and even intrinsic osteogenicity, an issue that was investigated and described in chapter 6. The question whether regional bioactivity leads to better performing bone regenerative scaffolds remains unanswered and more research is needed to address this issue, but *in vitro* important steps towards solving this issue have been made in this thesis. Regional deposition of an angiogenic growth factor was achieved and local increased vessel formation appeared (chapter 3).

CONTROLLED RELEASE OF BIOACTIVE FACTORS FOR BONE TISSUE ENGINEERING

In order to create scaffolds with defined architecture (local) application of bioactive factors is pivotal. Timing of growth factor availability is important to ensure durability that can induce regional differentiation in the scaffold [40]. The growth factors that we applied are bone morphogenetic protein 2 (BMP-2), a strong osteoinductive stimulant, vascular endothelial growth factor (VEGF), an important factor for vasculogenesis and vasculogenesis, and stromal cell derived factor 1α (SDF1-α), a chemokine that is known to attract endogenous cells. These growth factors have in common that they are all quickly degraded in the bloodstream. BMP-2, VEGF, and SDF1-α have half life times of less than an hour. We chose to work with gelatin microparticles (MP), a well-known release vehicle with the main benefit that growth factor loading could be performed via simple diffusion [41,42]. No potentially damaging chemical reactions were necessary, and all tested growth factors retained their biological activity. Release from gelatin MP of any of the growth factors tested could be characterized by a small initial burst, presumably based on diffusion from the outer regions of the particles [43]. After this the release rate could be tailored by altering sphere diameter or crosslink density. Release of growth factors was successfully tailored to match the regenerative goals, for example, BMP-2 was aimed to be present for a month, whereas VEGF and SDF1-α are presumably needed in the first days to weeks after implantation. Growth factor laden GMPs could be incorporated into bioprintable hydrogels, an important step in producing scaffolds with defined regional functions (chapter 2).

FUTURE PERSPECTIVES

Understanding natural bone healing

The knowledge on molecular signaling and cell coordination during natural bone healing is limited. Investigation of growth factor expression during fracture healing is challenging, as the concentrations are low and subject to preliminary degradation. The available literature shows there is an abundance of growth factors and cytokines expressed during bone healing (for example TNF-α, VEGF, SDF1-α BMPs, interleukins) [44]. Understanding more about timing, location and interaction of growth factors throughout the different phases of natural bone healing could shed a new light on scaffold design and functionality.

Customized bone grafts

When state of the art imaging and scaffold production techniques are combined this creates novel possibilities in design and production of bone tissue substitutes. Non-invasive imaging techniques such as computed tomography (CT) and magnetic resonance imaging (MRI) can generate accurate anatomical shapes for scaffold design, and translate these to 3D printed individualized scaffolds. This principle is currently gaining popularity in joint replacement surgery, in which cutting blocks for implant placement in the operating theater are custom made for each patient, based on their anatomy [45]. When this approach is combined with application of suitable growth factors, cells and scaffold materials in certain predefined regions, this could add to the effectivity of these smart scaffolds.

Genetic engineering

Application of gene therapy could be an effective alternative to protein delivery. In this thesis gene therapy was used to transfect cells to produce endogenous BMP-2. Transfection of MSCs with the BMP-2 transfection agent rendered a low-cost non-viral BMP-2 delivery system, with high transfection efficiency. The BMP-2 that was produced as a result of transfection was biologically active and led to improved bone formation (chapter 4). Further research on transfection of other growth factors and translation to safe clinical application of the technique is needed.

SUMMARY AND FINAL REMARKS

The overall aim of this thesis was to improve scaffold architecture and functionality for bone tissue engineering compared to existing scaffolds.

The beneficial effect of prolonged growth factor availability was investigated. In chapter 2 prolonged presence of BMP-2 in scaffolds could be accomplished by applying GMPs. It proved to be feasible to incorporate these GMPs into a bioprinted alginate construct containing BCP and gMSCs where the presence of BMP-2 led to osteogenic differentiation *in vitro* and *in vivo*. In chapter 3, EPCs and GMPs were embedded into hydrogel plugs and subsequently implanted subcutaneously in mice, prolonged presence of VEGF led to a significant increase in scaffold vascularization compared to fast release or control groups. This is in accordance with literature regarding VEGF release from other delivery systems. Growth factors were combined in chapters 5 and 7. BMP-2, VEGF and the chemokine SDF1-α, were placed in bone chambers or laden on GMP for controlled release in ceramic ectopic scaffolds. Analysis of bone formation indicated that growth factor combinations induced significantly more bone than control scaffolds. Addition of VEGF or SDF1-α did not increase bone formation in an ectopic rat model compared to BMP-2 laden scaffolds, but addition of SDF1-α was significantly more effective than addition of VEGF. These results are unexpected when compared to the results of our mice study, indicating that in these scaffolds vascularization was not the limiting factor for bone formation and underlining the pivotal influence of scaffold material, scaffold location and host animal.

The influence of growth factor location within the scaffolds was also subject of investigation. Combining bioprinting with controlled growth factor release allowed scaffold properties to be fine-tuned in a temporal as well as a spatial manner and our results point to a location-dependent outcome in tissue regeneration as a first step. For example, a future scaffold could contain a bone cortex region containing ceramics, BMP-2 and SDF1-α, and a bone marrow region containing Matrigel with VEGF. It would be very interesting to compare bone formation in a pre-defined regional scaffold to scaffolds that contain a mixture of all these components. We hypothesise that a biomimicking scaffold leads to more bone formation, based mainly on superior early vascularization properties, endogenous cell attraction and local combined osteogenic stimuli.

Overall this thesis marks an important step in smart scaffold design, since combining the described techniques enables researchers to reach a higher level of scaffold biomimicry. The development of hydrogel-based scaffold materials that are cell friendly, allow cell differentiation and are bioprintable is ongoing, and embodies a pivotal step in this research field.

REFERENCES

1. Petite H, Viateau V, Bensaid W, Meunier A, de Pollak C, Bourguignon M, Oudina K, Sedel L, Guillemin G. Tissue-engineered bone regeneration. *Nat Biotechnol 2000;18-9:959-63*.
2. Zhang ZY, Teoh SH, Chong MS, Lee ES, Tan LG, Mattar CN, Fisk NM, Choolani M, Chan J. Neovascularization and bone formation mediated by fetal mesenchymal stem cell tissue-engineered bone grafts in critical-size femoral defects. *Biomaterials 2010;31-4:608-20*.
3. Tortelli F, Tasso R, Loiacono F, Cancedda R. The development of tissue-engineered bone of different origin through endochondral and intramembranous ossification following the implantation of mesenchymal stem cells and osteoblasts in a murine model. *Biomaterials 2010;31-2:242-9*.
4. Caplan AI, Bruder SP. Mesenchymal stem cells: building blocks for molecular medicine in the 21st century. *Trends Mol Med 2001;7-6:259-64*.
5. Krebsbach PH, Kuznetsov SA, Satomura K, Emmons RV, Rowe DW, Robey PG. Bone formation in vivo: comparison of osteogenesis by transplanted mouse and human marrow stromal fibroblasts. *Transplantation 1997;63-8:1059-69*.
6. Janicki P, Kasten P, Kleinschmidt K, Luginbuehl R, Richter W. Chondrogenic pre-induction of human mesenchymal stem cells on beta-TCP: enhanced bone quality by endochondral heterotopic bone formation. *Acta Biomater 2010;6-8:3292-301*.
7. Bruder SP, Kurth AA, Shea M, Hayes WC, Jaiswal N, Kadiyala S. Bone regeneration by implantation of purified, culture-expanded human mesenchymal stem cells. *J Orthop Res 1998;16-2:155-62*.
8. Boos AM, Loew JS, Deschler G, Arkudas A, Bleiziffer O, Gulle H, Dragu A, Kneser U, Horch RE, Beier JP. Directly auto-transplanted mesenchymal stem cells induce bone formation in a ceramic bone substitute in an ectopic sheep model. *J Cell Mol Med 2011;15-6:1364-78*.
9. Geuze RE, Everts PA, Kruyt MC, Verbout AJ, Alblas J, Dhert WJ. Orthotopic location has limited benefit from allogeneic or autologous multipotent stromal cells seeded on ceramic scaffolds. *Tissue Eng Part A 2009;15-11:3231-9*.
10. Geuze RE, Kruyt MC, Verbout AJ, Alblas J, Dhert WJ. Comparing various off-the-shelf methods for bone tissue engineering in a large-animal ectopic implantation model: bone marrow, allogeneic bone marrow stromal cells, and platelet gel. *Tissue Eng Part A 2008;14-8:1435-43*.
11. Marcacci M, Kon E, Moukhachev V, Lavroukov A, Kutepov S, Quarto R, Mastrogiacomo M, Cancedda R. Stem cells associated with macroporous bioceramics for long bone repair: 6- to 7-year outcome of a pilot clinical study. *Tissue Eng 2007;13-5:947-55*.
12. Vacanti CA, Bonassar LJ, Vacanti MP, Shufflebarger J. Replacement of an avulsed phalanx with tissue-engineered bone. *N Engl J Med 2001;344-20:1511-4*.
13. Quarto R, Mastrogiacomo M, Cancedda R, Kutepov SM, Mukhachev V, Lavroukov A, Kon E, Marcacci M. Repair of large bone defects with the use of autologous bone marrow stromal cells. *N Engl J Med 2001;344-5:385-6*.
14. Scott MA, Levi B, Askarinam A, Nguyen A, Rackohn T, Ting K, Soo C, James AW. Brief review of models of ectopic bone formation. *Stem Cells Dev 2012;21-5:655-67*.
15. Eman RM, Oner FC, Kruyt MMP, Dhert W, Alblas J. Stromal cell-derived factor-1 stimulates cell recruitment, vascularization and osteogenic differentiation. *Tissue Eng Part A 2013*.
16. Claes L, Recknagel S, Ignatius A. Fracture healing under healthy and inflammatory conditions. *Nat Rev Rheumatol 2012;8-3:133-43*.
17. Bara JJ, Richards RG, Alini M, Stoddart MJ. Concise review: Bone marrow-derived mesenchymal stem cells change phenotype following in vitro culture: implications for basic research and the clinic. *Stem Cells 2014;32-7:1713-23*.

18. Dawson JI, Kanczler J, Tare R, Kassem M, Oreffo RO. Concise review: bridging the gap: bone regeneration using skeletal stem cell-based strategies - where are we now? *Stem Cells 2014;32-1:35-44*.
19. Quent VM, Theodoropoulos C, Hutmacher DW, Reichert JC. Differential osteogenicity of multiple donor-derived human mesenchymal stem cells and osteoblasts in monolayer, scaffold-based 3D culture and in vivo. *Biomed Tech (Berl) 2016;61-3:253-66*.
20. Levenberg S, Rouwkema J, Macdonald M, Garfein ES, Kohane DS, Darland DC, Marini R, van Blitterswijk CA, Mulligan RC, D'Amore PA, Langer R. Engineering vascularized skeletal muscle tissue. *Nat Biotechnol 2005;23-7:879-84*.
21. Seebach C, Henrich D, Kahling C, Wilhelm K, Tami AE, Alini M, Marzi I. Endothelial progenitor cells and mesenchymal stem cells seeded onto beta-TCP granules enhance early vascularization and bone healing in a critical-sized bone defect in rats. *Tissue Eng Part A 2010;16-6:1961-70*.
22. Eman RM, Meijer HA, Oner FC, Dhert WJ, Alblas J. Establishment of an Early Vascular Network Promotes the Formation of Ectopic Bone. *Tissue Eng Part A 2016;22-3-4:253-62*.
23. Krishnan L, Willett NJ, Guldberg RE. Vascularization strategies for bone regeneration. *Ann Biomed Eng 2014;42-2:432-44*.
24. Oryan A, Alidadi S, Moshiri A, Maffulli N. Bone regenerative medicine: classic options, novel strategies, and future directions. *J Orthop Surg Res 2014;9-1:18*.
25. Visser J, Melchels FP, Jeon JE, van Bussel EM, Kimpton LS, Byrne HM, Dhert WJ, Dalton PD, Hutmacher DW, Malda J. Reinforcement of hydrogels using three-dimensionally printed microfibres. *Nat Commun 2015;6:6933*.
26. Wegman F, Bijenhof A, Schuijff L, Oner FC, Dhert WJ, Alblas J. Osteogenic differentiation as a result of BMP-2 plasmid DNA based gene therapy in vitro and in vivo. *Eur Cell Mater 2011;21:230-42; discussion 42*.
27. Wegman F, Geuze RE, van der Helm YJ, Cumhur Oner F, Dhert WJ, Alblas J. Gene delivery of bone morphogenetic protein-2 plasmid DNA promotes bone formation in a large animal model. *J Tissue Eng Regen Med 2012*.
28. Thomson RC, Yaszemski MJ, Powers JM, Mikos AG. Fabrication of biodegradable polymer scaffolds to engineer trabecular bone. *J Biomater Sci Polym Ed 1995;7-1:23-38*.
29. Loozen LD, van der Helm YJ, Oner FC, Dhert WJ, Kruyt MC, Alblas J. Bone morphogenetic protein-2 nonviral gene therapy in a goat iliac crest model for bone formation. *Tissue Eng Part A 2015;21-9-10:1672-9*.
30. Pawar SN, Edgar KJ. Alginate derivatization: a review of chemistry, properties and applications. *Biomaterials 2012;33-11:3279-305*.
31. Vukicevic S, Kleinman HK, Luyten FP, Roberts AB, Roche NS, Reddi AH. Identification of multiple active growth factors in basement membrane Matrigel suggests caution in interpretation of cellular activity related to extracellular matrix components. *Exp Cell Res 1992;202-1:1-8*.
32. Oudshoorn MHM RR, Bouwstra JA, Hennink WE. Synthesis of methacrylated hyaluronic acid with tailored degree of substitution. *Polymer 2007;48-7:1915-20*.
33. Narayanan NK, Duan B, Butcher JT, Mazumder A, Narayanan BA. Characterization of multiple myeloma clonal cell expansion and stromal Wnt/beta-catenin signaling in hyaluronic acid-based 3D hydrogel. *In Vivo 2014;28-1:67-73*.
34. Sewell-Loftin MK, DeLaughter DM, Peacock JR, Brown CB, Baldwin HS, Barnett JV, Merryman WD. Myocardial contraction and hyaluronic acid mechanotransduction in epithelial-to-mesenchymal transformation of endocardial cells. *Biomaterials 2014;35-9:2809-15*.
35. Bose S, Tarafder S. Calcium phosphate ceramic systems in growth factor and drug delivery for bone tissue engineering: a review. *Acta Biomater 2012;8-4:1401-21*.

36. Sariibrahimoglu K, An J, van Oirschot BA, Nijhuis AW, Eman RM, Alblas J, Wolke JG, van den Beucken JJ, Leeuwenburgh SC, Jansen JA. Tuning the degradation rate of calcium phosphate cements by incorporating mixtures of polylactic-co-glycolic acid microspheres and glucono-delta-lactone microparticles. *Tissue Eng Part A 2014;20-21-22:2870-82.*
37. Viateau V, Manassero M, Sensebe L, Langonne A, Marchat D, Logeart-Avramoglou D, Petite H, Bensidhoum M. Comparative study of the osteogenic ability of four different ceramic constructs in an ectopic large animal model. *J Tissue Eng Regen Med 2016;10-3:E177-87.*
38. Fedorovich NE, Kuipers E, Gawlitta D, Dhert WJ, Alblas J. Scaffold Porosity and Oxygenation of Printed Hydrogel Constructs Affect Functionality of Embedded Osteogenic Progenitors. *Tissue Eng Part A 2011.*
39. Loh QL, Choong C. Three-dimensional scaffolds for tissue engineering applications: role of porosity and pore size. *Tissue Eng Part B Rev 2013;19-6:485-502.*
40. Geuze RE, Theyse LF, Kempen DH, Hazewinkel HA, Kraak HY, Oner FC, Dhert WJ, Alblas J. A differential effect of bone morphogenetic protein-2 and vascular endothelial growth factor release timing on osteogenesis at ectopic and orthotopic sites in a large-animal model. *Tissue Eng Part A 2012;18-19-20:2052-62.*
41. Hayashi K, Tabata Y. Preparation of stem cell aggregates with gelatin microspheres to enhance biological functions. *Acta Biomater 2011.*
42. Ratanavaraporn J, Furuya H, Kohara H, Tabata Y. Synergistic effects of the dual release of stromal cell-derived factor-1 and bone morphogenetic protein-2 from hydrogels on bone regeneration. *Biomaterials 2011;32-11:2797-811.*
43. Ikada Y, Tabata Y. Protein release from gelatin matrices. *Adv Drug Deliv Rev 1998;31-3:287-301.*
44. Marsell R, Einhorn TA. THE BIOLOGY OF FRACTURE HEALING. *Injury 2011;42-6:551-5.*
45. Bali K, Walker P, Bruce W. Custom-fit total knee arthroplasty: our initial experience in 32 knees. *J Arthroplasty 2012;27-6:1149-54.*

Nederlandse samenvatting

Bot is een weefsel met goed regeneratief vermogen. De meeste botbreuken genezen daardoor zonder problemen. Soms geneest een fractuur niet, dit kan komen door inadequate (gips) immobilisatie of een tekort aan vaatvoorziening, soms is een botdefect primair te groot om te overbruggen. In deze gevallen kan het nodig zijn een bottransplantatie te doen om operatief alsnog een goed resultaat te bewerkstelligen. Transplantatiebot moet dan worden geoogst op een plek waar het gemist kan worden, bijvoorbeeld uit de bekkenkam. Dit levert vaak het gewenste bot, maar het levert ook een verlengde operatietijd, verhoogd infectiegevaar en pijn met name in het donorgebied. Er kan ook gedoneerd bot gebruikt worden, van heupkopdonatie of overleden donoren, maar doordat er vele bewerkingen nodig zijn om dit donorbot veilig en zonder ziekteoverdracht te kunnen gebruiken is dit bot van mindere kwaliteit.

In de regeneratieve geneeskunde wordt er gezocht naar een oplossing voor dit probleem. Idealiter zou het mogelijk zijn een scan te maken van het te behandelen defect, om dit daarna in de juiste vorm te 3D-bioprinten, met eigenschappen die zo veel mogelijk lijken op de natuurlijke situatie. In de natuurlijke situatie zijn er locaties voor het vormen van botweefsel (gemaakt van hard materiaal, met botcellen en actieve stoffen), evenals locaties met uitsparingen voor ingroei van bloedvaten (van zacht materiaal, met vaatcellen) om overleving van het nieuwe weefsel te bewerkstelligen.

Voor het regeneren van weefsel spelen klassiek drie componenten een rol: cellen, dragermateriaal en bioactieve stoffen. Al deze factoren komen in dit proefschrift aan de orde. Het doel van dit onderzoek was om middels 3D bioprinten de architectuur van constructen te verbeteren en middels zorgvuldige plaatsing en afgifte van groeifactoren de regeneratie van de beoogde weefsels te stimuleren.

In **hoofdstuk 2** werd onderzocht hoe de groeifactor BMP-2 (bone morphogenetic protein), al dan niet geladen op microspheres (kleine bolletjes die een trage afgifte bewerkstelligen), botvorming kan stimuleren. Hiervoor werd alginaat gebruikt als drager, met beenmergstamcellen (die dienen als voorlopercellen voor botvormende osteoblasten) hieraan toegevoegd. Er werd voor stevigheid keramiek toegevoegd. Al deze componenten werden in de alginaatgel ingebed en ge-3D-print. Deze constructen werden geimplanteerd in ratten en muizen om botvorming te meten. Er werd osteoblastdifferentiatie gezien in de cellen in de gel. Er werd geen toegevoegde waarde gezien van verlengde afgifte van BMP-2.

In **hoofdstuk 3** werd Matrigel gebruikt met toevoeging van humane navelstrengbloedcellen en de vaatgroeifactor VEGF (vascular endothelial growth factor), al dan niet op microspheres. Het was mogelijk gebieden te printen met en zonder groeifactor, en na implantatie in muizen was er verschil te zien ten gunste van vertraagde afgifte van groeifactor, resulterend in een betere doorbloeding van de constructen. Om de Matrigel beter te kunnen printen werd de viscositeit verhoogd door middel van toevoeging van alginaat, maar dit had een negatief effect op de vaatvorming. Na implantatie konden de

verschillende regio's van de constructen (met en zonder microspheres) teruggevonden worden. Het bleek dus mogelijk regionale verschillen te incorporeren in de constructen.

In **hoofdstuk 4** werd gekeken naar de toevoegde waarde van SDF-1α (stromal cell derived factor 1α) in constructen die BMP-2 bevatten. SDF-1α is een bioactieve stof waarvan bekend is dat deze lichaamseigen stamcellen kan aantrekken. Er werden opnieuw hybride alginaatconstructen ontworpen, waarin BMP-2 werd gecombineerd met SDF-1α en stamcellen. Celvrije constructen werden bestudeerd om te kijken of SDF-1α voldoende eigen stamcellen zou kunnen aantrekken om botvorming te bewerkstelligen. Dit gebeurde in dit experiment niet. In de constructen met cellen werd wel gezien dat er eerder en meer botvorming plaatsvond wanneer de groeifactoren gecombineerd werden geïmplanteerd.

In **hoofdstuk 5** werden combinaties van de genoemde groeifactoren gemaakt en apart toegepast in een nieuw diermodel, de plastic bone chamber. Hiermee werd onderzocht hoe osteoblastdifferentiatie in een botomgeving gereguleerd is. De bone chamber is een hol buisje, dat met een schroef met gaatjes direct op het bot geplaatst kan worden. Doordat het kamertje geen signaal geeft bij röntgendoorlichting, kan het in dierexperimenten gebruikt worden om botvorming in de tijd te volgen middels microCTscans. Dit kan belangrijke informatie opleveren over het verloop van de botvorming binnen individuele proefdieren, en het aantal benodigde proefdieren verminderen. Het bleek mogelijk botvorming te bewerkstelligen in deze botkamers, en dit kon met de scans geobjectiveerd worden.

In **hoofdstuk 6** hebben we een printbare gel met gunstige eigenschappen voor regeneratieve geneeskunde gemaakt, en deze getest op het gebied van celoverleving, mogelijkheid tot osteogene differentiatie van cellen en printbaarheid. Het bleek mogelijk deze gel, gebaseerd op hyaluronzuur, dat voorkomt in natuurlijke weefsels, zo te veranderen dat deze met uv-licht overgaat van vloeibaar naar gel-vorm. De overleving van de cellen en mate van celdifferentiatie (een voorstadium van botvorming) hingen nauw samen met de stijfheid van de gel. Voor het 3D-printen van constructen met duidelijke architectuur gaat de voorkeur vaak uit naar een stijvere gel, terwijl de cellen in een zachtere gel beter functioneren.

In **hoofdstuk 7** werd de effectiviteit van bovenstaande groeifactoren gecombineerd en apart bestudeerd in een keramisch dragermateriaal in de vorm van schijfjes welke onderhuids geïmplanteerd werden. De constructen werden middels geavanceerde microCT met hoge resolutie gescand aan het einde van de implantatie om de botvorming te bepalen. Omdat keramiek op de scan vergelijkbaar is met bot, was tot nu toe differentiatie tussen de twee niet mogelijk, waardoor constructen altijd moesten worden uitgenomen voor weefselanalyse. Het bleek met onze nieuwe software mogelijk betrouwbare metingen te doen, hoewel de hoeveelheid botvorming altijd een beetje een overschatting bleek wanneer werd vergeleken met traditionele weefselanalyse.

Alle hoofdstukken bij elkaar genomen hebben we belangrijke stappen gezet naar verbeterde constructen voor botregeneratie. Door de afgifte van groeifactoren op het juiste moment op de juiste plaats kunnen we een hoger niveau van organisatie en architectuur in constructen bewerkstelligen.

Dankwoord

Prof. dr. Öner, beste Cumhur,
Ons contact begon met een mooi gesprek over de röntgenfoto van een Maine Coon in een college dat je ons gaf. Toen ik daarna vroeg hoe de orthopedie zich verhield tot de traumatologie zei je dat ik dat moest komen ervaren. Ik was meteen verkocht. Ik ben ontzettend trots dat je mijn promotor bent. Je bent altijd beschikbaar voor nuchter commentaar en goede tips. Ik bewonder je warmte en je blik op de wereld.

Prof. dr. Dhert, beste Wouter,
Onder jouw begeleiding kwamen de klinische blikken en basic science op het gebied bot en kraakbeen bij elkaar. Je hebt mijn promotietraject zeer hands-on begeleid, van wetenschappelijke presentatie tot de papers, iets wat bijzonder is met het aantal promovendi dat je hebt begeleid. Je bent altijd benaderbaar, correct, en een groot voorbeeld.

Dr. Alblas, beste Jacqueline,
Waar moet ik beginnen om jou te bedanken. Elke dinsdagochtend botmeetings, de vele tussentijdse gesprekken om onze plannen en mijn voortgang samen in de gaten te houden. Je hebt eindeloze versies van elke letter die op papier stond bekeken en je had tips op alle gebieden, tot fotografie aan toe. Ik ben dankbaar voor hoe je me in vier jaar hebt omgeschoold tot een basale wetenschapper. We hebben samen de mooiste congressen bezocht in San Francisco, Venetië, New Orleans dierbare herinneringen. Dank voor het geduld wat je altijd met me gehad hebt.

Prof. dr. Saris, beste Daan,
Ik wil je bedanken voor het vertrouwen wat ik vanaf de eerste minuut bij je heb ervaren. Toen ik moest wachten op het starten van dit promotietraject heb je een prachtige baan voor me gecreëerd, die veel deuren voor me geopend heeft. Je zorgt op een bijzondere manier voor de 'Utrechtclub' en ik weet dat ik altijd op je kan rekenen. Heel bijzonder. Ik wens je alle goeds met je prachtige kans in de Verenigde Staten, stay in touch!

Prof. dr. Verbout, beste Ab,
U bent de reden dat ik überhaupt ben gaan promoveren. Het was toeval dat mijn eindgesprek geneeskunde bij u was, het was geen specifiek orthopediegesprek. Dat hield u niet tegen om gehakt te maken van mijn plan om voor een klinische baan te solliciteren. Ik zie ons gesprek als een belangrijk kruispunt waarbij de thuisbasis Utrecht echt gevestigd is. Ik vind het fantastisch dat u komt opponeren. Dank voor alles.

Prof. dr. Weinans, beste Harrie,
Veel dank voor de fijne samenwerking, eerst in Rotterdam en later in Utrecht. Het heeft geleid tot 2 mooie manuscripten.

Graag wil ik de beoordelingscommissie bedanken voor hun bereidheid een oordeel te vellen over mijn thesis in manuscript: Prof. dr.ir. W.E. Hennink, Prof. dr. J.A. Jansen, Prof. dr L.P.H. Leenen, Prof. dr. J.A.N. Verhaar en dr. D.H.R. Kempen.

Paranimfen

Jessica Bakker, ik ben zo ontzettend blij dat we elkaar in Antwerpen ontmoet hebben. Ook al groeiden we een steenworp van elkaar op, we hadden elkaar nooit ontmoet. Onze jaren in Antwerpen waren een aaneenschakeling van briljante gekkigheid waarbij we altijd samen op pad waren. Je bent er al 15 jaar altijd voor me en ik ben stapelgek op je. Dank voor de mooie stapavonden, saunadagen, eindeloze shopsessies, citytrips en goede gesprekken.

Yvonne van der Helm, jij hebt me vol passie begeleid en stond altijd voor me klaar. Ik schiet weer in de lach als ik denk aan die keer dat je me moest zeggen dat ik niet met mijn hele hoofd in de zuurkast mocht. Je secuurheid en correctheid hebben me veel geholpen, en wat waren we vaak samen aan het sprokkelen als ik weer aparte spulletjes nodig had om microspheres te maken. Je bent zeer betrokken geweest tijdens mijn onderzoek en ik waardeer het erg dat je 'terug' wilt komen om aan mijn zijde te staan.

De onderzoek collegae

Anika Tsuchida, lieve An, je was de eerste orthopediecollega met wie ik kennismaakte, en wat mooi dat we samen van semiarts tot gepromoveerde orthopeden in opleiding zijn gekomen. Ik bewonder je klasse en beheerstheid en waardeer je vriendschap.

Kim Benders, Bendie, in een recordtempo kwam jij het lab in, was je opeens het lab weer uit, ben je nu bijna orthopeed en heb je ook nog je proefschrift verdedigd. Wow. Je superpowers zijn ook op andere plekken opgevallen en ik weet zeker dat je bijzondere dingen gaat doen. Laten we sterrenrestaurants blijven bezoeken! En zorgen dat we een 'whatever, whenever'-knop beschikbaar hebben.

Fiona Wegman, liefste Fi, je was mijn researchcoach, lachte me uit bij maxiparticle, lachte me uit als ik beyond chagrijnig was. Altijd bereid te helpen, altijd een open blik. Ik ben blij dat je mijn vriendin bent en hoop dat we vaker onze kinderen gaan opdringen ook vrienden te worden ;-).

Mattie van Rijen, lieve Matski, jij bent het cement dat de researchafdeling bij elkaar houdt. Een wandelende encyclopedie, fotograaf, interactieve rekenmachine, technicus. Je zorgt voor kwaliteit, sfeer, continuïteit Zonder jou was het niet hetzelfde geweest.

De andere Q-warriors: Hsiao-Yin Yang, let's keep the borrel/dinner-club going. Michiel Beekhuizen, Beekie, Iron Man, ik word altijd vrolijk van je. Wouter Schuurman, ik hoop dat we nog lang af en toe een borrel doen. Loek Loozen, ik zie je veel te weinig, je bent prachtig gezelschap. Tommy de Windt, tropische baas, ik zal altijd Michael Jackson blijven aanvragen als je in de buurt bent. Tom Schlösser, fijne vent, onnavolgbaar ben je.

Jetze Visser, onze fijne liaison met ROGO Oost. Rhandy Eman, mijn bone-IP maatje met de mooie schaterlach. Lucienne Vonk, hurricane Lucy, wat hebben we een lol gehad in New Orleans. Michiel Croes, jouw promotie is de volgende, gaaf. Tip: niet de ventilatie van je hotelkamer uitzetten! Michiel Janssen, Sjansen, deze MacMiep zegt thanks. Anita Krouwels, ik hoop dat we samen ooit naar Marc Anthony gaan. Linda Kock, waarom hebben we elkaar nooit meer gezien? Dit moet op een fout berusten. Behdad Pouran, nooit eerder zag ik iemand zo vastberaden en goed Nederlands leren. Petje af! Vivian Mouser, dank voor de gezelligheid. Said Sadiqi, heel knap hoe jij onderzoek combineerde met een eigen zaak. Man wat heb jij hard gewerkt. Parisa Rahnamay Moshtagh, I am very happy you joined us in Utrecht. Huub de Visser, we hebben maar kort samengewerkt maar we blijven elkaar vast tegenkomen. Marianne Koolen, ik mis je goeie cappuccino's maar dat komt in het Antonius vast goed.

Laura Creemers, dank voor alles. Debby Gawlitta, heel veel dank voor al je wijze begeleiding. Naast al het serieuze heb je zelfs de piña colada naar een nieuw niveau getild. Ferry Melchels, dank voor je fijne bijdrage, masterprinter, en brouwer. Dino Colo, beer van de Balkan, fijne vent. Ik ben blij steeds met je te mogen samenwerken. Mechteld Lehr, jammer dat we geen bijna-buren meer zijn. Johan van der Stok, onze samenwerking werd beloond met mooie publicaties. Okan Bastian, fantastisch om na het onderzoek ook klinisch te mogen samenwerken. Angela Kragten, dank voor de vele gezellige koffiemomenten.

Hendrik Gremmels, wat een mooie paper is onze samenwerking geworden. En wat waren die meetings met broodjes gorgonzola van tricolore mooi meegenomen. Laten we snel weer eens MrBalls onveilig maken. Ik weet vast (en nu quote ik jou) 'Nelly Furtado-gerelateerde weetjes'. Een van mijn favoriete complimenten en beledigingen in één.

Researchstudenten,
Jeroen van Bemmel, veel dank voor je inzet. Kelly van Deventer, veel dank, ik vond het een eer op je afstuderen en verdediging te mogen zijn. De docenten waren diep van je onder de indruk. Marieke 't Hart, wat ontzettend knap was het van jou om (veel jonger dan de rest) als eerste studente van je opleiding bij ons in het lab te komen. In no time hoorde je thuis in de groep en won je daarna nog een mooie prijs met je stage. Chapeau.

Birgit Goversen, dank voor de fijne samenwerking, het heeft een mooie publicatie tot gevolg gehad.

Mylene de Ruijter, lieve Myl, als ik aan jou denk dekt het woord 'trots' de lading niet eens. Ik zag jouw cv en wist dat we wel moesten samenwerken. Wilrijk. Campi. TD. Daar kan je geen nee tegen zeggen. Gedurende de stage wist je op te vallen en je hebt het maar mooi om weten te zetten in een eigen promotietraject. Ik ben intens trots dat ik je 'gescout' heb. Dank dat je wilde proofreaden. En pas op jezelf. En je gouden E.

OLVG Collegae, jullie maken van het OLVG een ontzettend fijne werkplek waar we in hoog tempo veel kunnen leren. Jullie hebben met me meegeleefd tijdens mijn laatste promotie-loodjes. Ik ben trots om bij deze club te horen.

Summies,
Mag ik nu dan eindelijk de nerdaward? Ik zal hem daarna braaf teruggeven aan van Binsbergen, want laten we eerlijk zijn…

Friends
Dordtse B.U., Lieve Lotte Oostrom, Esther Koppelaar en Marieke de Visscher, ik ben zo blij dat ik mijn 'voor altijd' vriendinnen al in 2VWO mocht ontmoeten. Na dat ene beruchte slaapfeestje zijn we altijd hecht gebleven. De themadagen, tripjes, fake-vrijgezellen, hevige stapavonden, escape rooms en serieuze gesprekken, ik zou jullie voor geen goud willen missen.

Dordtse chicas, die ik zonder uitzondering veel te weinig zie: Tessa Noltee, we zijn echt al forever friends. Ik weet dat ik altijd bij je terecht kan en andersom. Maartje Brockbernd, wat is het gaaf dat je vandaag weer foto's wilt maken, ik weet zeker dat ze weer fantastisch zullen zijn. Jouw aanwezigheid is altijd onwijs fijn. Iris Fakkel, laten we weer eens gaan eten. Enne… 'ken het gerolen worden?'

Antwerpse ladies, Lotte de Jager, Elske Folkertsma, Iris Buunk; laten we weer eens proberen vega-knoflook-gluten-vrij gaan eten.

Renate Ottenheim, ik weet zeker dat we in de toekomst nog samen mooie orthopedische crossovers gaan maken. Samen je konijn opereren bijvoorbeeld. Je bent een fantastische vriendin.

Larense 'Gooische Vrouwen': Larissa Bonn, Annemieke Janssen, Sandra Cannariato, jullie hebben gezorgd dat we ons snel thuisvoelden en niet meer weg willen. Dank hiervoor.

Familia
Ik heb het geluk om 3 ouders te hebben:

Marjolein, wat een ongelofelijke force of nature ben je. Ik vergeet nooit de dag dat ik thuiskwam uit school en dat jij als single mom in één dag het hele huis knalgeel geschilderd had, gestopt was met roken en een opleiding was gestart ('We gaan het anders doen…'). Daarna volgden een avond post-HBO, avondstudie bedrijfskunde en enkele jaren geleden je eigen promotie. Je hebt nooit laten blijken dat het zwaar was. Altijd heb je alles voor ons over gehad. Wat een voorbeeld. 'And all of my childhood memories are full of all the sweet things you did for me.' (Tupac, 'Dear Mama'.)

Maarten, ik lijk belachelijk veel op je. Ik heb je creativiteit, handigheid en je koppigheid. Merel en ik werden gek van de eindeloze museumbezoeken waar je ons altijd naar

meesleepte, dit zijn nu de herinneringen die ik het meest koester. Ik vind het fantastisch je met je kleinkinderen te zien. De rust die je hebt gevonden in het Noorden werkt aanstekelijk.

Robbert, sinds ik 13 jaar oud was ben je in mijn leven. En sindsdien heb ik altijd geweten dat het niet uit maakt wat er is: je bent er altijd voor me. Wanneer ik mensen probeer uit te leggen hoe jij bent, gebruik ik meestal mijn mr. Wolf uit *Pulp Fiction* vergelijking: you fix problems. En hoe. Altijd een logische oplossing en geruststellende woorden. Ik kan er altijd op vertrouwen dat je me uitlacht en van me houdt. En ik van jou. Dank dat je ervoor kiest mijn vader te zijn.

Merel, bird, liefste zus die er is. Zo verschillend en zo hetzelfde. Ik geniet van onze inside jokes (eindeloos veel zijn het er) en dat we net zo goed vriendinnen zijn als zussen. Ik denk dat het weer tijd wordt om samen de volle *P&P* te kijken, in slaap te vallen, weer een poging te doen, etc. Dank voor het super proofread-werk. Erg handig als je zus zo absurd goed is met taal.

Koos, dank dat je zo'n mooi stel maakt met Merel. Ik wil nu toch echt die zelfgemaakte pizza weer eens komen eten. En komen kijken bij Apelazerus.

Opa Harry ten Holter, wat fantastisch dat u op de verdediging aanwezig bent. U bent altijd een voorbeeld geweest op het gebied van hard werken en brede interesse. En ook simpelweg de liefste opa van de wereld.

Familie Wetzels: liefste Wiel, je bent een geweldige schoonvader en opa voor de kinderen. Het is fijn dat je ondanks de grote afstand zo vaak bij ons bent en altijd klaar staat om te helpen. Heel veel dank. Liefste schoonfamilie: dank voor jullie warmte, Bourgondische gezelligheid en bereidheid en geduld om voor mij te vertalen. 55 blijft het favoriete getal.

San & Matt, wat een voorrecht dat onze kinderen ook weer vrienden zijn. Wie was nou ook alweer de tante?

Lilian, Ronald, Bert, Dorine, Tristan, Coralie, Charlotte, Madeleine, Friso, Job. Laten we erin houden om elkaar te zien, om de verjaardag van Lidy te vieren, evenals andere feesten en partijen. We zijn een te mooi zooitje ongeregeld om dat niet te doen.

Liefste Kevin, waar jij bent is thuis. En niets is zo fijn als thuiskomen bij jou en onze prachtkinderen. Ik ben trots op wat we samen de afgelopen jaren bereikt hebben en kijk uit wat de komende jaren ons gaan brengen. Droomvent!

Pieter en Jasmijn. Niets maakt me gelukkiger dan jullie moeder te mogen zijn.

List of Publications

1. Poldervaart MT, Goversen B, de Ruijter M, Abbadessa A, Melchels FPW, Oner FC, Dhert WJA, Vermonden T, Alblas J. 3D bioprinting of methacrylated hyaluronic acid (MeHA) hydrogel with intrinsic osteogenicity. *PLoS ONE 2017;12-6:e0177628*.

2. Feyen DA, Gaetani R, Deddens J, van Keulen D, van Opbergen C, Poldervaart M, Alblas J, Chamuleau S, van Laake LW, Doevendans PA, Sluijter JP. Gelatin Microspheres as Vehicle for Cardiac Progenitor Cells Delivery to the Myocardium. *Adv Healthc Mater 2016;5-9:1071-9*.

3. Poldervaart MT, van der Stok J, de Haas MF, t Hart MC, Oner FC, Dhert WJ, Weinans H, Alblas J. Growth factor-induced osteogenesis in a novel radiolucent bone chamber. *Eur Cell Mater 2015;29:35-41; discussion*

4. Wegman F, Poldervaart MT, van der Helm YJ, Oner FC, Dhert WJ, Alblas J. Combination of bone morphogenetic protein-2 plasmid DNA with chemokine CXCL12 creates an additive effect on bone formation onset and volume. *Eur Cell Mater 2015;30:1-10; discussion -1*.

5. Poldervaart MT, Gremmels H, van Deventer K, Fledderus JO, Oner FC, Verhaar MC, Dhert WJ, Alblas J. Prolonged presence of VEGF promotes vascularization in 3D bioprinted scaffolds with defined architecture. *J Control Release 2014;184:58-66*.

6. Poldervaart MT, Wang H, van der Stok J, Weinans H, Leeuwenburgh SC, Oner FC, Dhert WJ, Alblas J. Sustained Release of BMP-2 in Bioprinted Alginate for Osteogenicity in Mice and Rats. *PLoS ONE 2013;8-8:e72610*.

7. Meuffels DE, Poldervaart MT, Diercks RL, Fievez AW, Patt TW, Hart CP, Hammacher ER, Meer F, Goedhart EA, Lenssen AF, Muller-Ploeger SB, Pols MA, Saris DB. Guideline on anterior cruciate ligament injury. *Acta Orthop 2012;83-4:379-86*.

8. Poldervaart MT, Breugem CC, Speleman L, Pasmans S. Treatment of lymphatic malformations with OK-432 (Picibanil): review of the literature. *J Craniofac Surg 2009;20-4:1159-62*.

Curriculum vitae

Michelle Poldervaart was born in Dordrecht, the Netherlands on December 1st 1981. She graduated high school (Titus Brandsma College, Dordrecht) in 2001. Due to the numerus fixus she studied biology in Utrecht and veterinary science at the University of Antwerp in Belgium before entering the Selective Utrecht Medical Master (SUMMA) in 2005. After her graduation in 2009 she joined a task force (led by prof. dr. D.B.F. Saris, and dr. D.E. Meuffels) assigned by the Netherlands Orthopaedic Association (Nederlandse Orthopedische Vereniging, NOV) to perform research for a new guideline about anterior cruciate ligament injury.

In 2010 she started as a PhD candidate on the subject of bone regeneration at the department of orthopaedics of the University Medical Center (UMC) Utrecht, under supervision of prof. dr. W.J.A. Dhert, prof. dr. F.C. Öner and dr. J. Alblas. The results of this research were presented on national and international conferences. She completed the Graduate School of Life Sciences training on regenerative medicine in Utrecht.

In 2014 Michelle started her clinical training at the department of surgery at the Meander Medical Center in Amersfoort (head: dr. E. Consten). She continued her orthopaedic residency in the Onze Lieve Vrouwe Gasthuis (OLVG) in Amsterdam (head: dr. R.W. Poolman and drs. D.F.P. van Deurzen). She will continue her orthopaedic training at the Antonius Hospital (head: dr. M.R. Veen), and UMC Utrecht (head: prof. Dr. D.B.F. Saris). After this she will return to the OLVG to complete her orthopaedic residency.

Michelle currently lives in Laren with her partner Kevin Wetzels and their children, Pieter and Jasmijn.